



**HAL**  
open science

## Basin geodynamics and sequence stratigraphy of Upper Triassic to Lower Jurassic deposits of Southern Tunisia

Cédric Carpentier, Suhail Hadouth, Samir Bouaziz, Bernard Lathuilière,  
Jean-Loup Rubino

► **To cite this version:**

Cédric Carpentier, Suhail Hadouth, Samir Bouaziz, Bernard Lathuilière, Jean-Loup Rubino. Basin geodynamics and sequence stratigraphy of Upper Triassic to Lower Jurassic deposits of Southern Tunisia. *Journal of African Earth Sciences*, 2016, 117 (2), pp.358-388. 10.1016/j.jafrearsci.2016.01.029 . insu-03712781

**HAL Id: insu-03712781**

**<https://insu.hal.science/insu-03712781>**

Submitted on 5 Mar 2024

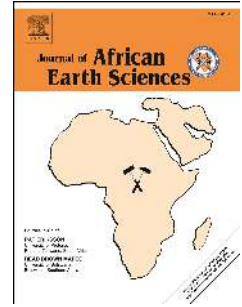
**HAL** is a multi-disciplinary open access archive for the deposit and dissemination of scientific research documents, whether they are published or not. The documents may come from teaching and research institutions in France or abroad, or from public or private research centers.

L'archive ouverte pluridisciplinaire **HAL**, est destinée au dépôt et à la diffusion de documents scientifiques de niveau recherche, publiés ou non, émanant des établissements d'enseignement et de recherche français ou étrangers, des laboratoires publics ou privés.

# Accepted Manuscript

Basin geodynamics and sequence stratigraphy of Upper Triassic to Lower Jurassic deposits of central and southern Tunisia

Cédric Carpentier, Suhail Hadouth, Samir Bouaziz, Bernard Lathuilière, Jean-Loup Rubino



PII: S1464-343X(16)30045-0

DOI: [10.1016/j.jafrearsci.2016.01.029](https://doi.org/10.1016/j.jafrearsci.2016.01.029)

Reference: AES 2489

To appear in: *Journal of African Earth Sciences*

Received Date: 27 May 2015

Revised Date: 10 September 2015

Accepted Date: 29 January 2016

Please cite this article as: Carpentier, C., Hadouth, S., Bouaziz, S., Lathuilière, B., Rubino, J.-L., Basin geodynamics and sequence stratigraphy of Upper Triassic to Lower Jurassic deposits of central and southern Tunisia, *Journal of African Earth Sciences* (2016), doi: 10.1016/j.jafrearsci.2016.01.029.

This is a PDF file of an unedited manuscript that has been accepted for publication. As a service to our customers we are providing this early version of the manuscript. The manuscript will undergo copyediting, typesetting, and review of the resulting proof before it is published in its final form. Please note that during the production process errors may be discovered which could affect the content, and all legal disclaimers that apply to the journal pertain.

1 **Basin geodynamics and sequence stratigraphy of Upper Triassic**  
2 **to Lower Jurassic deposits of central and southern Tunisia**

3  
4 **Cédric Carpentier<sup>(1)</sup>; Suhail Hadouth<sup>(1)</sup>; Samir Bouaziz<sup>(2)</sup>; Bernard Lathuilière<sup>(1)</sup>; Jean-Loup**  
5 **Rubino<sup>(3)</sup>**

6  
7 **(1) Université de Lorraine, CNRS, CREGU, GeoRessources lab., Faculté des Sciences et Technologies, BP 70239, F-**  
8 **54506 Vandoeuvre-lès-Nancy, France**

9 **(2) Laboratoire Eau-Energie-Environnement (AD-10-02), Ecole Nationale d'Ingénieurs de Sfax, Université de Sfax,**  
10 **BP 1173, 3038 Sfax, Tunisia**

11 **(3) Total S.A., CSTJF, avenue Larribau, 64000 Pau, France**

12  
13 **Corresponding author :**

14 Cédric CARPENTIER

15 Université de Lorraine, CNRS, CREGU, GeoRessources lab., Faculté des Sciences et Technologies, BP 70239,  
16 F-54506, Vandoeuvre-lès-Nancy, France.

17 E-mail: [cedric.carpentier@univ-lorraine.fr](mailto:cedric.carpentier@univ-lorraine.fr)

18 Tel: +33 (0)3 83 68 47 39

19 Fax: +33 (0)3 83 68 47 01

20

## 21 **Abstract**

22 Aims of this paper are to propose a geodynamic and sequential framework for the late Triassic and early Jurassic  
23 of central and south Tunisia and to evidence the impact of local tectonics on the stratigraphic architecture. Facies  
24 of the Upper Triassic to Lower Jurassic of Central and Southern Tunisia have been interpreted in terms of  
25 depositional environments. A sequential framework and correlation schemes are proposed for outcrops and  
26 subsurface transects. Nineteen middle frequency sequences inserted in three and a half low frequency  
27 transgression/regression cycles were evidenced. Despite some datation uncertainties and the unknown durations  
28 of Lower Jurassic cycles, middle frequency sequences appear to be controlled by eustasy. In contrast the  
29 tectonics acted as an important control on low frequency cycles. The Carnian flooding was certainly favored by  
30 the last stages of a rifting episode which started during the Permian. The regression accompanied by the  
31 formation of stacked angular unconformities and the deposition of lowstand deposits during the late Carnian and  
32 Norian occurred during the uplift and tilting of the northern basin margins. The transpressional activity of the  
33 Jeffara fault system generated the uplift of the Tebaga of Medenine high from the late Carnian and led to the  
34 Rhaetian regional angular Sidi Stout Unconformity. Facies analysis and well-log correlations permitted to  
35 evidence that Rhaetian to Lower Jurassic Messaoudi dolomites correspond to brecciated dolomites present on the  
36 Sidi Stout unconformity in the North Dahar area. The Early-cimmerian compressional event is a possible origin  
37 for the global uplift of the northern African margin and Western Europe during the late Carnian and the Norian.  
38 During the Rhaetian and the early Jurassic a new episode of normal faulting occurred during the third low  
39 frequency flooding. This tectonosedimentary evolution ranges within the general geodynamic framework of the  
40 north Gondwana margin controlled by the opening of both Neotethys and Atlantic oceans.

41

42 **Keywords:** late Triassic, early Jurassic, Tunisia, sequence stratigraphy, basin geodynamics

43

## 44 **1. Introduction**

45 After the late Palaeozoic collision with Laurasia, North Africa recorded the early stages of the opening of the  
46 Neotethys during late Paleozoic and Triassic times (Gabtni *et al.*, 2006; Memmi *et al.*, 1986; Stampfli and Borel,  
47 2002). In this geodynamic context, an intensive rifting affected the northern African margin during an anti-  
48 clockwise movement of Africa (Muttoni *et al.*, 2001). As a consequence of the westward opening of the  
49 Neotethys, the age of the transition between the active rifting and the passive margin stages is supposed to be  
50 younger in this direction. On seismic profiles, tilted blocs and overlaying passive margin geometries were

51 documented from Morocco to the Levant margin (Frizon de Lamothe, 2009; Galeazzi *et al.*, 2010; Gardosh *et*  
52 *al.*, 2010). However in some places the timing of this transition is different according to authors. In Tunisia,  
53 Stampfli *et al.* (1991) and Stampfli and Borel (2002) propose a late Permian onset of thermal subsidence with a  
54 short rifting in back-arc context during the Triassic on the northern Neotethyan margin. In contrast other authors  
55 considered that rifting was active until the middle-late Triassic (Galeazzi *et al.*, 2010, Piqué *et al.*, 1998), early  
56 Jurassic times (Golonka, 2007; Kamoun *et al.*, 2001; Raulin *et al.*, 2011; Schettino and Turco, 2011) or  
57 continuous until the early Cretaceous (Frizon de Lamote *et al.*, 2009). Turner *et al.*, (2001) also documented  
58 rifting episode during middle-late Triassic times in the Algerian Berkine Basin.

59  
60 Detailed stratigraphic study is a powerful tool to better constrain the geodynamic history of a region. However,  
61 while studies on Triassic deposits have been done in many north African localities such as Southeast Algeria  
62 (Bourquin *et al.*, 2010; Turner *et al.*, 2001), Jordan (Makhlouf, 2006), United Arab Emirates (Maurer *et al.*,  
63 2008), Levant (Korngreen and Benjamini, 2011), no detailed tectonosedimentary and sequence stratigraphy  
64 study of the Upper Triassic and Lower Jurassic deposits was performed in Central Tunisia. In addition,  
65 siliciclastic Triassic deposits contain large quantities of hydrocarbons in Algeria and southern Tunisia (Tigi  
66 Field). Middle-Upper Triassic dolomites may constitute targets for hydrocarbon exploration and the  
67 understanding of controls on their distribution in time and space is a challenge.

68  
69 The aim of this paper is to investigate the sequence stratigraphy of mixed carbonates, siliclastic, and evaporites  
70 of the Upper Triassic and Lower Jurassic deposits in Central and Southern Tunisia. In addition, major objectives  
71 are to constrain the timing of local deformations, to compare these results with depositional sequences, and to  
72 point out possible controls by local or more regional tectonics on sedimentation. To achieve this goal,  
73 sedimentological studies of outcrop and well logs using sequence stratigraphy methods were performed to  
74 propose local or basin scale correlations. Based on the locations of main faults, the geometries will be interpreted  
75 in terms of local variations in subsidence, eustasy, and sediment supply. Finally, results will be compared with  
76 structural frameworks of neighbouring areas in order to propose a model of geodynamical evolution of the  
77 Central and Southern Tunisia.

78

## 79 **2. Geological and structural setting**

80

81 The studied area extends from central Tunisia to the extreme south and east near Algerian and Libyan borders  
82 (Fig.1a). Northern Tunisia is affected by the recent alpine compressive tectonics, which generated thrusts and  
83 folding of evaporitic Triassic series. In central Tunisia, the normal and strike slip Jeffara fault system borders the  
84 Jeffara plain and the offshore Subratah Basin to the north (Fig.1). A minor synthetic fault coincides with the  
85 present cuesta profile delimiting the Dahar plateau to the southwest and the Jebel Rehach (J. Rehach) to the  
86 south (Fig.1b). The Dahar plateau covers the northern margin of the Paleozoic Talemzane High (Fig.1). In  
87 Southern Tunisia the western continuity of the Libyan Ghadames Basin is characterized by a broadly monoclinial  
88 geometry with a gentle southwestward dipping. In Algeria, the Berkine Basin constitutes the western extension  
89 of the Ghadames Basin. The Middle-Upper Triassic-Lower Jurassic rocks are exposed in two geographic and  
90 geological provinces:

- 91
- 92 - (1) The northern outcrop on the northern margin of the Dahar Plateau extends from the south of the  
93 Jebel Tebaga massif to the Oarjaijin village to the southeast (Fig. 1b). In the North Dahar, the structure  
94 is a monocline. Upper Triassic to Lower Jurassic dolomites are gently dipping ( $1-2^\circ$ ) southwestward  
95 (Bouaziz *et al.*, 2002) and overlay Lower and Middle Triassic deposits presenting a dipping of about 2  
96 to  $15^\circ$  to the south.
  - 97 - (2) In the J. Rehach, the Middle Triassic to Lower Jurassic series are outcropping along a 70 km long  
98 cuesta oriented northwest-southeast between the Tataouine city and the southeast of the Kirchaou  
99 village (Fig.1b). Formations are gently dipping to the south-west. Sidi Toui outcrops in the southeast of  
100 Tunisia exhibits only Ladinian to Carnian strata (Kamoun *et al.*, 2001) (Fig.1b).

101

102 During the Late Triassic, emerged lands bordered the Ghadames Basin to the south and provided siliciclastic  
103 material to the North African margin (Fig.2). Shallow carbonate and evaporite sedimentation occurred in a large  
104 part of the basin that was connected to the north to the western ending of the Neotethys (Sicanian Basin).  
105 Westward, during the first stages of the Atlantic rifting, NW-SE faulting formed a corridor between the emerged  
106 Iberian Massif and North Africa. Oceanic spreading was active in the Neotethys but did not extend as far as the  
107 Sicanian Basin. The Cimmerian orogeny started during the Carnian and subductions zones relieved by strike-slip  
108 faults developed on the northern margin of the Neotethys during the closure of the Paleotethys (Golonka, 2007;  
109 Sengör, 1984).

110

### 3. Method

Thirty five sedimentological sections have been logged and twenty eight are presented in this paper. Their GPS coordinates are given in Table1. To build sedimentary logs, thicknesses were measured on outcrops using a Jacob staff. Cartography was performed locally to determine the geometry and the stratigraphic position of formations or facies (e.g. Kronab Fm.). Facies interpretations are based on petrography, faunal associations, sedimentary structures and microfacies (150 thin sections). A sequence stratigraphic interpretation was performed on each section. Since they were not ever easy to evidence in each section, sea level fall unconformities have not been used as sequence boundaries according to classical models of sequence stratigraphy (Schlager, 2004; Posamentier and Morris, 2000; Posamentier and James, 1993; Vail *et al.*, 1991; Van Wagoner *et al.*, 1988). In contrast, transgression surfaces sometimes merged with subaerial exposure surfaces and characterized by a sharp deepening of depositional environments, above a shallowing-up trend, are the most obvious in the studied sections and have then been used to delimit sequences (Embry, 2009). Early diagenetic features were also investigated in optical microscopy and cathodoluminescence on thin sections. Outcrops and subsurface correlations are based on available biostratigraphy and sequence stratigraphy. The subsurface analysis was done by the interpretation of electric facies (see below) on well logs and using available petrographic descriptions. A sequence stratigraphy interpretation consistent with the outcrop study was established for each well according to the vertical stacking of facies.

### 4. Stratigraphy

The Triassic system is separated from Paleozoic deposits by the Hercynian angular unconformity probably of local extension (Raulin, 2013) (Fig.3). In the J. Rehach Lower and Middle Triassic deposits correspond to the alternation of fluviodeltaic siliciclastics (Bir El Jaja and Ras Hamia formations) and marginal dolomites and limestones (Kamoun *et al.*, 2001; Mejri *et al.*; 2006). The Ras Hamia Fm. comprises the siliciclastic and carbonate Ouled Chebbi Member and the fluvial siliciclastic Kirchaou Member separated by marine carbonates and shales of the *Myophoria* Limestones (Mennig *et al.* 1963; Buroillet, 1963). Those formations were also described in subsurface in South Tunisia where the TAG-I Fm. corresponds to the lateral equivalent of the Kirchaou Fm. (Hamouche, 2006). In the North Dahar, Anisian siliciclastics of the Ouled Chebbi member occur below the Sidi Stout Unconformity. In eastern Algeria, Anisian to Lower Carnian deposits consist of continental

139 sandstones of the TAG-I (Trias Argilo-Gréseux Inférieur) Fm. dated with vertebrates (Jalil, 1999) and  
140 palynomorphs (Bourquin *et al.*, 2010).

141  
142 In the J. Rehach, the Carnian deposits are characterized from base to top by the Mekraneb dolomites, the Tourag  
143 sandstones and the Rehach dolomites. Mekraneb dolomites are attributed with confidence to early Carnian  
144 (Kamoun *et al.*, 2001) and conodonts suggest a Cordevolian age (Rakus, 1981; Mock *et al.*, 1987). This first  
145 carbonate unit is considered as the base of the “*Trias Argilo Carbonaté* (TAC)” in Algeria (Busson, 1972). The  
146 Touareg sandstones are attributed to the middle Carnian due to their stratigraphic position between well dated  
147 Carnian dolomites. The second dolomite formation corresponds to the Rehach Fm. and is dated to the middle-  
148 late Carnian on the basis of foraminifera (Kamoun *et al.* 2001). In the North Dahar, dolomite breccias have also  
149 been dated to the Carnian (Kamoun *et al.*, 2001). They grade laterally northward into conglomerates of the  
150 Mougor Formation. However, on the basis of facies similarities between Messaoudi Fm. and Rehach Fm. (see  
151 below) Mello and Bouaziz (1987) assign a Rhaetian age to dolomite breccias of the North Dahar. In central  
152 Algeria and in south Tunisia TAG-I sandstones are covered by carbonates and shales of the TAC (Trias Argilo-  
153 Carbonaté) Fm. The age of this interval was not directly constrained in south Tunisia while a Carnian age was  
154 proposed for central Algeria by Galeazzi *et al.* (2010) on the basis of regional correlations and a Carnian to  
155 Norian age was envisioned by Bourquin *et al.* (2010) for the Zarzaitine area.

156  
157 In the J. Rehach, dolomites of the Rehach Fm. are overlain by the evaporitic red shales of the Mhira Fm. This  
158 formation is attributed to late Carnian to Norian by most authors (Visscher and Kystyn, 1978; Kamoun *et al.*,  
159 2001), on the basis of rich spores and palynomorphs assemblages found in its lower part (Bouaziz *et al.*, 1987).  
160 In the North Dahar, from base to top, red shales, polygenic conglomerates and green shales with thin evaporites  
161 and dolomites beds lay above the brecciated dolomites. Ages of these deposits are unknown. In south Tunisia  
162 TAC dolomites are overlaid with the non dated evaporitic Djeneien Fm. and evaporitic red shales of the Emzab  
163 Fm. (Ben Ismail, 1982). In Algeria sandstones of the TAG-S Fm. (Trias Argilo-Gréseux Supérieur) grade  
164 laterally into evaporites of the S4 salt Fm. Bourquin *et al.* (2010) assigned a Rhaetian age to these deposits on  
165 the basis of regional correlations. In central Algeria S4 salts were also described in subsurface and a Norian age  
166 was proposed by Galeazzi *et al.* (2010). In Algeria D2 shales overlaying S4 salts are not directly dated but  
167 Bourquin *et al.* (2010) propose a Hettangian age. In the saliferous Ghadamis/Berkine Basin, Mejri *et al.* (2006)

168 described the Mekraneb dolomites, Touareg sandstones, Rehach dolomites as Infra-D2 deposits and overlaying  
169 Mhira shales as D2.

170  
171 In the J. Rehach a major unconformity occurs at the base of the dolomitic and evaporitic deposits of the Rhaetian  
172 Messaoudi Fm. (Mello and Bouaziz, 1987). Until now, the Kronab conglomerates were considered as local and  
173 deposited above the unconformity (Mello and Bouaziz, 1987; Peybernès et al., 1993). The stratigraphic position  
174 of the conglomerates will be discussed further in the paper. Several oolite rich dolomitic strata corresponds to the  
175 Zerzour Fm. (Mello and Bouaziz 1987) which separates the Messaoudi Fm. below from evaporite rich Bhir Fm.  
176 above. Based on the presence of benthic foraminifera associations, the Zerzour Dolomite was assigned to  
177 Rhaetian time (Peybernès *et al.*, 1993; Kamoun *et al.*, 1994, 1997, 2001). The Bhir Formation is azoic and not  
178 well dated but may be tentatively attributed to Hettangian-Sinemurian age according to its stratigraphic position.  
179 In southern Tunisia the Emzab Fm. is overlain by the non dated halite of the Keskesa Fm. and by dolomites  
180 and anhydrite of the Larich Fm. In Algeria D2 red shales are covered by halite of the S3 salt and anhydrite of the  
181 Bhir Fm. Despite the lack of direct datations Bourquin *et al.* (2010) propose a Hettangian age for S3 salt.

182  
183 The oolitic and dolomitic Zmilet Haber Fm. also called B-Horizon in subsurface is capping the Bhir Fm. in the  
184 Tataouine area (Ben Ismail, 1982). In Tunisia this formation was assigned to the Pliensbachian (Busson, 1967;  
185 Ben Ismail, 1982; Ben Ferjani, 1990). Peybernès *et al.*, (1985) also proposed a Pliensbachian age on the basis of  
186 one echinid identified as *Pseudodiadema cf. prisciniacense*.

187

## 188 5. Results

189

### 190 5.1 Facies Analysis

191 Upper Triassic and Lower Jurassic deposits of Tunisia consist of the stacking of carbonate, siliciclastic and  
192 evaporite facies. Since dolomitization affecting the totality of facies is mainly mimetic, initial facies can be  
193 determined. The main facies characteristics are summarized in Table 2.

194

#### 195 **Carbonate facies**

#### 196 - Green Marls (Mgr)

197 This facies consists of green to yellow marls (Fig.4a). Marls are nodular locally and bioturbations are rare. They  
198 contain benthic fauna such as bivalves, echinoids. Rare ammonoids and nautiloids (*Nautilus klipsteini*),  
199 *Nothosaurus* and conodonts have been described in this facies (De Lapparent, 1954; Gorce, 1960; Rakus, 1981;  
200 Rieppel, 1997).

201 Interpretation: Lower offshore marls

202 The occurrence of pelagic organisms and diversified benthic fauna argues for an oxygenated marine  
203 environment. However the fine grain size indicates a calm depositional environment below the storm wave base  
204 in a lower offshore environment.

205

### 206 **-Nodular peloidal dolomite (Dn)**

207 This facies is generally alternating with the Mgr marls. It consists of yellow to beige nodular beds of peloidal  
208 dolomite with an initial packstone texture (Fig.5a). Except few *Thalassinoides* burrows, the bioturbation is  
209 generally diffuse but intensive. Where primary sedimentary structures have not been erased by bioturbation, the  
210 top of beds are characterized by wavy undulations with wavelengths of about 50cm (Fig. 4a). Aggrading  
211 hummocky cross stratifications and thin shell beds (less than 5cm thick) with clasts of brachiopods, oysters,  
212 echinoid spines and crinoids articles occur (Fig.4a and b).

213 Interpretation: Storm influenced upper offshore

214 The intensive bioturbation indicates a normal oxygenation of the sediment. The nodular aspect of beds is  
215 probably due to the intensive bioturbation (Clari and Martire, 1996). Bioclastic beds imply the reworking of  
216 benthic fauna by high energy events and their re-sedimentation in a calm offshore environment. Storm events are  
217 considered here as the most probable mechanisms able to produce such shell beds. In addition, the occurrence of  
218 storm wave structures such as HCS alternating with offshore marls indicates an environment between the storm  
219 wave base and the fair weather wave base. The euhaline nature of brachiopods and echinoderms also suggest an  
220 open marine life environment.

221

### 222 **- Bioclastic peloidal dolomite (Dbp)**

223 This facies consists of massive beds of peloidal dolomite with an initial packstone to grainstone texture (Fig.5b).  
224 Skeletal clasts such as oysters, echinoid spines and tests, crinoid articles and brachiopods are common.  
225 Crenulated coprolites occur locally (Fig.5c). The upper surface of beds is often characterized by wave ripples

226 with a centrimetric wavelength. Bioturbation can be abundant and represented by *Thalassinoides* and  
227 *Rhizocorallium jenense* burrows (Fig.4c)

228 Interpretation: Wave influenced shoreface

229 The packstone/grainstone texture and the bioclastic content indicate an agitated depositional environment and  
230 the diversified benthic euhaline fauna implies an open marine context. The occurrence of wave ripples and the  
231 lack of marl alternations suggest sedimentation above the storm wave base. The local abundance of coprolites  
232 was described in facies located just below the lower intertidal zone in Jurassic limestones of the SE France  
233 (Gaillard, 1983). Such an interpretation is consistent with the occurrence of *Thalassinoides* and *Rhizocorallium*  
234 *jenense* burrows (Knaust, 2013).

235

### 236 **-Oolitic and bioclastic dolomite (Do)**

237 This facies is subdivided in two subfacies. The first subfacies (Dos) is characterized by decimeter thick beds of  
238 well sorted, and dolomitized bioclastic and oolitic grainstones (Fig.5d). Locally, this facies can be enriched in  
239 angular quartz grains (fig.5e). Bioclasts consist mainly of bivalve shells and gastropods are common (Fig.5d,  
240 5e). Current ripples, bidirectional trough stratifications and micritic drapes forming flaser bedding occur in this  
241 facies (Fig. 4d). Horizontal or low angle stratifications have also been observed. The second subfacies (Dof)  
242 consists mainly of regular centimeter thick alternations of oolitic current ripples and dolomitic mudstones. This  
243 alternation forms lenticular or wavy bedding. A cyclicity in the relative amount and thicknesses of oolite beds  
244 with current ripples and mud layers occurs (Fig.4e). This facies can locally alternate with algal mats (Fig.5f).

245 Interpretation: Tide dominated oolitic shoal and flat

246 In the Ods subfacies, the grainstone texture, the ooid content and the dominance of broken shells indicate a high  
247 hydrodynamism. Inversions in the progradation directions of megaripples and mud drapes suggest sedimentation  
248 in a tidally influenced environment. This facies is interpreted as an oolitic shoal in the intertidal zone. The  
249 megaripples probably formed in shallow tidal channels cutting across the barrier while horizontal and low angle  
250 stratifications formed in beach environments on the top of the shoal. In the Odf subfacies, the cyclicity in  
251 thickness of calcarenite and mud beds is interpreted as neap and spring tide cycles (Fig. 4e). The small current  
252 ripples suggest a weak hydrodynamism compared to the Ods subfacies. Stromatolites indicates calmer  
253 hydrodynamic conditions such an intertidal backshoal area on a mud flat. The local enrichment in quartz grains  
254 in both subfacies indicates local inputs of terrigenous material from the hinterland in the vicinity of a stream  
255 mouth.

256

**257 Homogeneous dolomite (Dh)**

258 This facies is not widely represented. It consists of decimetric to metric beds of dolospar with an idiotopic  
259 texture (Fig.5g). Bioturbation is diffuse. When present, benthic fauna is poorly diversified and only represented  
260 by molds of dissolved shells of bivalves. Molds are often filled by fibrous dickite identified with infra-red  
261 microscopy (Fig.5g). Alignments of centimetric vugs are sometimes present (Fig. 4f). Vugs have a spherical or  
262 slightly irregular shape. They are also filled by fibrous dickite (Fig.5h) or contain pendant and laminated fibrous  
263 calcite cements on their upper edge (Fig.5i). The massive beds can alternate with nodular bioturbated dolomitic  
264 beds poor in fauna. Thrombolitic structures have also been observed sporadically in this facies.

265 Interpretation: Shallow evaporitic lagoon

266 The poorly diversified and exclusively benthic fauna and the occurrence of thrombolitic structures indicate an  
267 environmental stress such as low oxygen renewal or/and hypersaline conditions. However the occurrence of  
268 bioturbation indicates that the seafloor was oxygenated. The scarcity in allochems suggests that the initial  
269 sediment was a mudstone. This texture and the lack of current structures imply a calm depositional environment.  
270 As a consequence, this facies is interpreted as an initially muddy restricted subtidal lagoonal environment. The  
271 aligned vugs are similar to those described in shallow subtidal and intertidal environments of the Middle Triassic  
272 of the German Basin and of the Catalan Coastal Range (Mercedes-Martin *et al.* 2013, Koehrer *et al.* 2010). They  
273 are interpreted as the result of leaching of evaporite nodules formed in the sediment in a hypersaline lagoon.  
274 Such an interpretation is consistent with the occurrence of vugs only in muddy facies (Dh and Ds). The dickite in  
275 vugs is due to the transformation of initial kaolinite during burial at temperatures above 80°C (Ehrenberg *et al.*,  
276 1993; Morad *et al.*, 1994). This means that the dissolution of evaporites and the infill by kaolinite occurred  
277 before burial probably during periods of subaerial exposure. Since they are posterior to dickite, pendant cements  
278 indicate a late cementation in the vadose zone during telogenesis and recent exposure.

279

**280 Stromatolitic dolomite (Ds)**

281 This facies consists of algal mats alternating with peloidal packstones forming agglutinated stromatolites (*sensu*  
282 Ridding, 1991). The facies is dolomitized and a fenestral structure characterizes the sediment between algal mats  
283 (Fig.5j). The inter-crystalline and vuggy porosity is extensive. The upper surface of beds can be hardgrounds  
284 heavily perforated by *Gastrochaenolites* borings (Fig. 4g). Dissolution vugs similar to those observed in the  
285 facies Dh also occur in this facies (Fig. 4h). Desiccation cracks and polygons are locally present (Fig.4i).

286 Interpretation: Intertidal to lower supratidal inner ramp

287 The dominance of agglutinated stromatolites is typical of intertidal to lower supratidal environments (Ridding,  
288 2000; Alsharhan and Kendall, 2003). The occurrence of desiccation features and fenestral structures is consistent  
289 with this interpretation and indicates periods of subaerial exposure in the upper intertidal to lower supratidal  
290 zone (James, 1984). Hardgrounds indicate lithification of algal mats in an often immersed environment. Such  
291 hardgrounds have been described in the lower intertidal zone in the Holocene of Abu Dhabi (Kendall *et al.*,  
292 1994). These intertidal to low supratidal sediments were impacted by in situ evaporite precipitation in a  
293 hypersaline environment as attested by the occurrence of evaporite dissolution vugs.

294

### 295 **Dolomitic breccias (Db)**

296 This facies consists of dolomitic and often stromatolitic angular clasts in a dolomitic and sandy matrix (Fig.4j).  
297 The facies is clast supported and in some places breccias pass laterally to continuous dolomitic and stromatolitic  
298 beds (Fig.4k). Remains of nodular chicken wire, enterolithic or fibrous gypsum can be intercalated within  
299 breccias. In thin sections, cores of dolomite rhombs are frequently dissolved (Fig.5k).

300 Interpretation: Collapse breccias

301 The lateral continuity between algal mats and breccias indicates that these latter correspond to the breakup of  
302 stromatolites. No clue of tepee structure such as pisolitic and vadose cementation or anticlinal geometry  
303 (Assereto and Kendall, 1977) has been observed. In contrast the presence of evaporite remains or dissolution  
304 vugs argues for collapse process. Chicken wire and enterolithic evaporites suggest an *in situ* precipitation in a  
305 supratidal sebkha environment under an arid climate. Their dissolution implies prolonged periods of subaerial  
306 exposure and leaching by freshwaters (James, 1984). Impact of freshwater is also suggested by dedolomitization  
307 features such as dissolution of cores of dolomite rhombs.

308

### 309 **Graded oolitic dolomites (Dg)**

310 The facies is characterized by centimetric to decimetric oolitic and bioclastic beds with a grainstone to packstone  
311 texture. The facies is fine grained and well sorted. The contact between oolites and underlying sediments is sharp  
312 and erosive (Fig.6a). Above these surfaces, deposits are fining upward and contain planar oblique or less  
313 frequently horizontal bedding. This facies is intercalated in shallow evaporitic lagoonal facies Ev (see below).

314 Interpretation: Washover deposits

315 The sharp and erosive bases and the upward fining indicate sudden increases in hydrodynamism and a gradual  
316 return to calm conditions. This oolitic and bioclastic facies intercalated in shallow evaporitic lagoonal facies  
317 suggests that material was transported landward from a shoal environment. Oblique angular laminations indicate  
318 a gradual lateral accretion by avalanching in a calm environment while horizontal laminations suggest a laminar  
319 upper flow regime. These features are typical of storm washover deposits (Sedgwick and Davis Jr, 2003; Roep *et*  
320 *al.*, 1998).

321

### 322 ***Evaporitic facies***

#### 323 **Evaporites, shales and stromatolites alternations (Ev)**

324 This facies can be subdivided in two subfacies. The first (Evs) consists of an alternation of evaporites and  
325 dolomitic algal mats (Fig.6b). Evaporites are constituted by chicken wire nodules or enterolitic beds of anhydrite  
326 alternating with selenite gypsum. Chicken wire texture appears in replacement of gypsum prisms. Washover (Dg  
327 facies) and dolomitic breccias (Db) alternate with this subfacies. The second subfacies (Evm) consists of yellow  
328 and green silty shales poor in fauna and with thin centimetric layers of fibrous gypsum. Bioturbated dolomitic  
329 beds with rare algal mats occur sporadically in marls.

#### 330 Interpretation: Hypersaline lagoon

331 In the Evs subfacies, thin laterally continuous and vertically aligned gypsum prisms (selenite) are typical of  
332 subtidal environments in a restricted hypersaline lagoon (Warren and Kendall, 1985). Such an interpretation is  
333 supported by intercalations of washover deposits. The replacement of gypsum by nodular anhydrite is certainly  
334 due to dehydration during burial. Stromatolitic intervals indicate temporary transition toward marginal intertidal  
335 environments (Peryt, 2001). The Evm subfacies indicates a similar depositional environment with higher  
336 siliciclastic inputs. Intercalations of bioturbated dolomites point to episodes of oxygenation on the sea-floor due  
337 to a more significant renewal of seawater. Such conditions were most probably possible during moderate  
338 flooding events.

339

#### 340 **Evaporitic red shales (Fre)**

341 This facies is characterized by red to green shales. Shales contain laterally continuous layers of clean fibrous  
342 gypsum or lenticular crystals of gypsum enriched in sand inclusions and forming desert roses (Fig.6c). Meter  
343 thick layers of chicken wire nodules of gypsum are also intercalated in shales. Locally, petrified rootlets occur in  
344 layers of lenticular gypsum (Fig.6d)

345 Interpretation: Continental sabkha and playa lake.

346 The red color of shales enriched in iron oxides and the occurrence of petrified rootlets suggest that this facies  
347 deposited in a continental environment (Benison and Goldstein, 2000; Gibert *et al.*, 2007). Lenticular gypsum  
348 crystals rich in sand inclusions and chicken wire nodules are typical of evaporitic flat of sabkha type (Warren,  
349 2006). Layers of clean fibrous gypsum indicate precipitation in the water column probably when ephemeral salt  
350 lake developed (Warren, 2010; Salvany *et al.*, 1994). Consequently, the Frs facies recorded variations of the base  
351 level in a continental playa lake with alternation of soil development and peripheral sabkha facies with fibrous  
352 gypsum deposited during moderate floodings.

353

### 354 ***Siliciclastic facies***

#### 355 **Massive conglomerates (Gm)**

356 This facies is characterized by massive and unsorted polygenic conglomerates. Clasts consist of dolomites,  
357 sandstones, and basement pebbles to cobbles (Fig.6e). The conglomerate is mainly clast supported with some  
358 matrix supported intercalations. Obvious stratification and bedding are lacking. Clasts are angular to subrounded  
359 and their sizes vary between 2 cm to 35 cm.

360 Interpretation: Alluvial fan.

361 The polygenic composition indicates an allochthonous origin of clasts and a sedimentation after transport. The  
362 reduced sizes of outcrops allow not to determine the geometry of deposits at a large scale. However, the absence  
363 of tractive current structures is not consistent with deposition in a perennial stream. In contrast the heterometric  
364 nature of clasts and the presence of matrix supported beds rather indicate that cohesive debris flows was the  
365 main sedimentation process. The dominance of this transport and sedimentation mechanism suggests deposition  
366 on a slope and/or on the vicinity of a relief at the surface of an alluvial fan (Baltzer and Purser, 1990; Harvey *et*  
367 *al.*, 2005; Miall, 2006).

368

#### 369 **Red silty shales (FI)**

370 This facies consists of ten of centimeter to several meters thick layers of red to brown and locally green shales  
371 (Fig. 6f). They are silty and devoid of marine fauna. Fine grained sandstones with climbing ripples are locally  
372 intercalated within shales (Fig.6g)

373 Interpretation: Floodplain

374 The lack of marine fauna, the red color and the fine granulometry of shales indicate a sedimentation by  
375 decantation in a calm continental environment under oxidizing conditions. Such conditions are common in  
376 floodplains. Sandstone beds with climbing ripples are interpreted as overbank facies deposited in the floodplain  
377 during waning of flood events (Farrel, 2001; Miall, 2006).

378

### 379 **Graded sandstones (Sg)**

380 Sg facies is characterized by metric sequences of graded sandstone. A basal erosive surface is covered by coarse  
381 grained sandstones or conglomerate with a crude oblique stratifications (Fig. 6h). Vertically they pass to medium  
382 sands with trough cross-bedding (Fig.6h). Sequences are stacked and locally erosional surfaces truncate the top  
383 of cross-bedded sandstones (Fig. 6h). Sandstones and conglomerates sequences are erosional on top of red silty  
384 shales (Fsr facies) (Fig.6f).

385 Interpretation: Braided alluvial stream.

386 Trough cross-bedding in conglomerates and sandstones indicate perennial tractive currents in a lower flow  
387 regime (Miall, 2006). Basal erosional surfaces overlain by graded sequences with conglomerate and sandstones  
388 are interpreted as fluvial channel-fills. The stacking of graded and cross stratified fillings separated by erosional  
389 surfaces is typical of a scour and fill dynamics (Miall, 2006) and is interpreted as braided stream deposits.

390

### 391 **Cross stratified sandstones (Std)**

392 This facies is made of medium to coarse and moderately sorted sandstones. Sandstones contain both large  
393 troughs and 20 to 50 cm thick sigmoidal oblique cross-bedding (Fig.5i). The toes of foresets can be rippled and  
394 contain thin centimetric clay drapes (Fig.5j). Bioturbation is rare and consists of *Skolithos* burrows. On the basis  
395 of progradation directions of foresets, scarce paleo-flow reversals have been observed and measured.

396 Interpretation: Fluvial tidally influenced

397 Trough and sigmoidal cross-bedding indicate deposition under tractive lower flow regime. However clay drapes  
398 and small ripples on the toes of foresets imply regular decrease of flow velocities with settling events. These  
399 features and the clues of paleo-flow reversals suggest a tidal influence with muddy slack deposits alternating  
400 with coarse facies carried by dominant and opposite subordinate currents (Weimer *et al.*, 1982). However, the  
401 scarcity of subordinate current structures, the scarcity of clay deposits and the reduced abundance and diversity  
402 of bioturbation, represented only by *Skolithos* burrows, argues for a fluvial tidally influenced environment with  
403 brackish waters (Dalrymple and Choi, 2007; Fischbein *et al.*, 2009, Martinius *et al.*, 2012).

404

**405 Dolosandstone with megaplygons (Sdm)**

406 This facies consists of silty and/or sandy dolomitized mudstone with algal mats. The tops of beds show  
407 desiccation cracks with one bed rich in *Gyrophyllites* burrows. In addition, meter to several meter large polygons  
408 with concave upward shapes and separated by vertical cracks exist locally (Fig.41). Fractures connected to  
409 vertical ones between polygons spread horizontally between algal mats. They are filled with mammillary  
410 radial calcite (*sensu* Assereto and Kendall, 1977) and a last stage of micro-stalactitic cement (Fig.51).  
411 Dolosandstones alternate with decimetre to meter thick intervals of green marine shales.

**412 Interpretation: Supratidal tepees**

413 Large concave up polygons associated with horizontal fractures filled with mammillary radial and micro-  
414 stalactitic calcite cements are features described in tepee structures (Assereto and Kendall, 1977). Pendant  
415 cements imply precipitation in a vadose environment and tepee structures are typical of prolonged exposure in  
416 the lower supratidal zone (Warren and Kendall, 1985). Beds with desiccation cracks suggest less prolonged  
417 exposures. The occurrence of green marls and *Gyrophyllites* burrows indicates period of shallow subtidal  
418 sedimentation (Pandey *et al.*, 2014; Pemberton *et al.*, 2001) during small flooding between exposure events.

419

**420 5.2 Outcrop correlations**

421 Outcrop strips are discontinuous between North Dahar and J. Rehach areas (Fig.1). Consequently correlation  
422 transects in both areas will be described separately.

**423 5.2.a Transect 1: J. Rehach****424 Carnian Sequence 1 (RM1)**

425 In the southern part of the transect (Kef Touareg and Kef El Galalah) the lower part of the Mekraneb formation  
426 is marked by the appearance of offshore marls directly above the fluvial sandstones and red shales of the  
427 Kirchaou Fm. (Fig.7). Marls are overlain by thickening upward beds of upper offshore bioclastic, peloidal and  
428 bioturbated dolomites. Northward, the lower part of the Mekraneb Fm. consists mainly of bioclastic and peloidal  
429 dolomites of upper offshore and shoreface environment. The first facies above the Kirchaou Fm. generally  
430 contains a high amount of quartz grains. The upper part of the Mekraneb Fm. shows a gradual disappearance of  
431 dolomite beds in favor of green offshore marls (Fig.7). This marly upper part is locally truncated or entirely  
432 eroded by the basal erosive surface of the overlying Touareg Fm consisting of fluvial sandstones in its lower  
433 part. The basal erosive surface of the Touareg Fm. is locally covered by a lag of reworked and ferruginized

434 dolomite clasts (Fig.8b). This formation consists of alternations of braided fluvial sandstones (Sg) and red shales  
435 (Fl), in the lower and upper parts, surrounding tidally influenced fluvial sandstones (Std) in the middle part of  
436 the formation. The thicknesses of fluvial and tidally influenced facies are highly variable between sections (Fig.  
437 7) and basal fluvial facies are absent in the northern part of the transect (Galib Lamsen SE 2 section, Fig.7).

438  
439 Interpretation: The rapid transition from fluvial sandstones and red shales of the Kirchaou Fm. to marine  
440 dolomites and marls of the Mekraneb Fm. characterizes the first Carnian flooding. In the south of the transect,  
441 the maximum flooding interval is located in the lower part of the formation where offshore marls are the  
442 dominant or unique facies. The northward lateral transition from offshore marls to upper offshore to shoreface  
443 dolomites in the Rejjilah area suggests a shallowing of depositional environments in this direction. The erosive  
444 basal surface of the Touareg Fm. and the local reworking of the upper part of the Mekraneb formation indicate a  
445 fall in the base level that generated an incision and a seaward shift of facies with deposition of fluvial facies  
446 during a lowstand. The sharp irregular basal surface of tidally influenced sandstones of the Touareg Fm. is  
447 interpreted as a tidal ravinement surface (*sensu* Zaitlin *et al.*, 1994) at the base of the high frequency RS3  
448 sequence. The alternation of estuarine and fluvial facies corresponds to high frequency sequences during a  
449 middle frequency lowstand period at the end of the middle frequency RM1 sequence.

450

### 451 **Carnian sequences 2 and 3 (RM2 and RM3)**

452 The vertical transition from the Touareg Fm. to the Rehach Fm. is sharp. In this latter formation, deposits consist  
453 of shallow subtidal to intertidal dolomitic deposits organized in two to eight meter thick shallowing upward  
454 parasequences (Fig.8a). Above few meter thick beds of shoreface peloidal dolomites enriched in quartz grains,  
455 alternation of offshore marls (Mgr facies), subtidal lagoonal (Dh) and intertidal dolomites (Ds) constitute the  
456 predominant facies (Fig.7). As a whole, the oolitic facies are rare and the proximal facies are more abundant  
457 toward the northwest. The total thickness of the Rehach Fm. and thicknesses of parasequences increase  
458 southeastward (Fig.7). In the upper part of the Rehach quarry section, offshore green marls and are sharply  
459 overlain by a ten centimeters thick bed of nodular chalky carbonates with rhizoliths filled by red silts and fine  
460 grained sandstones (Fig.8d). A similar interval of mottled clays and root traces exists in the Kef El Galalah  
461 section but is located directly above marine lagoonal deposits.

462

463 Interpretation: In order to identify middle frequency sequences, a stacking pattern study has been performed on  
464 the Kef El Galala section constituting the most complete and vertically continuous section (Fig.9). Seven high  
465 frequency and two middle frequency sequences have been evidenced in the southern part of the transect (Fig.7).  
466 The sharp transition between the fluvial facies of the Touareg Fm. and the marine Rehach Fm. indicates a marine  
467 flooding through a basal erosional transgression surface. In high frequency sequences, maximum flooding  
468 intervals consist of green offshore marls (Mgr facies) while lagoonal dolomites and intertidal stromatolitic  
469 deposits are predominant during highstands (Dh and Ds facies) (Fig.7 and 9). The maximum flooding interval of  
470 the middle frequency RM2 sequence is reached in the lower part of the Rehach Fm. where the lower offshore  
471 facies is dominant (Fig.9). The highstand is characterized by the gradual increase in shoreface and shallow  
472 lagoonal dolomites with vugs of evaporite dissolution. A third middle frequency sequence named RM3 was  
473 evidenced in the upper part of the Rehach Fm. (Fig.9). The transgressive interval consists of a gradual deepening  
474 of depositional environments leading to a 8 metres thick unit of offshore green shales. Highstand deposits are  
475 characterized by the transition to shoreface and lagoonal dolomites. The mottled clays with carbonate nodules  
476 and rootlets are interpreted as alluvial deposits with calcisols. The sharp transition from offshore green marls to  
477 the thick paleosol corresponds to a rapid basinward shift of facies. Northwestward, the paleosol occurs directly  
478 above marine dolomites and the high frequency sequence RS10 is absent. This implies that the paleosol  
479 coincides with an angular unconformity truncating progressively the upper part of the Rehach formation toward  
480 the northwest (Fig.7). The rare occurrence of oolitic facies indicates that shoals were not widely developed and  
481 formed only little topographic highs on the sea floor. The gradual thickening of the Rehach Fm. toward the  
482 southeast and the increase in distality of facies in this direction indicate that the northwest-southeast polarity of  
483 the depositional system already deduced for the Mekraneb Fm. was valid during all the Carnian.

484

#### 485 **Carnian sequence 4 (RM4)**

486 Above the paleosol and up to the top of the Rehach Fm., facies consist mainly of intertidal stromatolitic or  
487 shallow lagoonal facies organized in parasequences (Fig.8c). Upper surfaces of parasequences are generally red  
488 coloured and underlying stromatolitic facies present millimetric rootlets traces observed in thin sections. Locally,  
489 10 to 20 cm thick intervals of mottled clays with root traces cap the top of parasequences. No clear vertical  
490 evolution of depositional environments in the stacking pattern of parasequences was observed. However oolitic  
491 and bioclastic facies are predominant toward the top. This formation is directly overlain by the Kronab  
492 conglomerates through a sharp erosional surface (Fig.10). Until now, the Kronab Fm. was placed in a

493 stratigraphic position between the Mhira Fm. below and the Messaoudi Fm. above (Kamoun *et al.*, 2001; Mejri  
494 *et al.*, 2006; Mello and Bouaziz, 1987). This interpretation was mainly based on observations in the Achaab El  
495 Messaoudi area where Kronab conglomerates pinch out northwestward below dolomitic facies of the Messaoudi  
496 Fm. However, a cartography work between Achaab Messaoudi and the southeast of the Beni Ahmed village  
497 allowed to evidence that the Kronab Fm. is located below the Mhira Fm. which is present in the neighboring  
498 Beni Ahmed well. Conglomerates are in direct contact above the Rehach dolomites (GPS point Beni Ahmed II in  
499 Table 2) (Fig. 10). The facies consisting of a highly cemented polygenic clast supported conglomerate in a red  
500 sandy matrix is clearly different from conglomeratic carbonate crusts corresponding to recent alluvial terraces  
501 described in this area (Bouaziz *et al.*, 1987). The Kronab Fm. consists of fluvial deposits (Sg facies) made of  
502 massive conglomerates in its lower part and sandstones and red shales in its upper part. Workable outcrops of the  
503 Kronab Fm. have been observed only in the Achaab El Messaoudi and Beni Ahmed area. Consequently, the  
504 southwestward extension of the formation is still unknown.

505  
506 Interpretation: The upper part of the Rehach consisting of parasequences deposited in a shallow lagoonal to  
507 supratidal environment with common subaerial exposures, as suggested by abundance of root traces and at the  
508 top of parasequences, indicates a moderate flooding after the subaerial exposure characterized by the paleosol at  
509 the top of the RM3 sequence (Fig.7). Because of the lack of obvious evolution of facies, high and middle  
510 frequency sequences are difficult to evidence. However the maximum flooding surface of the RM4 sequence  
511 may be placed in oolitic facies in the Achaab El Messaoudi and Rehach quarry sections. Since the contact is  
512 sharp between the shallow marine dolomites of the Rehach Fm. and the braided fluvial conglomerates of the  
513 Kronab Fm. and since this transition indicate a rapid basinward shift of facies at the top of the RM3 sequence  
514 without intermediate marginal facies, the basal surface of the Kronab Fm. is interpreted as a relative sea-level  
515 fall unconformity rather than only an increase in sediment supply. The predominance of sandy channels in  
516 floodplain red shales in the upper part of the formation above massive conglomerates attests to a gradual  
517 backstepping. Consequently we consider that only the massive conglomeratic fluvial facies of the lower part of  
518 the Kronab Fm. constitute the lowstand deposits.

519

#### 520 - **Late Carnian to Norian sequences 5 and 6 (RM5 and RM6)**

521 The Mhira Fm. can be observed only in sporadic outcrops. Consequently no complete and vertically continuous  
522 section has been logged. In the Achaab El Messaoudi section, the lower 6 meters of the Mhira Fm. are

523 characterized by alternations of shallow lagoonal shales and dolosandstones with mudcracks and *Gyrophyllites*  
524 burrows (Sdm facies). This interval is topped by large tepee structures (Fig.10). The upper part of the Mhira Fm.  
525 is observable in the Sebket Leguine area and near the Beni Mhira village. It is made up of alternations of red  
526 shales with fibrous gypsum layers and a several meters thick interval of lenticular gypsum with petrified rootlets  
527 deposited in an evaporitic flat (Fre facies). The formation thickens southwestward and pinches out below the  
528 Messaoudi Fm. northwestward in the Achaab El Messaoudi area (Mello and Bouaziz, 1987) (Fig. 10).

529  
530 Interpretation: The stacking of shallow intertidal and supratidal facies in the lower part of the Mhira Fm. above  
531 floodplain and fluvial sandy channel of the top of the Kronab Fm. characterizes a moderate flooding during the  
532 RM5 sequence. The maximum flooding interval is located in facies dominated by green shales of shallow  
533 subtidal lagoonal environment (Fig. 10). Above, the transition to intertidal and supratidal facies with tepee  
534 structures indicates a progradation during a highstand. The tepee structures mark a prolonged subaerial  
535 exposure merged with a transgression surface constituting the boundary between RM5 and RM6 sequences. The  
536 thick interval of lenticular gypsum with petrified rootlets observed in the Sebket Leguine area indicates a period  
537 of intensive evaporation during a drying of the playa during a regressive event. However, the sporadic  
538 distribution of outcrops allowed not determining a complete sequential framework in the upper part of the Mhira  
539 Fm. Middle frequency sequences will be discussed below by mean of the well-log study.

540

#### 541 - **Rhaetian and Lower Jurassic evaporites**

542 As for the Mhira Fm., the reconstitution of the vertical evolution of facies in Rhaetian deposits (Messaoudi, Bhir,  
543 and Zerzour Fm.) is not possible due to the scarcity of outcrops. Dolomites of the Messaoudi Fm. consist of  
544 oolitic tidal flat deposits (Dof) alternating with dolomite collapse breccias (Db). The basal contact with  
545 underlying formations is sharp. The Messaoudi Fm. overlays Norian Mhira shales in the Achaab El Messaoudi  
546 and Beni Ahmed area while northwestward it covers directly Rehach dolomites in the Rejjilah area or Kirchaou  
547 sandstones in the Guelib Lemsane area (Fig.7). In the Beni Ahmed section, the Messaoudi Fm. is represented by  
548 five meters of evaporites, stromatolites and collapse breccias (Db and Ev facies). The first tidal oolitic facies  
549 appear above this first evaporitic interval (Fig.7). The Zerzour Fm. has been observed only in the Galib El  
550 Zarzour section. The observed facies are characterized by a 3 meters thick interval of oolitic washover deposits  
551 (Dg facies) intercalated in salina facies (Ev facies) of the Bhir Fm.

552

553 Interpretation: The progressive disappearance of Norian and Carnian formations toward the northwest below the  
554 Rhaetian Messaoudi Fm. corresponds to a well documented regional angular unconformity (Mello and Bouaziz,  
555 1987). As a consequence, the boundary between the Messaoudi Fm. and underlying deposits corresponds to a  
556 major subaerial exposure, truncation and transgression surface of the subsequent re-flooding of the basin. The  
557 scarcity of outcrops and the lack of continuous sections in Rhaetian deposits makes difficult a detailed sequential  
558 interpretation and stratigraphic correlations. From outcrops only the identification of low frequency sequences  
559 can be envisioned. In the Messaoudi Fm., the distribution of facies (predominance of Dof and Db facies between  
560 Achaab El Messaoudi and Guelib Lemsane, Ev facies predominant toward the southwest) suggests a more  
561 proximal and shallower area in the northwest and a quite deeper restricted subtidal lagoon in the southeast. The  
562 washover deposits of the Zerzour Fm. intercalated between evaporitic facies of the Bhir Fm. is interpreted as a  
563 slight opening of the depositional environment and a maximum flooding interval during a rise of base level. As  
564 for the Mhira Fm. middle frequency sequences will be discussed below using subsurface data.

565

## 566 - **Transect 2: North Dahar**

567 Seven sections have been logged along the outcrop strip between Mougor in the northwest and Ouarjajin in the  
568 southeast (Fig.11). Upper Triassic deposits rest unconformably on Permian and Lower Triassic formations  
569 (Fig.12). This angular unconformity was named Sidi Stout Unconformity by Mello and Bouaziz (1987).

570

## 571 **Dahar sequence 1 (DS1)**

572 As a whole, the thickness of deposits increases from the Mougor in the northwest to the Kef El Amba area in the  
573 southeast (Fig.11). First marine deposits correspond to sandy dolomites of shallow lagoonal environment (Dh  
574 facies) alternating with intertidal stromatolites (Ds facies). Locally (Sidi Stout area) a basal lag of sandstone  
575 pebbles reworked from underlying middle Triassic deposits occurs. Vertically, facies changes to quartz free  
576 bioturbated subtidal deposits (Dh facies) in most of sections. In the northern Mougor area deposits correspond to  
577 alluvial fan conglomerates with two, decimeters thick, intercalations of lagoonal dolomites or dolomite breccias  
578 (Fig.13a). Above, in the northern part of the transect (Ouadi Hallouf and Sidi Stout sections) dolomites are  
579 enriched in sandstone layers. Those dolomites are covered by stromatolitic facies (Dh facies) in the Ouadi  
580 Hallouf section and by quartz rich cross stratified oolitic grainstones (Dos facies), brecciated dolomites or sand  
581 rich facies in the Sidi Stout area (Fig.11). Red continental shales or micro-breccias cap the marine facies in most

582 of the sections. In the Ouarjajin area, subtidal and stromatolitic dolomites are covered by a three meter thick  
583 interval of collapse breccias (Db facies).

584

585 Interpretation: The pebble lag at the base of dolomitic deposits corresponds to a transgressive lag above a major  
586 sequence boundary corresponding to the Sidi Stout unconformity. The vertical decrease in the quartz content and  
587 the appearance of subtidal dolomites illustrate the continuation of the flooding. A maximum flooding was  
588 reached during the deposition of oolitic facies. The occurrence of alluvial fan deposits and the reduced thickness  
589 of deposits in the Mougor area suggest a more proximal and less subsiding area. The thin dolomitic  
590 intercalations in conglomerates characterize the maximum flooding interval (*sensu* Pittet and Strasser; 1998).  
591 The regressive part of the sequence is marked by the vertical increase in siliciclastic inputs, the appearance of  
592 stromatolitic facies and continental shales at the top. In the Ouarjajin area the thick interval of brecciated  
593 dolomites at the top of the sequence points out a prolonged episode of subaerial exposure not recorded in other  
594 sections.

595

## 596 **Dahar sequence 2 (DS2)**

597 Between Sidi Stout and Kef El Amba, alluvial facies of the top of the DS1 sequence are covered by marine  
598 dolomites organized in meter thick parasequences. Facies correspond to shallow lagoon (Dh), intertidal  
599 stromatolitic (Ds), oolitic bioclastic and sandy shoal (Dos) and subtidal peloidal dolomites (Dbp). The upper part  
600 of dolomitic facies is represented by collapse breccias in most of the sections. They are sharply covered by  
601 fluvial sandstones and alluvial red shales (Sg and Fl facies). Northward, in the Ouadi Hallouf area, facies consist  
602 of matrix supported conglomerates alternating with dolomite breccias (Gm and Db facies) while in the Mougor  
603 section only alluvial fan conglomerates have been observed. In the Ouarjajin section the facies is exclusively  
604 constituted by an alternation of intertidal stromatolitic dolomites and collapse breccias.

605

606 Interpretation: The reappearance of marine dolomitic facies above continental facies indicates a flooding at the  
607 base of the DS2 sequence. The maximum flooding interval corresponds to shallow subtidal facies grading  
608 laterally northward to sandy oolitic and bioclastic shoal in the more proximal Sidi Stout area. In the Mougor  
609 section the maximum flooding interval is characterized by a thirteen centimeter thick intercalation of dolomite  
610 between alluvial fan conglomerates. A sharp transition to fluvial facies marks the top of the sequence. Below this  
611 surface, the thick interval of collapse breccias suggests a prolonged episode of subaerial exposure prior to

612 fluvial sedimentation. Variations in the thicknesses of fluvial facies and dolomitic deposits preserved below the  
613 basal surface of fluvial deposits argue for an incised valley geometry generated by a base-level fall (Fig. 11). In  
614 the Ouarjajin area, the predominance of collapse breccias attests of important events of freshwater infiltrations  
615 during prolonged subaerial exposures. Here, stromatolitic beds between brecciated facies constitute the  
616 maximum flooding interval. The regional geometry characterised by a gradual thickening and deepening of  
617 deposits from the Mougor section to Kef El Amba and the occurrence of a southern shallower and less subsiding  
618 zone in the Ouarjajin area suggests the occurrence a normal synsedimentary fault between Ouarjajin and Kef El  
619 Amba (Fig.11).

620

### 621 **Dahar sequence 3 (DS3)**

622 Between Kef El Amba and Sidi Stout, alluvial and fluvial deposits overlay brecciated dolomites of the top of the  
623 DS2 sequence. The thickness of fluvial deposits is variable between sections with a broadly southward  
624 thickening. However, in the Ouarjajin section, fluvial facies are absent and only a ferruginous crust covering  
625 dolomite breccias with a ferruginous matrix occurs (Fig.13b). In the Kef El Amba 1 and 2 sections, the lower  
626 part of continental deposits corresponds to red shales of alluvial plain environment (FI facies). A five centimeters  
627 thick bed of pink oolitic dolomite appears at the top of this interval in the Kef El Amba 1 section. This bed is  
628 partly eroded by sandy channels and dolomitic pebbles constitute the basal conglomeratic lag of sandstones in  
629 the Kef El Amba 1 section (Fig.11). The top of fluvial deposits consists of the amalgamation of several sandy  
630 fluvial channels.

631

632 Interpretation: The vertical transition from alluvial plain shales to oolitic dolomite indicates a backstepping of  
633 marginal marine environments. A maximum flooding is reached in the dolomitic bed which characterizes the  
634 only marine incursion between alluvial and fluvial deposits. This bed appears only in the Kef El Amba section  
635 because of its local erosion by sandy fluvial channels. The reappearance of fluvial deposits characterized by  
636 amalgamated channels in the upper part constitutes the highstand of the DS3 sequence. The absence of the DS3  
637 sequence, the intensive brecciation with only intertidal stromatolitic dolomites, the absence of subtidal deposits,  
638 and the lower thickness of the DS2 sequence suggest that the Ouarjajin area was still less subsident compared to  
639 northern sections.

640

### 641 **Dahar sequences 4 and 5 (DS4 and DS5)**

642 Yellow-green marls with intercalations of thin fibrous gypsum layers overlay lagoonal bioturbated dolomites in  
643 Sidi Stout and evolve laterally to oolitic tidal flat facies (Dof) in the Ouadi Hallouf section (Fig.11). Evaporitic  
644 marls are replaced northwestward by shallow subtidal and intertidal dolomites. A quartz enrichment occurs in  
645 this direction. The Pliensbachian Zmilet Haber Fm. covers marls and consists of bioturbated oolitic dolomites of  
646 lagoonal environment.

647  
648 Interpretation: Lagoonal or oolitic dolomites above fluvial deposits of the end of the DS3 sequence illustrate a  
649 marine flooding at the base of the DS4 sequence. The maximum flooding interval is located in these dolomitic  
650 facies since overlaying evaporitic marls mark a more restricted environment. The quartz enrichment, the  
651 transition to more proximal facies, and the thinning of deposits toward the northwest indicate that this area was  
652 still less subsident. However, the absence of alluvial fan deposits in Mougor shows that the preexisting  
653 topographic high that existed during the Carnian was partially erased or flooded during the DS4 sequence. The  
654 Zmilet Haber Fm. illustrates a new opening of the depositional environment accompanied by the reappearance of  
655 oolitic and bioturbated facies. Consequently, the basal surface of the Zmilet Haber Fm. corresponds to a  
656 transgression surface and to the boundary between DS4 and DS5 sequences. The constant thickness and the lack  
657 of change of depositional environment in the Ouarjajin area suggest that the synsedimentary fault activity  
658 supposed during the Carnian stopped during sequences DS4 and DS5.

659  
660 A stacking pattern analysis allowed to evidence a low frequency maximum flooding during the DS1 cycle  
661 (Fig.9). A major sequence boundary corresponds to the transgression surface at the top of the DS3 sequence,  
662 above fluvial deposits. A second low frequency flooding led to the deposition of the B Horizon.

663

## 664 **5.4 Subsurface correlations**

665 In order to clarify the correlations between the J. Rehach and the North Dahar, to propose correlations between  
666 outcrops and formations described in subsurface in eastern Algeria or south Tunisia (Ben Ismaïl, 1982,  
667 Hamouche, 2006, Bourquin *et al.*, 2010, Turner *et al.*, 2001, Turner and Sherif, 2007) and to refine the relation  
668 between depositional sequences and the regional geodynamic history, several transects of well logs correlations  
669 located south of the outcrop strip have been studied (Fig.14).

670

### 671 **5.4.1 Outcrop – subsurface correlations**

672 A composite log merging the Achaab El Messaoudi and Kef El Galala sections was correlated with the El Borma  
673 Nord Est 1 (EB-NE-1) well located 165 km away to the southwest (Fig.14). This well was chosen because of its  
674 proximity with the wells described by Galeazzi et al. (2010) in Algeria and because it crosses one of the thickest  
675 and most complete series of upper Triassic and lower Jurassic deposits in south Tunisia. Electric log patterns and  
676 petrographic descriptions available in drill reports have been used to determine changes in depositional  
677 environments and sequences. Shales are characterized by higher Gamma Ray (GR) values compared to  
678 dolomites or evaporites. Resistivity and Neutron logs allowed differentiating evaporites (high values) from pure  
679 dolomites (low values). In contrast, since sandstones are arkosic their identification was difficult using Gamma  
680 Ray logs. Consequently, their occurrence was mainly determined using drill reports.

681  
682 The sequences RM1 to RM5 evidenced in the J. Rehach have been identified in subsurface (Fig.15). The  
683 Mekraneb Fm. is characterized by dolomite and evaporite alternations in the lower part of the Trias Argilo  
684 Carbonaté (TAC). Sandstones of the Touareg Fm. constitute the lowstand deposits of the upper part of the  
685 middle frequency RM1 sequence and are present in the EB-NE-1 well. In subsurface, the flooding of the RM2  
686 sequence is characterized by green shales and dolomites. Basinward, the highstand of RM2 consists of an  
687 enrichment in anhydrite and gypsum forming the Lower Evaporites (Fig.15). The inverse evolution of facies due  
688 to an opening of depositional environments illustrates the transgression of RM3 in the upper part of the TAC. In  
689 the El Borma Nord Est 1 well the top of RM3 is characterized by the sharp transition to sandstones interpreted as  
690 the result of an increase in terrigenous inputs and a basinward shift of facies. This interval constitutes the lower  
691 boundary of S4 salt (Bourquin *et al.*, 2010; Galeazzi *et al.*, 2010; Hamouche, 2006; Turner and Sherif, 2007) and  
692 is correlated with the exposure characterized by paleosol in the upper part of the Rehach Fm in the Rehach  
693 quarry section (Fig.7). In subsurface, and as in the J. Rehach, the flooding during the RM4 sequence is  
694 materialized by the appearance of variegated clays and shallow marine dolomitic facies. The maximum flooding  
695 is reached when dolomitic facies are predominant. The top of this sequence is characterized by halite and gypsum  
696 deposits interpreted as lowstand deposits coeval to the incision and the deposition of the Kronab conglomerates  
697 in the J. Rehach. The first deposits of RM5 illustrate a new flooding with the gradual reappearance of shallow  
698 marine dolomites and evaporites. A new lowstand characterized by halite beds constitutes the top of RM5 and is  
699 interpreted as coeval with the subaerial exposure characterized by tepee structures in the lower part of the Mhira  
700 Fm. in the J. Rehach. The flooding of the sequence RM6 is represented by marine shales with scarce gypsum  
701 beds. The highstand is characterized by a thick halite unit constituting the upper part of S4 salt. In the Achaab El

702 Messaoudi section this sequence is absent because of its truncation by the Sidi Stout unconformity. Two  
703 sequences RM7 and RM8 have been observed in the playa facies (Fre facies) of the D2 Fm (Emzab Fm. of Ben  
704 Ismaïl, 1982). The top of RM7 corresponds to a gypsum and halite unit. This evaporitic unit is correlated with  
705 the regressive event characterized by lenticular gypsum with petrified rootlets observed on outcrop in the Mhira  
706 Fm. in the Sebkhet Leguine area. This correlation scheme is coherent with the lithostratigraphic diagram of  
707 Mejri *et al.* (2006) who consider that the D2 Fm. is the lateral equivalent in subsurface of the Mhira shales. The  
708 top of the RM8 sequence consists of the transgressive surface at the base of overlaying S3 salts. The RM7 and  
709 RM8 sequences are lacking in the Achaab El Messaoudi section because of their truncation by the regional  
710 angular unconformity at the base of the Messaoudi Fm.

711  
712 In subsurface, the Mhira Fm. is overlain by a thick unit of evaporites with intercalations of dolomites and shales.  
713 Facies consist of anhydrite, massive halite beds, dolomite with anhydrite nodules or ooids and red or green  
714 shales. This unit corresponds in part to the equivalent of the Messaoudi and Bhir formations observed in the J.  
715 Rehach. The first basal halite unit is named S3 salt and, above, dolomite stringers in the middle part constitute  
716 the Zerzour Fm. below the evaporitic Bhir Fm. According to facies models and their relationships with sequence  
717 stratigraphy proposed for coastal evaporites and salterns (Kendall, 1988; Tucker, 1991; Warren, 2006),  
718 carbonates illustrate connections with the open-sea and an efficient renewal of seawater during periods of high  
719 relative sea-level when the sill is flooded. In contrast, as showed by Tucker (1991) in the Zechstein evaporites of  
720 Germany, isolation of the basin during regressive periods is characterized by precipitation of anhydrite and  
721 finally halite when closure is completed. On the basis of these considerations, eleven sequences (RM9 to RM19)  
722 have been evidenced into the S3 salt, Zerzour, and Bhir Fm. capped by the B Horizon (Fig.15). Sequences from  
723 RM9 to RM11 are dominated by halite deposits while from RM12 to RM16 anhydrite and dolomitic facies  
724 become predominant. Halite layers, reappear in the upper part of RM16 and RM17 sequences. RM18 is  
725 characterized by an increase in green shales and dolomitic deposits.

726  
727 The nineteen middle frequency cycles are inserted into three and a half low frequency transgression/regression  
728 cycles (MS). The first maximum flooding of MS1 is located in the Rehach Fm. during RM3. Above the  
729 shallowing of depositional environments constitutes the low frequency highstand until a regressive maximum  
730 and the confinement of the basin during deposition of Kronab conglomerates and coeval halite in a more distal  
731 position. A new moderate flooding during MS2 led to deposition of shallow marine dolomites and evaporites

732 during the early stage of the Mhira Fm. (RM5 sequence). The low frequency highstand consists of continental  
733 playa deposits of the upper part of the Mhira Fm. The third low frequency flooding started with restricted marine  
734 halite deposits of S3 salt and led to the deposition of Zerzour dolomites. The maximum flooding was reached  
735 during RM13 when dolomitic facies were the most widespread. A new highstand period led to the deposition of  
736 halite facies during RM16 and RM17. A final low frequency flooding during RM18 to RM19 was completed  
737 with deposition of dolomites of the Pliensbachian B Horizon.

738

#### 739 **5.4.2 Transect 1:**

740 The transect 1 is oriented NW-SE between Bir Soltane 1 and Garaet El Atsel 1 wells and is parallel to the  
741 outcrop strip (Fig.14). Deposits of the sequence RM1 are present only in the Garaet El atsel 1 well. This implies  
742 an onlap of those deposits northwestward. The thickness of the TAC is broadly constant between Bou Nemcha 1  
743 and Garaet El Atsel 1 wells (Fig.16). Those Carnian deposits are absent in the Ksar El Hallouf well, where only  
744 dolomites of the Messaoudi Fm. and evaporites of the Bhir Fm. are present. Sandstones and halite beds which  
745 deposited during lowstands at the end of sequences RM3 and RM4 respectively pinch-out northwestward. S4  
746 salts and the Mhira Fm. are present until the Bou Nemcha 1 well and disappear toward Ksar El Hallouf.  
747 Accordingly to outcrop observations in the J. Rehach, the most probable origin for the disappearance of Carnian  
748 and Norian deposits northwestward is their progressive truncation below the regional angular Sidi Stout  
749 unconformity rather than an onlap geometry. S3 salt is only present in the southeast of the transect while  
750 deposition started with dolomitic and evaporitic deposits of the RM12 sequence in the Ksar El Hallouf well. This  
751 geometry suggests a northward onlap of Rhaetian evaporites and dolomites. In the Bir Soltane 1 well Triassic  
752 and Lower Jurassic deposits are absent and Dogger carbonates rest unconformably on the Permian. Such a  
753 geometry indicating an increasing unconformity toward the northwest is consistent with observations of Raulin  
754 (2013) and Raulin *et al.* (2011) who described unconformity of the Vraconian on the Permian at the western  
755 termination of the Tebaga of Medenine.

756

#### 757 **5.4.3 Transect 2**

758 The transect 2 is located west of outcrops and is oriented N-S (Fig.14). The northern termination of the transect  
759 corresponds to the Kef El Amba section in the North Dahar. The equivalent of the Mekraneb Formation  
760 (dolomitic part of the RM1 sequence) and the Touareg sandstones are well represented in the southern part of the  
761 transect (Fig.17a). However, those deposits are absent north of BZ-1 (Fig.17a, 17b). Lower evaporites at the top

762 of the RM2 sequence are present on a wide part of the transect and disappear northward. South of PGA-1, the  
763 transgressive part of RM3 is characterized by black organic shales intercalated with evaporites at the base and  
764 replaced by dolomites to the top (Fig.17a). The thickness of RM3 increases gradually from south to north,  
765 decreases rapidly between BZ-1 and PGA-1 (Fig.17b), and fluctuates rapidly between OS-1 and the Tebaga of  
766 Medenine. In the southern part of the transect a maximum flooding is reached at the top of Carnian black  
767 argilites and above the reappearance of dolomites indicates a progradation during the highstand of RM3  
768 (Fig.17a). This regressive phase is interrupted by a sharp transition to intertidal and supratidal dolomites with  
769 sandstone intercalations in the lower part. This interval is interpreted as lowstand deposits equivalent of mottled  
770 clays and the paleosoil observed in the J. Rehach at the top of the RM3 sequence. In the south this sharp  
771 transition is accompanied by an erosional unconformity indicated by toplap geometries (Fig.17a). Lowstand  
772 deposits of RM3 pinch-out on the northern margin of the basin. A second unconformity is present in the upper  
773 part of RM4. Lowstand deposits of the top of RM4 represented by halite and sandstones pinch-out southward  
774 and northward with onlaps (Fig.17a, 17b). Transgressive and highstand evaporites of RM6 and RM7 are  
775 replaced by evaporitic shales northward (Fig.17b).

776  
777 As in transect 1, deposits of RM3 to RM8 are truncated northward by the Rhaetian regional unconformity  
778 (Fig.17b). The truncation is also present in the southern part of the transect where S4 salt and evaporitic red  
779 shales of the D2 Fm. are gradually truncated with toplap geometries below S3 salts (Fig.17a). In contrast, it is  
780 interesting to note that in the central part of the transect S3 salts overlain conformably the Mhira shales. Note  
781 also that the thickness of S3 salts and dolomite rich part of the Bhir Fm. increases locally in the vicinity of PGA-  
782 1. S3 salts onlap the unconformity southward (Fig.17a) and northward (Fig.17b) and grade laterally to anhydrite  
783 or red evaporitic shales in the KGH-1 area. According to geometries observed on the transect 1, only dolomites  
784 of the Messaoudi Fm. and evaporites of the Bhir Fm onlapped and flooded the Tebaga of Medenine. This suggests  
785 that brecciated dolomites of the North Dahar correspond to a lateral equivalent of those formations. The flooding  
786 of RM13 is accompanied by the generalisation of dolomitic facies in the saltern. Oolitic dolomites of the Zerzour  
787 Member grade laterally to Messaoudi dolomites which are directly overlaying the Rhaetian unconformity to the  
788 north. These facies suggest that connections with the open-sea were re-established and that the sill was flooded.  
789 Consequently we consider that dolomites of the North Dahar deposited during the RM14 and RM15 sequences  
790 during a low frequency maximum flooding period. This interpretation is consistent with the subsequent  
791 reappearance of confined conditions in the basin as attested by the occurrence of halite in the transect 1 and 2 at

792 the top of RM16 and RM17. This regressive period is correlated to the incision on the sill observed in the North  
793 Dahar at the base of fluvial deposits.

794

## 795 **6 Discussion**

### 796 **6.1 Facies models and climatic implications**

797 Two depositional models succeeded each other during late Triassic and early Jurassic times. During the Carnian  
798 the basin was open to the Neotethys, as attested by the common occurrence of storm deposits and open marine  
799 fauna. Evaporitic facies developed only in temporarily exposed proximal areas. Facies were mainly dolomitic and  
800 deepest environments consisted of offshore marls and storm dominated nodular dolomites. From the late Carnian  
801 and until the late Norian confined evaporitic and siliciclastic deposits of playa lake environment prevailed.  
802 During the Rhaetian and the early Jurassic, dolomitic facies developed on the sill formed by the Tebaga of  
803 Medenine. This relief bordered a confined saltern to the south. In intertidal to supratidal environments,  
804 stromatolitic dolomites with evaporites nodules, desiccation cracks and tepee structures were the dominant  
805 facies. The basin became confined and evaporites precipitated.

806

807 Several factors have certainly influenced changes in the depositional models. The closure of the basin during the  
808 Norian and the Rhaetian due in part to the emergence of the Tebaga of Medenine certainly favoured the  
809 precipitation of evaporites in central and south Tunisia (Turner and Sherif, 2007). This interpretation is conformed  
810 by the occurrence of less restricted environments in the evaporitic Rehouis Fm located north of the Tebaga of  
811 Medenine (Kamoun *et al.*, 2001). In the other hand, evaporitic facies were not exclusively restricted to the south  
812 of the Tebaga of Medenine but also deposited north of it, in the Tunisian Atlas (Kamoun *et al.*, 2001). As a  
813 consequence, the generalization of evaporitic facies also suggests an increase in the aridity. However, while  
814 transition to dry condition during the end of the Triassic have been described on the neighbouring Moroccan  
815 margin (Hofmann *et al.*, 2000) and in Libya (Muttoni *et al.*, 2001), an increase in humidity is observed on the  
816 northern tethyan margin during the Rhaetian (Berra *et al.*, 2010) and up to Sweden (Ahlberg *et al.*, 2002). The  
817 appearance of humid belts at high latitudes and on the northern Tethys margins coeval of an aridification of  
818 tropical areas is certainly due to the conjunction of both a strong monsoonal effect during the end of the late  
819 Triassic (Tanner *et al.*, 2004) and the displacement to the arid climatic belt during the anticlockwise rotation of  
820 the Gondwana (Muttoni *et al.*, 2001).

821

## 822 **6.2 Accommodation vs sediment supply**

823 During the Carnian, floodings led to the deposition of offshore marls. During regressive maximum intertidal to  
824 supratidal dolomitic environments prevailed without prolonged subaerial exposures. These features suggest  
825 that accommodation exceeded the sedimentation rate. Indeed, the chloralgal bentic association devoid of  
826 hermatypic corals and with scarce oolitic deposits which existed in hypersaline environments on the basin  
827 margins was certainly not able to produce important quantities of carbonate to counterbalance accommodation.  
828 During the desposition of the lower part of S3 salt the thickness of sequences decreased and intertidal deposits  
829 capped by prolonged subaerial exposure prevailed on the southeast margin of the Tebaga of Medenine (Fig.7).  
830 The overall shallowing of depositional environments cannot be explained by an increase in sediment supply  
831 given the persistence of chloralgal benthic associations and the lack of important volumes siliciclastic inputs. In  
832 contrast such an evolution rather suggests a decrease in the accommodation during the highstand of the low  
833 frequency RM1 sequence.

834

835 In contrast, during the late Norian (upper part of S4 salt and Mhira shales) the thick marine halite and playa lake  
836 deposits suggest that despite a positive accommodation the available space was filled by the sedimentation. This  
837 argues for an increase in the sediment supply during this period. This increase may be explained by either a less  
838 aride climate or the appearance of reliefs providing important quantities of terrigenous material.

839

840 During the Rhaetian and the early Jurassic middle frequency, despite the absence of carbonate producers and of  
841 siliciclastic sediment supply, sequences are thin and prolonged subaerial exposures prevailed at the end of  
842 progradations as attested by the abundance of collapse breccias. During the low frequency maximum flooding the  
843 predominance of washover deposits indicates that depth never exceeded few metres. All these features suggest  
844 that accommodation was less important than during the Carnian and the end of the Norian and that a low  
845 sediment supply was able to fill the accommodation space.

846

## 847 **6.3 Tectonosedimentary evolution**

848 Subsurfaces and outcrop correlations allow to propose a coherent tectonosedimentary scenario for the late  
849 Triassic and early Jurassic of central Tunisia. During the late Triassic and the early Jurassic the Central and  
850 Southern Tunisia were impacted by several tectonic events.

851 Ladinian-Carnian

852 The deposition of the Mekraneb Fm. occurred during the first Carnian flooding (RM1 sequence) (Fig.18a).  
853 During RM1 and RM2 a large and shallow carbonate ramp extended in the J. Rehach and the proximal area was  
854 located to the northwest on margins of the Paleozoic Talemzane high. However, the erosion toward the  
855 northwest due to the Sidi Stout unconformity allows not to know the extension of the transgression. Peritidal  
856 dolomites and limestones existed in the whole basin during periods of high relative sea-level. During regressive  
857 maximum and confinement of the basin at the end of the sequence RM1 and RM2, fluvial and estuarine  
858 sandstones (Touareg Fm.) and evaporites prevailed in the basin (Fig.18a). The lack of deposits of RM1 and RM2  
859 north of the BZ-1 well can be explained by the topography inherited from the Talemzane High on which Carnian  
860 deposits overlapped and which was still exposed at the end of the middle Triassic (Bibonne, 2014). During the  
861 transgression of RM3 condensed facies with black organic shales developed in south Tunisia. The upper part of  
862 the TAC equivalent of the Rehach Fm. indicates the continuation of the Carnian flooding. The high was flooded  
863 during RM3. The thinning of deposits south of PGA-1 and their thickening between OS-1 and MHB-1 can also  
864 be explained by the topography due to the Talemzaqne High (Figs.17a, 17b). In contrast, the local variations in  
865 thickness of the TAC north of MHB-1 suggest that syndimentary normal faults were active during the Carnian  
866 and generated local thickening of Rehach dolomites on hangingwalls (Fig.18a). No evidence of uplift of the  
867 Tebaga of Medenine during the deposition of the TAC has been observed. This extensional phase coeval with  
868 alkaline volcanism in the Chotts Basin (Bouaziz *et al.*, 2002, Piqué *et al.*, 1998; Raulin, 2013) coincides with the  
869 major Carnian flooding accompanied by the generalization of marine dolomitic ramp facies open to the  
870 Neotethys. This scenario is in disagreement with the geodynamic timing proposed by Stampfli and Borel (2002)  
871 who considered that the end of the rifting and the onset of thermal subsidence on the Tunisian margin occurred  
872 during the late Permian. In contrast our observations support the scenario proposed by several authors (Bouaziz  
873 *et al.*, 2002; Courel *et al.*, 2003; Galeazzi *et al.*, 2010; Piqué *et al.*, 1998; Raulin, 2013; Raulin *et al.*, 2011;  
874 Turner *et al.*, 2001) of a tectonic subsidence and rifting still active during the late Triassic. However, the Carnian  
875 corresponds to the last rifting stage after a rifting peak reached during the late Permian and the early Triassic  
876 (Raulin, 2013).

877

878 The first evidence of the uplift of the Tebaga of Medenine corresponds to the rapid transition to alluvial mottled  
879 clays and to formation of a paleosol in the J. Rehach at the top of RM3. In this area and in the northern part of  
880 the transect 2 (Fig.18b) the uplift of the northern region is responsible of an exposure while lowstand sandstones  
881 deposited southward (Fig.18b). This event corresponds to a major change in sedimentation during the late

882 Carnian with an increase in evaporitic deposition and siliciclastic inputs during a low frequency forced  
883 regression and a gradual isolation of the Ghadames Basin. This first uplift phase is contemporaneous with the  
884 onset of deposition of S4 salt. Partial emptying of the basin characterized by prolonged subaerial exposures  
885 with or without incision of the basin margin in the J. Rehach (Kronab conglomerates and tepee surface) coeval  
886 with halite deposition in the basin occurred during the late Carnian and the early Norian (RM4 and RM5  
887 sequences) (Fig.18c, 18d). They are separated by a reflooding during RM5 illustrated by the reinstallation of  
888 peritidal dolomites on margins grading to anhydrite in the basin.

889  
890 Kamoun *et al.* (2001) proposed that the Tebaga of Medenine was a horst formed during rifting. Another scenario  
891 based on paleostress and seismic studies (Bouaziz *et al.*, 2002; Raulin, 2013) proposed that Tunisia was mainly  
892 impacted by a transpressional regime along the Jeffara fault system. Even if the region located north of the  
893 Jeffara faults system was impacted by extensive tectonics and alkaline volcanism during the entire late Carnian  
894 and early Norian (Kamoun *et al.*, 2001), during the deposition of the sequences RM4 and RM5, no obvious local  
895 variations in subsidence can be deduced from outcrop and subsurface correlations south of the Tebaga of  
896 Medenine. This suggests that normal faults activity decreased south of the Jeffara fault system during the late  
897 Carnian. Except the uplift of the Tebaga of Medenine, the Ghadames Basin was broadly stable. Consequently  
898 our observations attest of an interruption or at least a decrease in the the rift activity during the late Carnian  
899 coeval with a change in stress regime. The rapid and constant southward thickening of deposits of the sequence  
900 RM5 suggests a new uplift of the northern margin of the basin (Fig.18d).

### 901 Norian

902 After a moderate flooding at the base of the Mhira Fm., a shallowing of depositional environments prevailed  
903 during the Norian and the deposition of playa red shales of the upper part of the Mhira Fm. Siliciclastic inputs  
904 increased in the basin and continental environments prevailed (Fig.18e). Sequences were characterized by  
905 deposition of shallow evaporitic playas during floodings and by generalization of continental sebkha facies and  
906 paleosoil during drying periods. During the Norian, alkaline volcanism was documented in the Chott region  
907 north of the Jeffara fault system (Kamoun *et al.*, 2001) and indicates the continuation of extensive tectonics in  
908 this area. On the transect 2 local thickening of D2 shales in the PGA-1 area suggests that a renewal of normal  
909 faulting also occurred during the late Norian in the Ghadames Basin (Fig.17a). However, location of faults are  
910 different from those of faults active during the Carnian (Fig.18e).

### 911 Rhaetian-early Jurassic

912 On the northern margin, the boundary between sequences RM8 and RM9 corresponds to the major Sidi Stout  
913 unconformity. Considering the late Norian age of the Mhira Fm. (Bouaziz *et al.*, 1987) and the Rhaetian age of  
914 the Messaoudi dolomites (Mello and Bouaziz, 1987), Bouaziz *et al.* (1987) attributed a late Norian to early  
915 Rhaetian age to the unconformity. This event corresponds to a major southward tilting of the Permo-Triassic  
916 block of the Tebaga of Medenine in the northern part of the Ghadames Basin (Fig.18e). The onlap of the S3 salt  
917 observed both in north direction on the transect 2 (Fig.17a and 17b) indicates that the basin was drained in part  
918 during a period of negative accommodation. This fall of base level also generated a slight erosion of southern  
919 part of the basin as attested by the toplap geometry of Mhira shales below the S3 salt (Fig.17a). As proposed by  
920 Bouaziz *et al.* (1987, 2002) and since the angular unconformity is the more developed in the vicinity of the  
921 Tebaga of Medenine, the compressional transpressive activity of the Jeffara system was probably still active  
922 during the early Rhaetian and was responsible of the southward tilting.

923  
924 The onlap geometry of the S3 salt on the Tebaga of Medenine illustrates the gradual marine reflooding of the  
925 basin after its entire or partial exposure (Fig.18f). However, the angular unconformity disappears in the central  
926 part of the basin (Fig.17a). If the basin was totally drained during a generalized uplift of the basin, the basal  
927 surface of S3 salts should consist of a surface of subaerial exposure coeval with lowstand deposits in deeper  
928 neighbouring basins (Fig.19a). In contrast, in the absence of unconformity and subaerial exposure, and since S3  
929 salts are marine, the basal surface of S3 salts should be a transgressive surface (Fig.19b). In Libya, the contact  
930 between Norian fluvial deposits of the Abu Shaybah Fm. and the overlaying shallow marine Abu Ghaylan Fm.,  
931 envisioned as the lateral equivalent of Tunisian Rhaetian evaporites (Mejri *et al.*, 2006), is conformable (Hallet,  
932 2002) and probably corresponds to the Rhaetian flooding (Rubino, 2003). If, such a surface exists at the base of  
933 S3 salts in the central part of Tunisia this implies that subaerial exposure on the uplifted Tebaga of Medenine is  
934 coeval with a flooding in the southern subsiding area without basinward shift of facies and lowstand deposits.  
935 This suggests that the folding that generated the uplift of the Tebaga de Medenine was accompanied by an  
936 increase in accommodation (subsidence or eustasy?) which exceeded the sedimentation rate in the basin. If this  
937 model is confirmed, as proposed by Dreyer *et al.* (1999) in the syndeformational Eocene Sobrarbe deltaic  
938 complex in the South Pyrenean foreland Ainsa Basin, a subaerial exposure in uplifted zones used as sequence  
939 boundary *sensu* Vail *et al.* (1991) could be correlated with a transgressive surface without lowstand deposits in  
940 active tectonic areas. Unfortunately, the absence of observations on cores allowed not to determine the nature of  
941 the surface in the central part of the basin.

942  
943 The reflooding of the sill was completed during the RM12 sequence (Fig.18f). During this period dolomitic  
944 facies were generalized. Oolitic shoals of the Messaoudi Fm. developed on the sill in the North Dahar while  
945 storm washover deposits extended southward and formed the Zerzour Member. This suggests that connections  
946 with the open-sea were completed during this period of high relative sea-level. However the alternation of  
947 collapse breccias and intertidal stromatolitic dolomites in the Messaoudi Fm. argues for a shallow and temporary  
948 exposed saltern. The abundance of siliciclastic material in dolomitic facies in the North Dahar suggests that  
949 erosion from exposed lands was more active than during the Carnian. This is confirmed by the occurrence of  
950 alluvial fan deposits certainly fed by exposed parts of the Tebaga of Medenine in most proximal parts (Mougor  
951 area). A normal fault was active in the North Dahar and the Ouarjaijin area recorded deposition of shallower  
952 intertidal to supratidal facies on the footwall. In addition, the local thickening of S3 salt and dolomitic facies in  
953 PGA-1 attests of normal faulting during RM7 to RM11 (Figs.17a and 18f) . Contrarily to Kamoun *et al.* (2001)  
954 who argued that Zerzour dolomites and Bhir evaporites deposited during a post-rift period, our observations  
955 suggest that normal faulting occurred during the long term reflooding of the Ghadames Basin. However, the  
956 scarcity of local subsidence differentials suggests that the rifting intensity was lower than during Carnian times.  
957 This interpretation is consistent with the continuation of shallow to emersive conditions, and the reduced  
958 thickness of sequences during the deposition of the Messaoudi and Bhir formations (Fig.18f). This implies that  
959 the overall subsidence was necessarily moderate in the Ghadames Basin and did not outpace the sedimentation  
960 rate.

961  
962 During the end of RM16 the basin became confined again. Halite and siliciclastics deposited in the deeper parts  
963 of the basin during a lowstand while an incision affected the North Dahar (Fig.18f). The prolonged subaerial  
964 exposure caused dissolution of evaporites interbedded with dolomitic facies and generated collapse breccias. The  
965 long term regression continued until the end of the RM17 sequence. A new low frequency reflooding started  
966 during RM18 and led to the deposition of the evaporites and dolomites of the Bhir Fm. (Fig.18f). No local  
967 variations in subsidence have been evidenced during this period suggesting that normal faulting ceased.

#### 968 969 **6.4 Comparisons with neighbouring regions and origin of depositional sequences**

970 A good correlation exists between Carnian to Norian sequences observed in the present study and the curve of  
971 coastal onlaps of European basins (Hardenbol *et al.*, 1998) (Fig.20). This observation suggests that middle

972 frequency cycles were certainly controlled by eustasy. For Raethian and Lower Jurassic deposits, sequences  
973 identified on well logs are matching with the coastal onlap curve. However, robust datations are lacking in the  
974 evaporitic deposits of the Bhir Fm. It makes difficult to estimate the duration of sequences and to discriminate  
975 possible mixing of different orders. In addition, Rhaetian and Lower Jurassic sequences are constituted by  
976 shallow subtidal to supratidal facies impacted by subaerial exposures. Consequently, considering these shallow  
977 depositional environments, sequences may be lacking in the sedimentary record especially during periods of low  
978 frequency lowstand (e.g. RM16 and RM17).

979  
980 From Morocco to Tunisia subsident troughs developed along transform Hercynian faults with a sinistral  
981 movement and oriented NW-SE or NE-SW (Galeazzi *et al.*, 2010; Piqué *et al.*, 1998; Piqué and Laville, 1995).  
982 The subsident Jeffara Basin constituted the western prolongation of one of these troughs and during the Carnian  
983 rifting, transpressional movement along the Jeffara fault system generated local folding in Tunisia (Raulin,  
984 2013). As mentioned by Raulin (2013) the strike-slip movements of the NW-SE Hercynian structures during the  
985 late Triassic accommodated the anticlockwise movement (Muttoni *et al.*, 2001) of the northern Gondwana  
986 during the Atlantic rifting which was still active during Norian and Rhaetian times (Laville *et al.*, 2004). As in  
987 Tunisia, Carnian rifting has been documented along the northern Gondwana margin such as in Morocco (Laville  
988 *et al.*, 2004; Manspeizer *et al.*, 1978), central Algeria (Courel *et al.*, 2003, Galeazzi *et al.*, 2010), Egypt (Hussein  
989 and Abd-Allah, 2001; Keeley, 1994) and Levant margin (Gardosh *et al.*, 2010; Korngreen and Benjamini, 2002).  
990 This rifting is related to the opening of the Neotethys in Tunisia and eastern region (Bouaziz *et al.*, 2002;  
991 Korngreen and Benjamini, 2002) while the Atlantic rifting impacted Morocco and probably Algeria (Bourquin  
992 *et al.*, 2010). The low frequency Carnian flooding has been observed from the Arabian platform to the Italian  
993 dolomites (Haq and Al-Qahtani, 2005; Gianolla and Jacquini, 1998). In south Algeria, Bourquin *et al.* (2010)  
994 considered that the maximum flooding occurred during a rifting phase and the deposition of the *Trias Argileux*  
995 *carbonaté* (TAC). These authors dated the maximum flooding to the early Norian. However in Central Algeria  
996 and for some of the same wells that those used by Bourquin *et al.* (2010), Galeazzi *et al.* (2010) envisioned a  
997 Carnian age for the TAC. This age is more consistent with our correlations scheme between the Carnian Rehach  
998 dolomites in outcrops and the TAC in subsurface. Overall, the low frequency flooding was probably favored by  
999 an active subsidence created by the rifting.

1000

1001 In the Ghadames Basin, Bouaziz *et al.* (2002) envisioned a short period of change in the stress regime during the  
1002 end of the Triassic linked to a significant transpressional activity of the Jeffara fault system. Such an  
1003 interpretation was also mentioned by Raulin (2013). Our observations are in agreement with these authors. In the  
1004 Ghadames Basin the activity of normal faulting stopped during the late Carnian when first evidences of the uplift  
1005 of the Tebaga of Medenine appeared. An abrupt shallowing in depositional environments accompanied this  
1006 change in stress regime and generated an unconformity at the base of the S4 salt. A similar unconformity with  
1007 shallowing of depositional environment was described between the TAC dolomites and the S4 salt in Algeria  
1008 (Galeazzi *et al.*, 2010) and between the Carnian marine dolomites of the Azizia Fm. and the fluvial Abu Shayba  
1009 Fm. in Libya (Rubino *et al.*, 2003; Hallet, 2002). Discontinuities are attributed to the Norian but could be dated  
1010 late Carnian since the ages of deposits directly above them are not constrained (Adlof *et al.*, 1985) (Fig.20). A  
1011 late Carnian uplift preceding a volcanic event was also envisioned on the Levant margin (Korngreen and  
1012 Benjamini, 2002).

1013  
1014 A low frequency regression led to the partial drying of the basin during the late Norian-early Rhaetian and to the  
1015 formation of the Sidi Stout unconformity. This period was accompanied by a major structural transpressive strike  
1016 slip event with a tilting in the vicinity of the Tebaga of Medenine. The unconformity was also generated in  
1017 southern Tunisia and Algeria. However rifting is documented in the Jeffara basin, in Morocco, and in Algeria  
1018 until the Norian to early Rhaetian at least and continued during the early Jurassic time (Fig.20). This suggests  
1019 that despite a continuation of normal faulting in troughs bounded by Hercynian faults, subsidence decreased in  
1020 central Tunisia. Galeazzi *et al.* (2010) and Stampfli *et al.* (2001) envisioned an uplift of rift shoulder during the  
1021 late Triassic. A similar interpretation was proposed for the late Carnian to Norian uplift phase preceding the  
1022 Rhaetian to early Jurassic rifting and volcanism on the Levant margin (Korngreen and Benjamini, 2002).  
1023 However, the structural rearrangement observed in Tunisia is probably linked to a more global event since  
1024 several angular unconformity and/or hiatus during a long term fall of base level from the middle Carnian to late-  
1025 Norian or early Rhaetian has also been described in Germany (Aigner and Bachmann, 1992) and on the Arabian  
1026 platform (Maurer *et al.*, 2008). In the Italian Dolomites, a major fall in the relative sea-level during the middle  
1027 Carnian coeval with a cessation of normal faulting precedes a second major fall at the Norian-Rhaetian boundary  
1028 (Berra *et al.*, 2010; Gianolla and Jacquin, 1998). In the Paris Basin, Bourquin and Guillocheau (1996) and  
1029 Bourquin *et al.* (1998) also described an angular unconformity in the *Marnes Irisées supérieures* Fm. This  
1030 unconformity is due to a global tilting of the Paris Basin and the activity of hercynian faults. Its age is intra-

1031 Norian. This unconformity was preceded by an important fall of relative sea-level as soon as the late Carnian and  
1032 the deposition of the Grès à roseaux Fm. Overall, the rapid shallowing of depositional environments in the  
1033 Ghadames Basin is coeval with a decrease in the subsidence linked to a decrease in the normal faulting and a  
1034 widespread structural event recorded at the scale of the northern Gondwana margin and Western Europe.  
1035 Guiraud *et al.* (2005) and Guiraud and Bosworth (1999) interpreted the late Triassic uplift and unconformities  
1036 from Syria to Libya as the distal effects of the Early-Cimmerian event due to the collision and subduction of the  
1037 Iranian plate with Eurasia from the Carnian (Wilsem *et al.*, 2009). Bourquin et al (2002) also proposed that the  
1038 Early-Cimmerian tectonic phase was at the origin of modifications in stress regime and of Norian and Rhaetian  
1039 unconformities in the Paris Basin. Such an event is a more probable origin for coeval unconformities observed  
1040 both in northern African margins and in Germany and the Paris Basin located on the northern Tethyan margin  
1041 where European plate deformations and reactivation of Hercynian structures due to variations in stress between  
1042 plates was envisioned (Bourquin and Guillocheau, 1996). This event is a plausible cause for the structural  
1043 rearrangements and the intensification of transpressive strike-slip movements along hercynian faults described in  
1044 central Tunisia (Bouaziz *et al.*, 2002).

1045  
1046 On the basis of gradual onlaps of Upper Triassic and Lower Jurassic deposits on the basin margins, Courel *et al.*  
1047 (2003) argued that in Algeria and Tunisia the flooding was continuous during this period. However, even if the  
1048 surface occupied by deposits increased from the Carnian to the Sinemurian, the flooding was interrupted from  
1049 the uppermost late Carnian to the rhaetian by several unconformities and lowstand sediments deposited in central  
1050 parts of the basin (S4 and S3 salts). In addition a partial drying of the basin certainly occurred when the Rhaetian  
1051 Sidi Stout unconformity formed. Galeazzi *et al.* (2010) proposed that in Algeria and Tunisia, the late Norian to  
1052 early Rhaetian uplift was the result of postrift thermal relaxation prior to a phase of thermal subsidence. Several  
1053 authors also envisioned that a postrift phase started during the Rhaetian or the early Jurassic (Kamoun *et al.*,  
1054 2001; Piqué *et al.*, 1998). However, as observed on outcrops in the North Dahar, in Central and Southern Tunisia  
1055 the Rhaetian flooding is coeval with normal faulting. As pointed by Kamoun *et al.* (2001) the extensional  
1056 tectonics was clearly attenuated compared to the Carnian. However this period is characterized by a renewal of  
1057 normal faulting in the Ghadames Basin after a short transpressional regime from the late Carnian to the early  
1058 Rhaetian. This suggests that a new rifting phase started during the Rhaetian. Despite the rifting was continuous  
1059 from the Permian to the early Jurassic in north Tunisian troughs (Schettino and Turco, 2011), it was interrupted  
1060 by an uplift during the Norian. Such an interpretation is in agreement with observations of Bouaziz *et al.* (2002)

1061 and Raulin *et al.* (2011) who proposed that during Rhaetian and early Jurassic rifting was active in Tunisia.  
1062 Neotethys rifting during the early Jurassic is also documented in Egypt (Keeley, 1994; Hussein and Abd-Allah,  
1063 2001) and on the Levant margin (Gardosh *et al.*, 2010; Hardy *et al.*, 2010). In this latter area, the rifting that  
1064 probably started during Permian times and continued until the Bajocian was interrupted by a period of reduced  
1065 tectonic activity and uplift during the Norian and early Jurassic (Garfunkel, 2004; Korngreen and Benjamini,  
1066 2002). As evidenced in the late Triassic and early Jurassic of Morocco (Le Roy and Piqué, 2001) and on the  
1067 Levant margin, in central Tunisia several rifting sequences certainly succeeded each other and were locally  
1068 interrupted by short periods of compressive stress regime due to intensive transpressional activity of Hercynian  
1069 structures delimiting subsident troughs. In summary, Tunisia was impacted by both N-S extension generated by  
1070 Neotethys rifting and the contemporaneous senestral displacement of Hercynian structures, which accommodated  
1071 the Atlantic rifting in a N20 to N70 direction from the Permian and the Early-Cimmerian collision on the  
1072 northern margin of the Neotethys from the Carnian. In Morocco, the thermal subsidence on the Atlantic margin  
1073 started during the early Jurassic (Le Roy and Piqué, 2001) and may have controlled subsidence in Algeria  
1074 (Galeazzi *et al.*, 2010) while eastward rifting of the Neotethys was still active from the Tunisian to the Levant  
1075 margin.

1076

## 1077 **7. Conclusion**

1078 Nineteen middle frequency sequences have been depicted within the Carnian to Pliensbachian deposits in  
1079 Central and Southern Tunisia. They are grouped in three and a half low frequency transgression/regression  
1080 cycles. Middle frequency sequences can be correlated to the eustatic curve of coastal onlaps of the European  
1081 basins. Low frequency sequences can be correlated to the successive steps in the geodynamic evolution of the  
1082 basin:

1083 - During most of late Carnian and the first low frequency flooding, marine open environments prevailed. This  
1084 flooding was probably favored by subsidence created by normal faulting during a rifting period, initiated during  
1085 the Permian.

1086 - During the uppermost late Carnian, an abrupt shallowing of depositional environments occurred and was  
1087 coeval with the first evidences of uplift of the Tebaga of Medenine high. Deposition occurred in shallow  
1088 intertidal or continental playa environments. Normal faulting declined and compressive regime on margins  
1089 southern compartment of the Hercynian Jeffara fault system prevailed. The area was uplifted and several angular  
1090 unconformities formed on edges of the basin contemporaneously with middle frequency lowstand deposits in its

1091 central part. The major Sidi Stout unconformity is present on edges of the uplifted Tebaga of Medenine where it  
1092 corresponds to a low frequency regressive maximum. In contrast the unconformity disappears southward where  
1093 Rhaetian S3 salt appears as transgressive in subsiding syncline zones. The uplift can be documented until late  
1094 Norian to early Rhaetian. This uplift and attenuation of the rifting documented as far as the Levant margin may  
1095 correspond to the conjunction of several mechanisms such as an uplift of rift shoulders preceding the second  
1096 rifting event and the local change in stress regime due to an intensive transpressional activity along the  
1097 Hercynian structures.

1098 - During the Rhaetian and possibly until the early Jurassic a second event of normal faulting impacted Central  
1099 Tunisia. During this period a second low frequency flooding invaded the Ghadames Basin. The Messaoudi  
1100 dolomites deposited on edges of the sill formed by the Tebaga of Medenine high, while evaporites predominated  
1101 in a saltern to the south in more distal parts.

1102  
1103 The change in depositional models between open marine Carnian deposits and Rhaetian to Lower Jurassic  
1104 restricted evaporites is certainly the result of both the appearance of the Tebaga of Medenine high, this relief was  
1105 acting as a sill, and a climatic change from humid to arid during the gradual anticlockwise migration of the  
1106 Gondwana. In the future, in order to better constrain durations and ages of sequences in Messaoudi and Bhir Fm.  
1107 datation must be better constrained. The nature of the basal surface of S3 salt in the basin has to be determined in  
1108 order to solve the question of a possible flooding in the subsident basin coeval with exposure on uplifted areas.  
1109 A complementary correlation work of well logs is actually in progress to refine correlations of Tunisian deposits  
1110 and unconformities with adjacent regions of Algeria and Libya and to test the stratigraphic scheme proposed in  
1111 this study.

1112

### 1113 **Acknowledgement**

1114 We would like to thank TOTAL Company who supported this study as part of the project of Sud Peri-Tethys.  
1115 We also acknowledge Romain Bibonne, Camille Raulin for discussion and exchange during field trips and  
1116 workshops. We are grateful to Sylvie Bourquin and the anonymous reviewer who allowed to improve the quality  
1117 of the manuscript through their comments and advices. We also thank A. Kalifi and M. Facon for their help for  
1118 well logs correlations.

1119

### 1120 **References:**

- 1121 Adloff, M.C., Doubinger, J., Massa, D., Vachard, D., 1985. Trias de la Tripolitaine (Libye) : Nouvelles données  
1122 biostratigraphiques et palynologiques. *Revue de l'Institut. Français du Pétrole*, 40, 8.
- 1123
- 1124 Ahlberg, A., Arndorff, L., Guy-Ohlson, D., 2002. Onshore climate change during the Late Triassic marine  
1125 inundation of the Central European Basin. *Terra Nova*, 14, 241-248.
- 1126
- 1127 Aigner, T., Bachmann, G., 1992. Sequence-stratigraphic framework of the German Triassic. *Sedimentary  
1128 Geology*, 80, 115-135.
- 1129
- 1130 Alsharhan A.S., Kendall C.G.S.C., 2003. Holocene coastal carbonate and evaporite of the southern Arabian Gulf  
1131 and their ancient analogues. *Earth-Science Reviews*, 61, 191-243.
- 1132
- 1133 Assereto, R. L. A. M., Kendall, C. G. St. C., 1977. Nature, origin and classification of peritidal tepee structures  
1134 and related breccias. *Sedimentology*, 24, 153-210
- 1135
- 1136 Baltzer, F., Purser, B.H., 1990. Modern alluvial fan and deltaic sedimentation in a foreland tectonic setting: the  
1137 lower Mesopotamian Plain and the Arabian Gulf. *Sedimentary Geology*, 67, 175-197.
- 1138
- 1139 Ben Ferjani, A., Burolet, P.F., Mejri, F. 1990. *Petroleum geology of Tunisia*, E. T. A. P. Tunis, 194 p.
- 1140
- 1141 Ben Ismaïl, M., 1982. Le Trias et le Jurassique inférieur et Moyen évaporitiques de l'extrême sud tunisien, étude  
1142 des sondages profonds et de terrain, synthèses paléogéographiques. Document du Laboratoire de géologie du  
1143 Muséum de Paris, Paris.
- 1144
- 1145 Benison, K.C., Goldstein, R.H., 2000. Sedimentology of ancient saline pans: An example from the Permian  
1146 Opeche Shale, Williston Basin, North Dakota, USA. *Journal of Sedimentary Research*, 70, 159-169.
- 1147
- 1148 Berra, F., Jadoul, F., Anelli, A., 2010. Environmental control on the end of the Dolomia principale/Hauptdolomit  
1149 depositional system in the central Alps: Coupling sea-level and climate changes. *Palaeogeography,  
1150 Palaeoclimatology, Palaeoecology*, 290, 138–150.

- 1151
- 1152 Bibonne, R., 2014. Sédimentologie et stratigraphie des séries clastiques du Trias inférieur à moyen du bassin de  
1153 Ghadamès et de la Jeffara (Tunisie et Libye), PhD thesis, Strasbourg University.
- 1154
- 1155 Bouaziz S., 1995. Étude de la tectonique cassante dans la plateforme et l'atlas sahariens (Tunisie méridionale) :  
1156 évolution des paléochamps de contraintes et implications géodynamiques. State Doctorate, University of  
1157 Sciences of Tunis, Tunisia.
- 1158
- 1159 Bouaziz, S., Barrier, E., Soussi, M., Turki, M., Zouari, H., 2002. Tectonic evolution of the northern African  
1160 margin in Tunisia from paleostress data and sedimentary record. *Tectonophysics*, 357, 227-253.
- 1161
- 1162 Bouaziz, S., Mello, J., Doubinger, J., 1987. Les argiles et évaporites de Mhira : Nouvelle formation d'âge  
1163 Carnien supérieur-Norien de la Jeffara (Tunisie méridionale) – Analyse palynologique. *Notes du Service*  
1164 *Géologique de Tunisie*, 54, 25-39.
- 1165
- 1166 Bourquin, S., Eschard, R., Hamouche, B., 2010 High-resolution sequence stratigraphy of Upper Triassic  
1167 succession (Carnian-Rhaetian) of the Zarzaitine outcrops (Algeria): A model of fluvio-lacustrine deposits.  
1168 *Journal of African Earth Sciences*, 58, 365-386.
- 1169
- 1170 Bourquin S., Robin C., Guillocheau F., Gaulier J.-M., 2002. Three-dimensional accommodation analysis of the  
1171 keuper of the Paris Basin: discrimination between tectonics, eustasy, and sediment supply in the stratigraphic  
1172 record. *Marine and Petroleum Geology*, 19, 469-498.
- 1173
- 1174 Bourquin, S., Rigollet, C., Bourges, P., 1998. High-resolution sequence stratigraphy of an alluvial fan–fan delta  
1175 environment: stratigraphic and geodynamic implications — An example from the Keuper Chaunoy Sandstones,  
1176 Paris Basin. *Sedimentary Geology*, 121, 207-237.
- 1177
- 1178 Bourquin, S., Guillocheau, F., 1996. Keuper stratigraphic cycles in the Paris Basin and comparison with cycles  
1179 in other Peritethyan basins (German Basin and Bresse-Jura Basin). *Sedimentary Geology*, 105, 159-182.
- 1180

- 1181 Burollet, P.F., 1963. Reconnaissance géologique dans le Sud-Est du bassin de Kufra. First Saharan Symposium,  
1182 Tripoli. Revue Institut Français du Pétrole, Paris, 18, pp. 1537–1545.
- 1183
- 1184 Busson, G., 1972. Principes, méthodes et résultats d'une étude stratigraphique du Mésozoïque saharien. Memoire  
1185 du Muséum National d'Histoire Naturelle., 26, 441 pp., Paris.
- 1186
- 1187 Busson, G. 1967. Le Mésozoïque saharien, 1<sup>ère</sup> partie: l'Extreme-Sud Tunisien, Publ. C. R. Z. A, Géologie, 8,  
1188 Paris, 194 p.
- 1189
- 1190 Clari, P.A., Martire, L., 1996. Interplay of cementation, mechanical compaction, and chemical compaction in  
1191 nodular limestones of the Rosso Ammonitico Veronese (Middle-Upper Jurassic, northeastern Italy). Journal of  
1192 Sedimentary Research, 63, 447-458.
- 1193
- 1194 Courel, L., Aït Salem, H., Benaouiss, N., Et-Touhami, M., Fekirine, B., Oujidi, M., Soussi, M., Tourani, A.,  
1195 2003. Mid-Triassic to Early Liassic clastic/evaporitic deposits over the Maghreb Platform. Palaeogeography,  
1196 Palaeoclimatology, Palaeoecology, 196, 157-176.
- 1197
- 1198 De Lapparent, A.F., 1954. Stratigraphie du Trias de la Jeffara (Extrême Sud tunisien et Tripolitaine). Abstract  
1199 book, XIX International Congress of Geology Alger, Ass. Serv. géol. afric., 21, 129-134.
- 1200
- 1201 Dalrymple, R.W., Choi, K., 2007. Morphologic and facies trends through the fluvial–marine transition in tide-  
1202 dominated depositional systems: A schematic framework for environmental and sequence-stratigraphic  
1203 interpretation. Earth-Science Reviews, 81, 135-174.
- 1204
- 1205 Dreyer, T., Corregidor, J., Arbues, P., Puigdefabregas, C., 1999. Architecture of the tectonically influenced  
1206 Sobrarbe deltaic complex in the Ainsa Basin, northern Spain. Sedimentary Geology, 127, 127-169.
- 1207
- 1208 Ehrenberg, S.N., 1993. Preservation of anomalously high porosity in deeply buried sandstones by grain-coating  
1209 chlorite: examples from the Norwegian Continental Shelf. AAPG Bulletin, 77, 1260–1286.
- 1210

- 1211 Embry, A.F., 2009. Practical sequence stratigraphy. Canadian Society of Petroleum Geologists, online at  
1212 [www.cspg.org](http://www.cspg.org), 79 p.  
1213
- 1214 Farrell, K.M., 2001. Geomorphology, facies architecture, and high-resolution, nonmarine sequence stratigraphy  
1215 in avulsion deposits, Cumberland Marshes, Saskatchewan. *Sedimentary Geology*, 139, 93-150.  
1216
- 1217 Fischbein, S.A., Joeckel, R.M., Fielding, C.R., 2009. Fluvial-estuarine reinterpretation of large, isolated  
1218 sandstone bodies in epicontinental cyclothems, Upper Pennsylvanian, northern Midcontinent, USA, and their  
1219 significance for understanding late Paleozoic sea-level fluctuations. *Sedimentary Geology*, 216, 15-28.  
1220
- 1221 Frizon de Lamotte, D., Leturmy, P., Missenard, Y., Khomsi, S., Ruiz, G., Saddiqi, O., Guillocheau, F., Michard,  
1222 A., 2009. Mesozoic and Cenozoic vertical movements in the Atlas system (Algeria, Morocco, Tunisia): An  
1223 overview. *Tectonophysics*, 475, 9-28.  
1224
- 1225 Gabtni, H., Jallouli, C., Mickus, K.L., Zouari, H., Turki, M.M., 2006. The location and nature of the Telemzan  
1226 High-Ghadames basin boundary in southern Tunisia based on gravity and magnetic anomalies. *Journal of*  
1227 *African Earth Sciences*, 44, 303-313.  
1228
- 1229 Gaillard, C., 1983. Les biohermes à spongiaires et leur environnement dans l'Oxfordien du Jura méridional,  
1230 Documents du Laboratoire de Géologie de Lyon, N°90.  
1231
- 1232 Galeazzi, S., Point, O., Haddadi, N., Mather, J., Druésne, D., 2010. Regional geology and petroleum systems of  
1233 the Illizi–Berkine area of the Algerian Saharan Platform: An overview. *Marine and Petroleum Geology*, 27, 143-  
1234 178.  
1235
- 1236 Gardosh, M.A., Garfunkel, Z., Druckman, Y., Buchbinder, B., 2010. Tethyan rifting in the Levant Region and its  
1237 role in Early Mesozoic crustal evolution. *Geological Society, London, Special publication*, 341, pp. 9-36.  
1238
- 1239 Garfunkel, Z., 2004. Origin of the Eastern Mediterranean basin: a reevaluation. *Tectonophysics*, 391, 11-34.  
1240

- 1241 Gianolla, P., Jacquin, T., 1998. Triassic sequence stratigraphic framework of western European basins, in: de  
1242 Graciansky, Hardenbol, J. Jaquin, T., Vail, P.R. (Eds.) Mesozoic and Cenozoic Sequence Stratigraphy of  
1243 European Basins, SEPM Special Publication, 60, pp. 643-650.
- 1244
- 1245 Gibert, L., Orti, F., Rossel, L., 2007. Plio-Pleistocene lacustrine evaporites of the Baza Basin (Betic Chain, SE  
1246 Spain). *Sedimentary Geology*, 200, 89-116.
- 1247
- 1248 Giraud, R., Bosworth, W., Thierry, J., Delplanque, A., 2005. Phanerozoic geological evolution of Northern and  
1249 Central Africa: an overview. *Journal of African Earth Sciences*, 43, 83-143.
- 1250
- 1251 Giraud, R., Bosworth, W., 1999. Phanerozoic geodynamic evolution of northeastern Africa and the northwestern  
1252 Arabian platform. *Tectonophysics*, 315, 73-108.
- 1253
- 1254 Golonka, J., 2007. Late Triassic and Early Jurassic palaeogeography of the world. *Palaeogeography,*  
1255 *Palaeoclimatology, Palaeoecology*, 244, 297-307
- 1256
- 1257 Gorce, F., 1960. Etude de quelques vertébrés du Muschelkalk du Djebel Rehach (Sud Tunisien). *Mem. Soc.*  
1258 *Geol. Fr. N. S.88B*, 1-33.
- 1259
- 1260 Hallet, D., 2002. *Petroleum Geology of Libya*. Elsevier, Amsterdam.
- 1261
- 1262 Hamouche, B., 2006. Sédimentologie du Trias saharien de l’affleurement à la subsurface : Modèle de dépôt et  
1263 architecture stratigraphique. Application aux affleurements de Zarzaitine et au bassin de Berkine (Sahara  
1264 oriental, Algérie). PhD thesis, Rennes University, France.
- 1265
- 1266 Haq, B.U., Al-Qahtani, A.M., 2005. Phanerozoic cycles of sea-level change on the Arabian Platform.  
1267 *GeoArabia*, 10, 2, 127-160.
- 1268
- 1269 Hardenbol, J., Thierry, J., Farley, M.B., Jacquin, T., De Graciansky, P.C., Vail, P.R., 1998. Mesozoic and  
1270 Cenozoic sequence chronostratigraphic framework of European basins, in: De Graciansky, P.C., Hardenbol, J.,

- 1271 Jacquin, T., Vail, P.R. (Eds.) Mesozoic and Cenozoic Sequence Stratigraphy of European Basins, SEPM Special  
1272 publication, 60, Tulsa, 3–15.  
1273
- 1274 Hardy, C., Homberg, C., Eyal, Y., Barrier, E., Müller, C., 2010. Tectonic evolution of the southern Levant  
1275 margin since Mesozoic. *Tectonophysics*, 494, 211-225.  
1276
- 1277 Harvey, A., Mather, A., Stokes, M., 2005. Alluvial fans: geomorphology, sedimentology, dynamics –  
1278 introduction. A review of alluvial-fan research, in: Harvey, A., Mather, A., Stokes, M. (Eds.) *Alluvial fans:  
1279 Geomorphology, Sedimentology, Dynamics*, Geological Society Special Publication, 251, London, pp. 1-7.  
1280
- 1281 Hofmann, A., Abdelilah, T., Reinhard, G., 2000. Cyclicity of Triassic to Lower Jurassic continental red beds of  
1282 the Argana Valley, Morocco: implications for palaeoclimate and basin evolution. *Palaeogeography,  
1283 Palaeoclimatology, Palaeoecology*, 161, 229-266.  
1284
- 1285 Hussein, I.M., Abd-Allah, A.M.A., 2001. Tectonic evolution of the northeastern part of the African continental  
1286 margin, Egypt. *Journal of African Earth Sciences*, 33, 49-68.  
1287
- 1288 Jalil, N.E., 1999. Continental Permian and Triassic vertebrate localities from Algeria and their stratigraphical  
1289 correlations. *Journal of African Earth Sciences*, 29, 219-226.  
1290
- 1291 James, N.P., 1984. Shallowing-upward sequences in carbonates, in: Walker, R.,G. (Ed.), *Facies Models*.  
1292 Geological Association of Canada Publications, second edition, 213-228.  
1293
- 1294 Kamoun, F., Peybernès, B., Ciszak, R., Calzada, S., 2001. Triassic palaeogeography of Tunisia.  
1295 *Palaeogeography, Palaeoclimatology, Palaeoecology*, 172, 223-242.  
1296
- 1297 Kamoun, F., Peybernès, B., Martini, R., Zaninetti, L., Vila, J.-M., Trigui, A., Rigane, A., 1997. Associations de  
1298 foraminifères benthiques dans les séquences de dépôt du Trias moyen?-supérieur de l'Atlas tunisien central et  
1299 méridional. *Geobios*, 31, 703-714.  
1300

- 1301 Kamoun, F., Martini, R., Peybernes, B., Zaninetti, L., 1994. Caractérisation micropaléontologique du « Rhétien »  
1302 dans l'axe Nord-Sud (Tunisie centrale) ; comparaison avec le Rhétien de la dorsale et de la plate-forme  
1303 saharienne. *Rivista Italiana di paleontologia e stratigrafia*, 100, 365-382.
- 1304
- 1305 Keeley, M.L., 1994. Phanerozoic evolution of the basins of northern Egypt and adjacent areas. *Geologische*  
1306 *Rundschau*, 83, 728-742.
- 1307
- 1308 Kendall, C.G.St.C., Sadd, J.L., Alsharhan, A.S., 1994. Holocene marine cement coatings on beachrocks of the  
1309 Abu Dhabi coastline (U.A.E.), an analog for cement fabrics in ancient limestone. *Carbonates and Evaporites*, 9,  
1310 119-131
- 1311
- 1312 Kendall, A.C., 1988. Aspects of evaporate basin stratigraphy, in: Schreiber, B.C. (Ed.), *Evaporites and*  
1313 *hydrocarbons*: New York, Columbia University Press, pp. 11-65.
- 1314
- 1315 Knaust, D., 2013. The ichnogenus *Rhizocorallium*: Classification, trace makers, palaeoenvironments and  
1316 evolution. *Earth-Science Reviews*, 126, 1-47.
- 1317
- 1318 Koehrer, B., Heymann, C., Prousa, F., Aigner, T., 2010. Multiple-scale facies and reservoir quality variations  
1319 within a dolomite body - Outcrop analog study from the Middle Triassic, SW German Basin. *Marine and*  
1320 *Petroleum Geology*, 27, 386-411.
- 1321
- 1322 Korngreen, D., Benjamini, C., 2011. Platform to shelf edge transect, Triassic of northern Israel, North Arabian  
1323 Plate. *Sedimentary Geology*, 236, 164-184.
- 1324
- 1325 Laville, E., Piqué, A., Amrhar, M., Charroud, M., 2004. A restatement of the Mesozoic Atlasic rifting  
1326 (Morocco). *Journal of African Earth Sciences*, 38, 145-153.
- 1327
- 1328 Le Roy, P., Piqué, A., 2001. Triassic–Liassic Western Moroccan synrift basins in relation to the Central Atlantic  
1329 opening. *Marine Geology*, 172, 359-381.
- 1330

- 1331 Makhlof, I., 2006. Late Triassic-early Jurassic Neotethyan evolution at Northern Gondwana (Jordan and Libya,  
1332 Mediterranean region). *Geologica Acta*, 4, 3, 371-376.
- 1333
- 1334 Manspeizer, W., Puffer, J., Cousminer, H., 1978. Separation of Morocco and eastern North America: A Triassic-  
1335 Liassic stratigraphic record. *Geological Society of America Bulletin*, 89, 901-920.
- 1336
- 1337 Marcoux, J., Baud, A., Ricou, L.E., Bellion, Y., Besse, J., Gaetani, M., Gallet, Y., Guiraud, R., Jaillard, E.,  
1338 Krystyn, L., Moreau, C., Theveniaut, H., 1993. Late Norian (215-212 Ma), in: Dercourt, J., Ricou, L.E.,  
1339 Vrielynck, B. (Eds.), *Atlas Tethys Palaeoenvironmental Maps*. BEICIP-FRANLAB.
- 1340
- 1341 Martinius, A.W., Hegner, J., Kaas, I., Bejarano, C., Mathieu, X., Mjøs, R., 2012. Sedimentology and  
1342 depositional model for the Early Miocene Oficina formation in the Petrocedeño Field (Orinoco heavy-oil belt,  
1343 Venezuela). *Marine and Petroleum Geology*, 35, 354-380.
- 1344
- 1345 Maurer, F., Rettori, R., Martini, R., 2008. Triassic stratigraphy, facies and evolution of the Arabian shelf in the  
1346 northern United Arab Emirates. *International Journal of Earth Sciences*, 97, 765-784
- 1347
- 1348 Mejri, F., Burolet, P.F., Ben Ferjani, A., 2006. *Petroleum geology of Tunisia. A renewed synthesis*. ETAP  
1349 Memoir, 22, Tunis.
- 1350
- 1351 Mello J., Bouaziz S. 1987. Mise en évidence de la discordance de Sidi Stout dans la province centrale du  
1352 Sud tunisien et de son terme transgressif: dolomies de Messaoudii (Rhétien). *Notes du Service Géologique*  
1353 *National de Tunisie* 45, 41-54.
- 1354
- 1355 Memmi, L., Burolet, P.F., Vitterbo, I., 1986. *Lexique stratigraphique de la Tunisie. Première partie:*  
1356 *Précambrien et Paléozoïque*. *Notes du Service Géologique de Tunisie*, 53, pp. 66.
- 1357
- 1358 Mennig, J.J., Vittimberga, P., Lehmann, P., 1963. Etude sédimentologique et pétrographique de la Formation  
1359 Ras Hamia (Trias moyen) du nord-ouest de la Libye, *Revue de l'Institut Français du Pétrole*, 18, pp. 1504-1519.
- 1360

- 1361 Mercedes-Martin, R., Salas, R., Arenas, C., 2013. Facies heterogeneity and depositional models of a Ladinian  
1362 (Middle Triassic) microbial-dominated carbonate ramp system (Catalan Coastal Ranges, NE Spain). *Marine and*  
1363 *Petroleum Geology*, 46, 107-128.
- 1364
- 1365 Miall, A.D., 2006. *The geology of fluvial deposits*, fourth edition, Springer-Verlag, Berlin.
- 1366
- 1367 Mock, R., Mello, J, Biely, A. Bouaziz, S., 1987. Microfaune cordévolienne (Carnien inférieur) de la base du  
1368 Trias carbonaté de la Plateforme Saharienne. *Notes du Service Géologique de Tunisie*, 55, 19-29.
- 1369
- 1370 Morad, S., Ben Ismail, H., De Ros, L.F., Al-Aasm, I.S., Serrhini, N.-E., 1994. Diagenesis and formation water  
1371 chemistry of Triassic reservoir sandstones from southern Tunisia. *Sedimentology*, 41, 1253-1272.
- 1372
- 1373 Muttoni, G., Garzanti, E., Alfonsi, L., Cirilli, S., Germani, D., Lowrie, W., 2001. Motion of Africa and Adria  
1374 since the Permian: paleomagnetic and paleoclimatic constraints from northern Libya. *Earth and Planetary*  
1375 *Science Letters*, 192, 159-174.
- 1376
- 1377 Pandey, D.K., Uchman, A., Kumar, V., Shekhawat, R.S., 2014. Cambrian trace fossils of the Cruziana  
1378 ichnofacies from the Bikaner-Nagaur Basin, north western Indian Craton. *Journal of Asian Earth Sciences*, 81,  
1379 129-141.
- 1380
- 1381 Pemberton, G.S., Spila, M., Pulham, A.J., Saunders, T., MacEachern, J.A., Robbins, D., Sinclair, I.K., 2001.  
1382 *Ichology and Sedimentology of Shallow to Marginal Marine Systems: Ben Nevis and Avalon Reservoirs,*  
1383 *Jeanne D'Arc Basin. Geological Association of Canada, Short Course, Notes 15.*
- 1384
- 1385 Peryt, T., 2001. Gypsum facies transitions in basin-marginal evaporites: middle Miocene (Badenian) of west  
1386 Ukraine. *Sedimentology*, 48, 1103-1119.
- 1387
- 1388 Peybernès, B., Kamoun, F., Ben Youssef, M., Trigui, A., Ghanmi, M., Zarbout, M., Frechengues, M., 1993.  
1389 *Sequence stratigraphy and micropaleontology of the Triassic series from the southern part of Tunisia. Journal of*  
1390 *African Earth Sciences*, 17, 3, 293-305.
- 1391

- 1392 Peybernès, B., Alméras, Y., Ben Youssef, M., Kamoun, F., Mello, J., Rey, J., Zargouni, F. 1985. Nouveaux  
1393 éléments de datation dans le Jurassique du Sud-Tunisien (Plateforme Saharienne). Comptes Rendus de  
1394 l'Académie des Sciences, Paris, 300, II, 3, 113-118.
- 1395
- 1396 Pittet, B., Strasser, A., 1998. Long-distance correlations by sequence stratigraphy and cyclostratigraphy:  
1397 examples and implications (Oxfordian from the Swiss Jura, Spain, and Normandy). *Geologische Rundschau*, 86,  
1398 852-874.
- 1399
- 1400 Piqué, A., Brahim, L.,A., Ouali, R.A., Amrhar, M., Charroud, M., Gourmelen, C., Laville, E., Rekhiss, F.,  
1401 Tricart, P., 1998. Evolution structurale des domaines atlasiques du Maghreb au Méso-Cénozoïque ; le rôle des  
1402 structures héritées dans la déformation du domaine atlasique de l'Afrique du Nord. *Bulletin de la Société*  
1403 *Géologique de France*, 169, 787-810.
- 1404
- 1405 Piqué, A., Laville, E., 1995. L'ouverture initiale de l'Atlantique central. *Bulletin de la Société géologique de*  
1406 *France*, 166, 6, 725-738.
- 1407
- 1408 Posamentier, H.W., Morris, W.R., 2000. Aspects of the stratal architecture of forced regressive deposits, in:  
1409 Hunt, D., Gawthorpe, R.L. (Eds.), *Sedimentary responses to forced regressions*, Geological Society Special  
1410 Publication, 172, London, pp. 19-46.
- 1411
- 1412 Posamentier, H.W., James, D.P., 1993. An overview of sequence stratigraphic concepts uses and abuses, in:  
1413 Posamentier, H.W., Summerhayes, C.P., Haq, B.U., Hallen G.P. (Eds.), *Sequence stratigraphy and facies*  
1414 *associations*. IAS Special Publication, 18, pp. 3-8.
- 1415
- 1416 Rakus, M., 1981. Découverte de *Pseudofurnishius murcianus* Boogaard (Conodonta) dans le Trias du Sud-  
1417 tunisien. Abstract book of the first National Congress of Earth Sciences, Tunis, September 1981, 241-248
- 1418
- 1419 Raulin, C., 2013. Histoire tectonique du bassin Sud-tunisien (Jeffara) du Paleozoïque au Tertiaire, PhD thesis,  
1420 Cergy-Pontoise University, France.
- 1421

- 1422 Raulin, C., Frizon de Lamotte, D., Bouaziz, S., Khomsi, S., Mouchot, N., Ruiz, G., Guillocheau, F., 2011. Late  
1423 Triassic–early Jurassic block tilting along E–W faults, in southern Tunisia: New interpretation of the Tebaga of  
1424 Medenine. *Journal of African Earth Sciences*, 61, 94–104  
1425
- 1426 Riding, R., 2000. Microbial carbonates: the geological record of calcified bacterial-algal mats and biofilms.  
1427 *Sedimentology*, 47, 179-214.  
1428
- 1429 Riding, R., 1991. Classification of microbial carbonates, in: Riding, R. (Ed.) *Calcareous Algae and*  
1430 *Stromatolites*. Springer-Verlag, Berlin, pp. 21-51.  
1431
- 1432 Rieppel, O., 1997. Sauropterygia from the Muschelkalk of Djebel Rehach, southern Tunisia. *Neues Jahrb. Geol.*  
1433 *Paläontol. Mitt.*, 9, 517-530.  
1434
- 1435 Roep, T.B., Dabrio, C.J., Fortuin, A.R., Polo, M.D., 1998. Late highstand patterns of shifting and stepping  
1436 coastal barriers and washover-fans (late Messinian, Sorbas Basin, SE Spain). *Sedimentary Geology*, 116, 27-56.  
1437
- 1438 Rubino, J.-L., Galeazzi, S., Sbeta, A., 2003. Guide Book Supplement Day 1, The Triassic Succession of Jabal  
1439 Nefusaj, NW Libya. *Sedimentary Basins of Libya, Second Symposium Geology of Northwest Libya*, Tripoli, 1-  
1440 23.  
1441
- 1442 Salvany, J.M., Munoz, A., Perez, A., 1994. Nonmarine evaporitic sedimentation and associated diagenetic  
1443 processes of the southwestern margin of the Ebro Basin (lower Miocene), Spain. *Journal of Sedimentary*  
1444 *Research*, 64, 190–203.  
1445
- 1446 Schettino, A., Turco, E., 2011. Tectonic history of the western Tethys since the Late Triassic. *GSA Bulletin*, 123,  
1447 89-105.  
1448
- 1449 Schlager, W., 2004. Fractal nature of stratigraphic sequences. *Geology*, 32, 185-188  
1450

- 1451 Sedgwick, P.E., Davis Jr, R.A., 2003. Stratigraphy of washover deposits in Florida: implications for recognition  
1452 in the stratigraphic record. *Marine Geology*, 200, 31-48.
- 1453
- 1454 Sengör, A.M., 1984. The Cimmeride Orogenic System and the Tectonics of Eurasia. *GSA Special Papers*, 195,  
1455 1-74.
- 1456
- 1457 Stampfli, G., Borel, G., 2002. A plate tectonic model for the Paleozoic and Mesozoic constrained by dynamic  
1458 plate boundaries and restored synthetic oceanic isochrones. *Earth and Planetary Science Letters*, 196, 17-33.
- 1459
- 1460 Stampfli, G., Mosar, J., Favre, P., Pillevuit, A., Vannay, J.C., 2001. Permo–Mesozoic evolution of the western  
1461 Tethys realm: the Neo-Tethys East Mediterranean Basin connection, in: *Muséum National d’Histoire Naturelle*  
1462 (Ed.), *Peri-Tethys Memoir 6: Peri-Tethyan Rift/Wrench Basins and Passive Margins*. *Mémoires du Muséum*  
1463 *National d’Histoire Naturelle*, 186, Paris, 51–108.
- 1464
- 1465 Stampfli, G., Marcoux, J., Baud, A., 1991. Tethyan margins in space and time. *Palaeogeography,*  
1466 *Palaeoclimatology, Palaeoecology*, 87, 373-409.
- 1467
- 1468 Tanner, L.H., Lucas, S.G., Chapman, M.G., 2004. Assessing the record and causes of Late Triassic extinctions.  
1469 *Earth-Science Reviews*, 65, 103-139.
- 1470
- 1471 Tucker, M.E., 1991. Sequence stratigraphy of carbonate–evaporite basins; models and application to the Upper  
1472 Permian (Zechstein) of Northeast England and adjoining North Sea. *Journal of the Geological Society of*  
1473 *London*, 148, 1019-1036.
- 1474
- 1475 Turner, P., Sherif, H., 2007. A giant Late Triassic-Early Jurassic evaporitic basin on the Saharan platform, North  
1476 Africa, in: Schreiber, B., Lugli, S., Babel, M. (Eds.) *Evaporites through space and time*. *Geological Society of*  
1477 *London, Special Publication*, 285, London, 87-105.
- 1478

- 1479 Turner, P., Pilling, D., Walker, D., Exton, J., Binnie, J., Sabaou, N., 2001. Sequence stratigraphy and  
1480 sedimentology of the late Triassic TAG-I (Blocks 401/402, Berkine Basin, Algeria). *Marine and Petroleum*  
1481 *Geology*, 18, 959-981.
- 1482
- 1483 Vail, P.R., Audemard, F., Bowman, S.,A., Eisner, P.N., Perez-Cruz, C., 1991. The Stratigraphic Signatures of  
1484 Tectonics, Eustasy and Sedimentology: an Overview, in: Einsele, G., Ricken, W., Seilacher, A., (Eds.) *Cycles*  
1485 *and Events in Stratigraphy*. Springer-Verlag, Berlin, pp. 617-659.
- 1486
- 1487 Van Wagoner, J.C., Posamentier, H.W., Mitchum, R.M., Vail, P.R., Sarg, J.F., Loutit, T.S., Hardenbol, J., 1988.  
1488 An overview of the fundamentals of sequence stratigraphy and key definitions, in: Wilgus, C.K., Hastings, B.S.,  
1489 Kendall, C.G. St C., Ross, C.A., Van Wagoner, J.C. (Eds.) *Sea-level changes an integrated approach*. SEPM  
1490 *Special Publication*, 42, pp. 39-45.
- 1491
- 1492 Visscher, H., Krystyn, L., 1978. Aspects of Late Triassic palynology. 4. A palynological assemblage from  
1493 ammonoid-controlled Late Karnian (Tuvallian) sediments of Sicily. *Review of palaeobotany and Palynology*, 26,  
1494 93-112.
- 1495
- 1496 Weimer, R., Howard, J., Lindsay, D., 1982. Tidal flats and associated tidal channels, in: Scholle, P., Spearing, D.  
1497 (Eds.), *Sandstone Depositional Environments*, AAPG Memoir, 31, Tulsa, 191-245.
- 1498
- 1499 Warren, J.K., 2010. Evaporites through time: Tectonic, climatic and eustatic controls in marine and nonmarine  
1500 deposits. *Earth-Science Reviews*, 98, 217–268.
- 1501
- 1502 Warren, J.K., 2006. *Evaporites: Sediments, Resources and Hydrocarbons*. Springer-Verlag, Berlin.
- 1503
- 1504 Warren, J.K., Kendall, C.G.S.C., 1985. Comparison of marine (subaerial) and salina (subaqueous) evaporites:  
1505 modern and ancient. *AAPG Bulletin*, 69, 1013-1023.
- 1506
- 1507 Wilsem, M., Fürsich, F., Seyed-Emami, K., Reza Majidifard, M., Taheri, J., 2009. The Cimmerian Orogeny in  
1508 northern Iran: tectono-stratigraphic evidence from the foreland. *Terra Nova*, 21, 211-218.

1509

1510 Zaitlin, B., Dalrymple, R., Boyd, R., 1994. The stratigraphic organization of incised-valley systems associated  
1511 with relative sea-level change, in: Dalrymple, R., Boyd, R., Zaitlin, B. (Eds.), *Incised-valley systems: origin and*  
1512 *sedimentary sequences*. SEPM Special Publication, 51, Tulsa, pp. 45-60.

1513

**1514 Table captions:**

1515

1516 Table 1: GPS coordinates of measured sections.

1517

1518 Table 2: Summary of principal Upper Triassic-Lower Jurassic facies.

1519

**1520 Figure captions:**

1521

1522 Figure 1: Structural and geological maps of the studied area; a) Main structural features of Tunisia and  
1523 neighbouring regions (after Hallet, 2002; Bouaziz *et al.*, 2002); b) Geological map of the studied area with  
1524 locations of outcrop sections (modified after Raulin *et al.*, 2011).

1525

1526 Figure 2: Palaeogeographical map of the western Neotethys during the Late Triassic (modified from Golonka,  
1527 2007; Marcoux *et al.*, 1993; Stampfli and Borel, 2002).

1528

1529 Figure 3: Lithostratigraphy of Triassic deposits of Tunisia and southeastern Algeria (modified from Bouaziz  
1530 1995; Bourquin *et al.*, 2010; Ben Ismail, 1982; Kamoun *et al.*, 2001; Hamouche, 2006; Galeazzi *et al.*, 2010)

1531

1532 Figure 4: Main carbonate facies in outcrops; a) Green marls (Mgr) of offshore environment alternating with  
1533 peloidal dolomitic beds of the facies Dn. Note the upper undulated surfaces of beds and the internal aggrading  
1534 HCS (Rehach formation, Rehach quarry section); b) Upper surface of a shelly bed interpreted as storm deposits  
1535 in the facies Dn (Rehach formation, Rehach quarry section); c) *Rhizocorallium jenense* burrow in the shallow  
1536 subtidal facies Dbp (Rehach formation, Rehach quarry section); d) Oolitic and sandy calcarenite of the Dos  
1537 subfacies showing tidal criterions such as current ripples (Cr) draped by mud drapes (Md) and bidirectional cross  
1538 beddings (Tb) containing reworked dolomitic clasts (Sc) (Rehach formation, Kef El Amba quarry); e) Dof

1539 subfacies with current ripples (arrows) and rhythmic variations in the calcarenite (Cr) and mud drapes (Md) ratio  
1540 interpreted as spring tides (St) and neap tides (Nt) cycles (Rehach formation, Kef El Amba quarry); f) Massive  
1541 dolomite of the facies Dh with aligned centimetric vugs interpreted as the result of dissolution of evaporite  
1542 nodules (Rehach formation, Rehach quarry section); g) Hardground with borings (B) at the top of a stromatolitic  
1543 dolomite bed in the Ds facies (Rehach formation, Warjaijine section); h) Thick stromatolitic dolomites (facies  
1544 Ds) with vugs of evaporite dissolution (arrows) (Rehach formation, Kef El Touareg section); i) Desiccation  
1545 polygons associated with stromatolites of the facies Ds (Rehach formation, Achaab Messaoudi section); j)  
1546 Chaotic monogenic dolomitic breccia (facies Db) interpreted as collapse breccias. Note the red sandy matrix  
1547 between dolomite clasts (Rehach formation, Ouadi Hallouf); k) Lateral relationship between dolomitic breccias  
1548 (Db) and stromatolitic dolomites (Ds). Breccia is the result of the break of algal mats by dissolution of evaporites  
1549 and collapse without transport (Messaoudi formation, Achaab, Rijjilah section); l) Tepee structures  
1550 characterized by megapolygons with buckled margins (facies Sdm). The sediment corresponds to a sandy  
1551 dolomite with algal mats. Circled hammer for scale (Mhira formation, Achaab Messaoudi section).

1552  
1553 Figure 5: Main carbonate microfacies. a) Peloidal and bioclastic packstone of the facies Dn (Ras3 sample, plane-  
1554 polarized light, Rehach formation, Achaab Messaoudi section); b) Peloidal grainstone (Dbp facies) with  
1555 extensive residual intergranular porosity (in blue) (RIJ-RE2 sample, plane-polarized light, Rehach formation,  
1556 Rijjilah section); c) Coprolithes (arrows) in the Dbp facies (RE-CS2 sample, plane-polarized light, Rehach  
1557 formation, Rehach quarry section); d) Dolomitized oolitic and bioclastic (B: bivalve; G: gastropod) grainstone of  
1558 the facies Do with a significant intergranular porosity (RQ5 sample, plane-polarized light, Rehach formation,  
1559 Rehach quarry section); e) Same facies that in picture d with a high content in subangular quartz grains (B:  
1560 Bivalve; G: gastropod) (ST4 sample, plane-polarized light, Rehach formation, Sidi Stout section); f) Grainstone  
1561 with ooids (arrows) alternating with laminated algal mats in the Do facies (RE-CS3 sample, plane-polarized  
1562 light, Rehach formation, Rehach quarry section), g) Homogeneous idiotopic dolomite of the Dh facies with  
1563 molds of shells filled by dickite (KAF9 sample, plane-polarized light, Rehach formation, Kef Touareg section);  
1564 h) Dissolution vug filled by dickite in homogeneous idiotopic dolomite (Dh facies) (KAF-RE2 sample, cross-  
1565 polarized light, Rehach formation, Kef Touareg section); i) Dissolution vug in the Dh facies with calcite pendant  
1566 cement (pink) precipitated during vadose diagenesis (KAS-AY3 sample, plane-polarized light, Rehach  
1567 formation, Achaab Messaoudi section); j) Fenestral structure between algal mats in stromatolitic dolomite of the  
1568 Ds facies. Note the extensive porosity due to the fenestral vugs (KAS-AY2 sample, plane-polarized light,

1569 Rehach formation, Achaab Messaoudi section); k) Dolomite rhombs with dissolved cores (in blue) in the Db  
1570 facies. Dedolomitization is probably due to dissolution by aggressive meteoric waters below surfaces of  
1571 prolonged subaerial exposure (MOG3 sample, plane-polarized light, Mogor formation, Mogor section); l)  
1572 Fracture infill below megapolygons of the facies Sdm. The matrix (Mx) is recrystallised as microspar and  
1573 fracture is mainly filled by mammillary radiaxial calcite (Rc) (*sensu* Assereto and Kendall, 1977); The last stage  
1574 of cementation consists of fibrous pendant cements formed in a vadose environment (RAS7 sample, plane-  
1575 polarized light, Mhira formation, Achaab Messaoudi section).

1576  
1577 Figure 6: Main siliciclastic and evaporitic facies; a) Stacking of storm washover deposits (facies Dg) on lagoonal  
1578 stromatolitic dolomite (Ds). Storm deposits are characterized by erosional basal surfaces (Es) and a positive  
1579 vertical grading with angular oblique laminations (Zerzour formation, Zerzour section); b) Alternation of  
1580 stromatolitic gypsum (*sensu* Peryt, 2001) (Stg), nodular anhydrite (Ns) and fibrous gypsum (Fg) in the facies Ev  
1581 (Messaoudi formation, Zerzour section); c) Rosette gypsum in red shales of the Fre facies (Mhira formation,  
1582 Sebkhet Leguine section); d) Gypsified rootlets (arrows) in the continental evaporitic flat facies Fre (Mhira  
1583 formation, Sebkhet Leguine section); e) Poorly sorted conglomerate with sandstone boulders (Sb), and  
1584 subangular dolomite and basement pebbles in the facies Gm. Db = brecciated dolomite, Mx = matrix (Moghor  
1585 formation, Moghor section); f) Red silty shales (Fl facies) overlain by microconglomeratic sandstones (Sg facies)  
1586 through an erosional surface (Es). The circled hammer is 33 cm long (Kef El Amba 2 section); g) Climbing  
1587 ripples in fine grained sandstones of the facies Fl (Touareg formation, Kef Touareg section); h) Trough cross  
1588 bedding in conglomerates and sandstones of the facies Sg. Note the occurrence of an erosional surface (Es)  
1589 between conglomerates and sandstones. The basal surface of the channel (Bc) is erosive on alluvial shales (Fl)  
1590 (Kef El Amba 2 section); i) Sigmoidal cross bedding in sandstones of the Std facies (Touareg formation, Rijjilah  
1591 section); j) Thin mud drapes (white arrows) associated with small current ripples (black arrow) in the bottomset  
1592 of sigmoidal cross beddings (facies Std) (Touareg formation, Rijjilah section).

1593  
1594 Figure 7: Correlation diagram in the J. Rehach area.

1595  
1596 Figure 8: Sedimentological features of Rehach dolomites. a) Complete shallowing upward semi cycle with the  
1597 vertical evolution of facies in the Rehach formation of the Achaab Messaoudi section; b) Lag of red dolomitic  
1598 clasts at the base of the Touareg formation (Rejjilah section); c) Parasequences from shallow lagoonal to

1599 intertidal stromatolites in the upper part of the Rehach Fm. Note the red colored surfaces (arrows) often  
1600 containing microscopic rootlets (Rehach quarry section); d) Multicolored shales below a carbonate paleosoil  
1601 (arrow). The upper surface corresponds to the sequence boundary of the sequence RM3 (Rehach quarry section).

1602

1603 Figure 9: Stacking pattern diagrams of the Kef El Galala and Kef El Amba sections.

1604

1605 Figure 10: Upper part of the Aachab El Messaoudi section and field distribution of the Kronab conglomerates  
1606 between Rehach dolomites and the Mhira Fm. in the Aachab El Messaoudi and Beni Ahmed area.

1607

1608 Figure 11: Correlation diagram in the North Dahar.

1609

1610 Figure 12: Panorama of the Sidi Stout unconformity in the Sidi Stout Bhyira area. Tilted lower Triassic  
1611 siliciclastic strata are truncated and unconformably covered by upper Triassic dolomites.

1612

1613 Figure 13: Key surfaces in the North Dahar area; a) Flooding characterized by a thin bed of brecciated dolomites  
1614 (Db) above a transgression surface (TS) in the alluvial fan conglomerate (Gm) of the Mogor section.; b) Surface  
1615 of prolonged subaerial exposure in the Ouarjajine section characterized by a hematitic crust at the top of a  
1616 highly brecciated dolomite.

1617

1618 Figure 14: Location map of studied outcrops and subsurface transects 1 and 2.

1619

1620 Figure 15: Correlation diagram between the J. Rehach outcrops and the Garaet El Atsel 1 well.

1621

1622 Figure 16: Geometries and sequence stratigraphy of Upper Triassic and Lower Jurassic deposits along the  
1623 transect 1.

1624

1625 Figure 17: Geometries and sequence stratigraphy of Upper Triassic and Lower Jurassic deposits along the  
1626 transect 2; a) southern part of the transect; b) northern part of the transect in the vicinity of the Tebaga of  
1627 Medenine.

1628

1629 Figure 18: Model of tectonosedimentary evolution of Central and Southern Tunisia between the Carnian and the  
1630 Pliensbachian.

1631

1632 Figure 19: Sketches of possible stratigraphic evolutions of Upper Norian to Rhaetian deposits in the Ghadames  
1633 basin. a) Stratigraphic evolution in a case of total draining of the basin; b) Stratigraphic evolution in the case of a  
1634 normal flooding of Rhaetian salts on Norian shales without draining and exposure of the basin. In this case  
1635 exposure on uplifted area can be correlated with a transgressive surface without lowstand deposits during an  
1636 increase of the subsidence in the basin. See text for explanations.

1637

1638 Figure 20: Synthesis diagram of sequential and geodynamic evolution of neighbouring regions with stratigraphic  
1639 location of main unconformities.

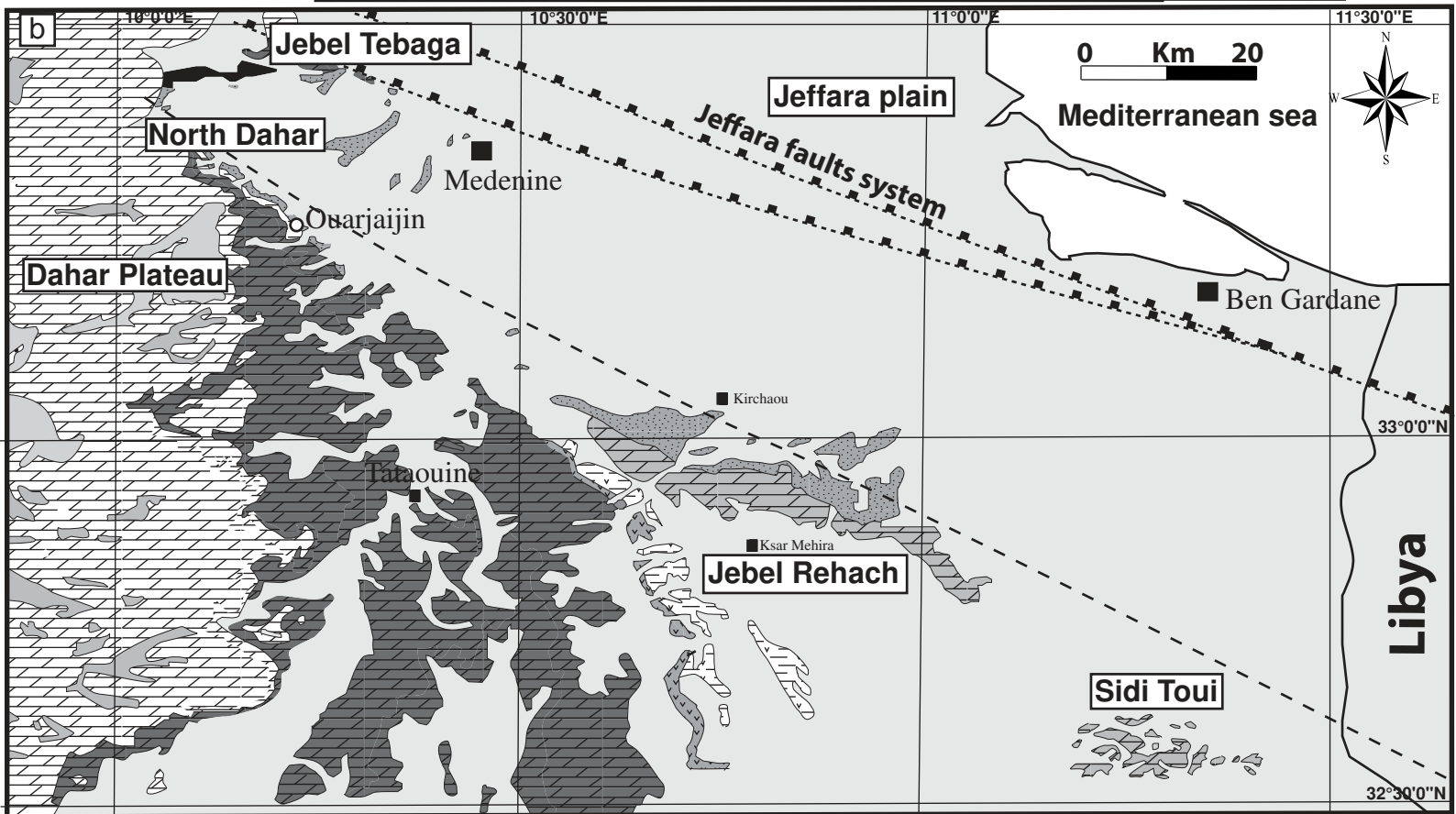
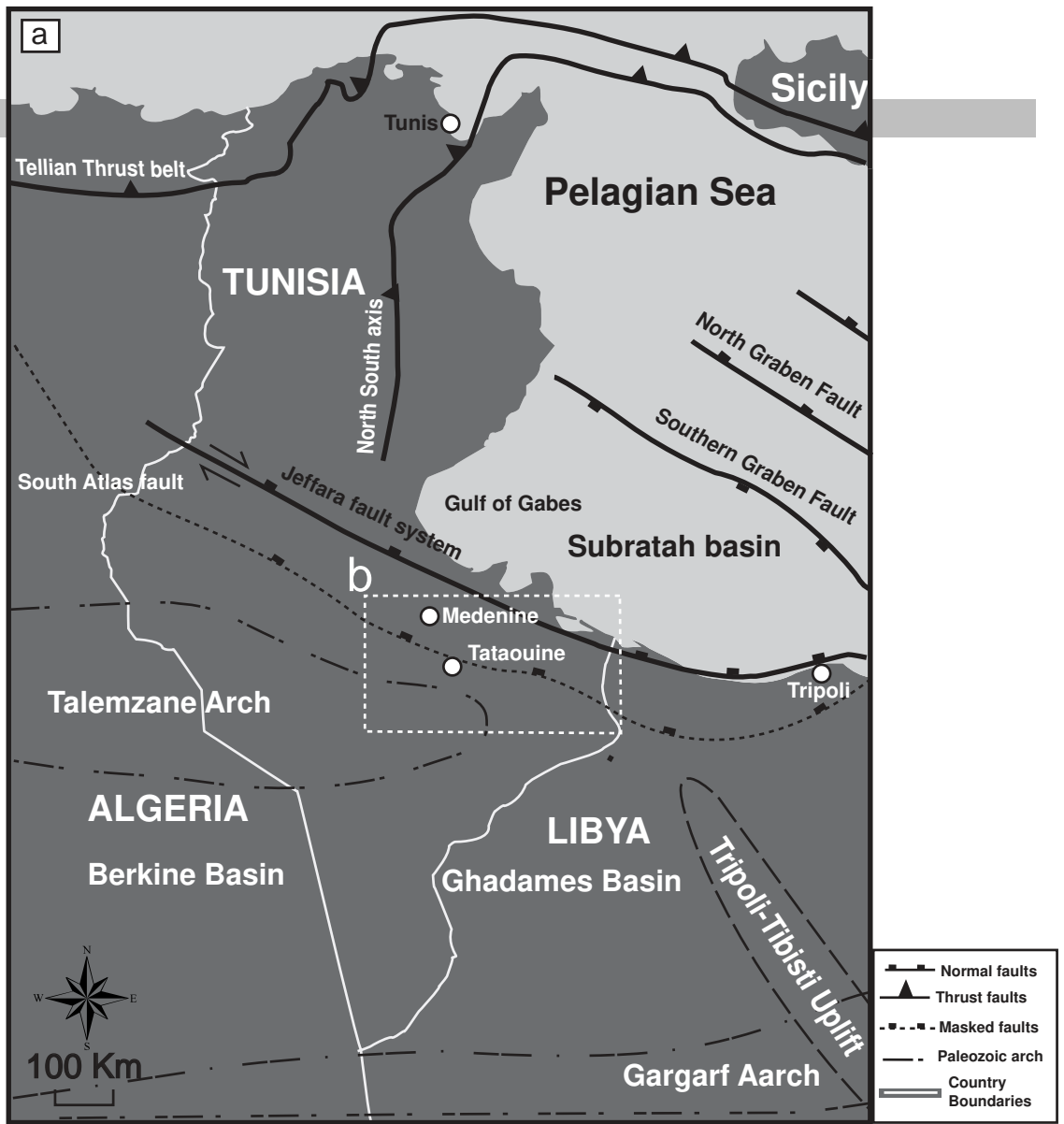
1640

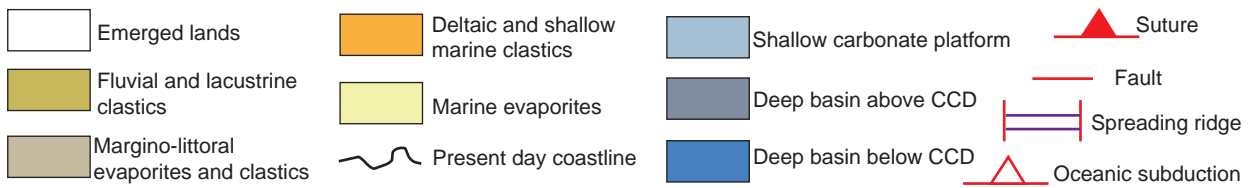
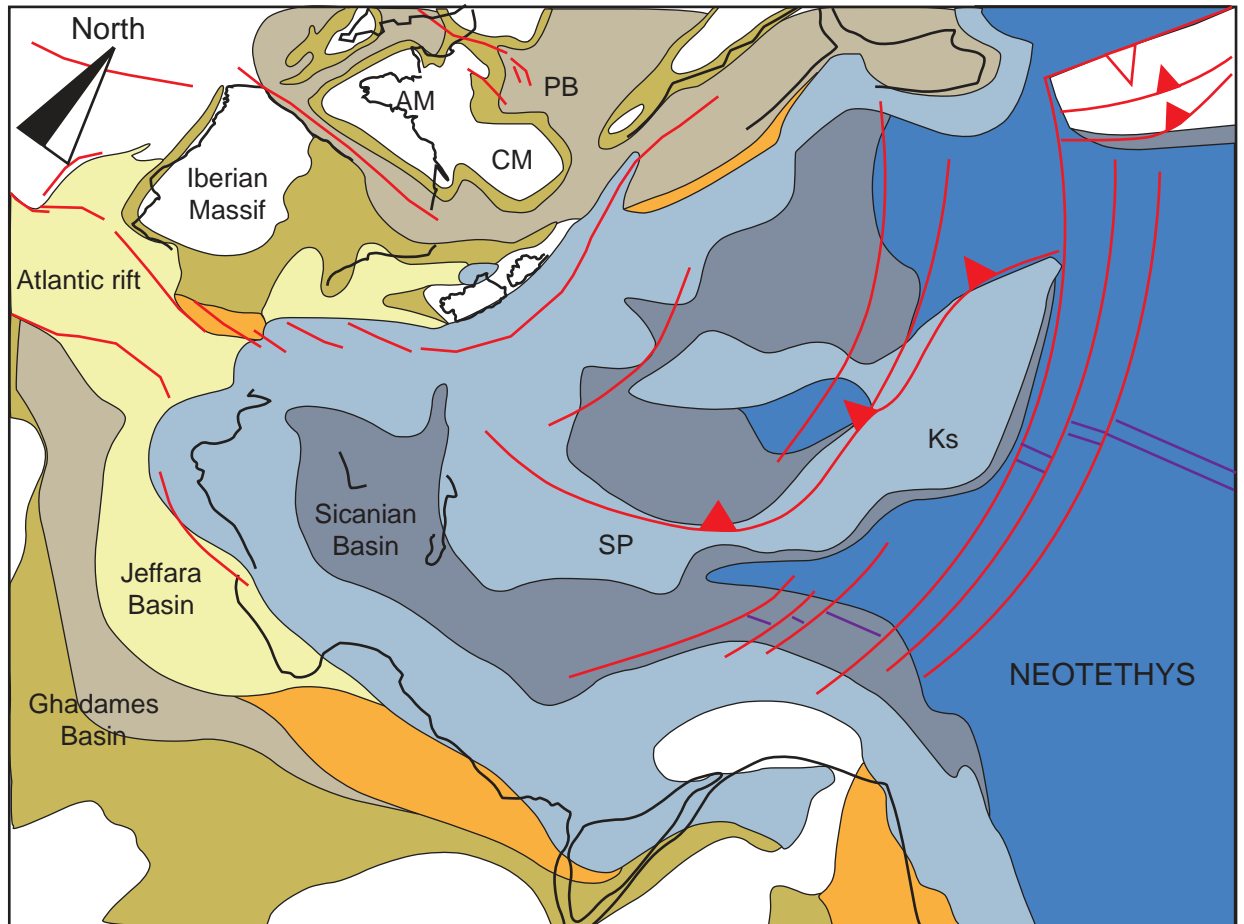
1641

1642

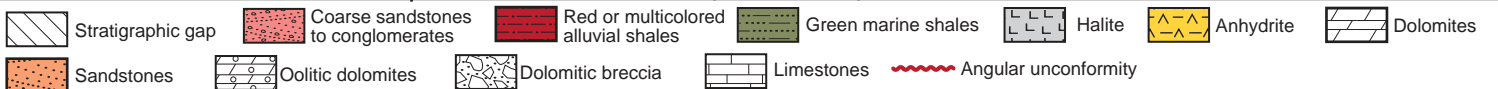
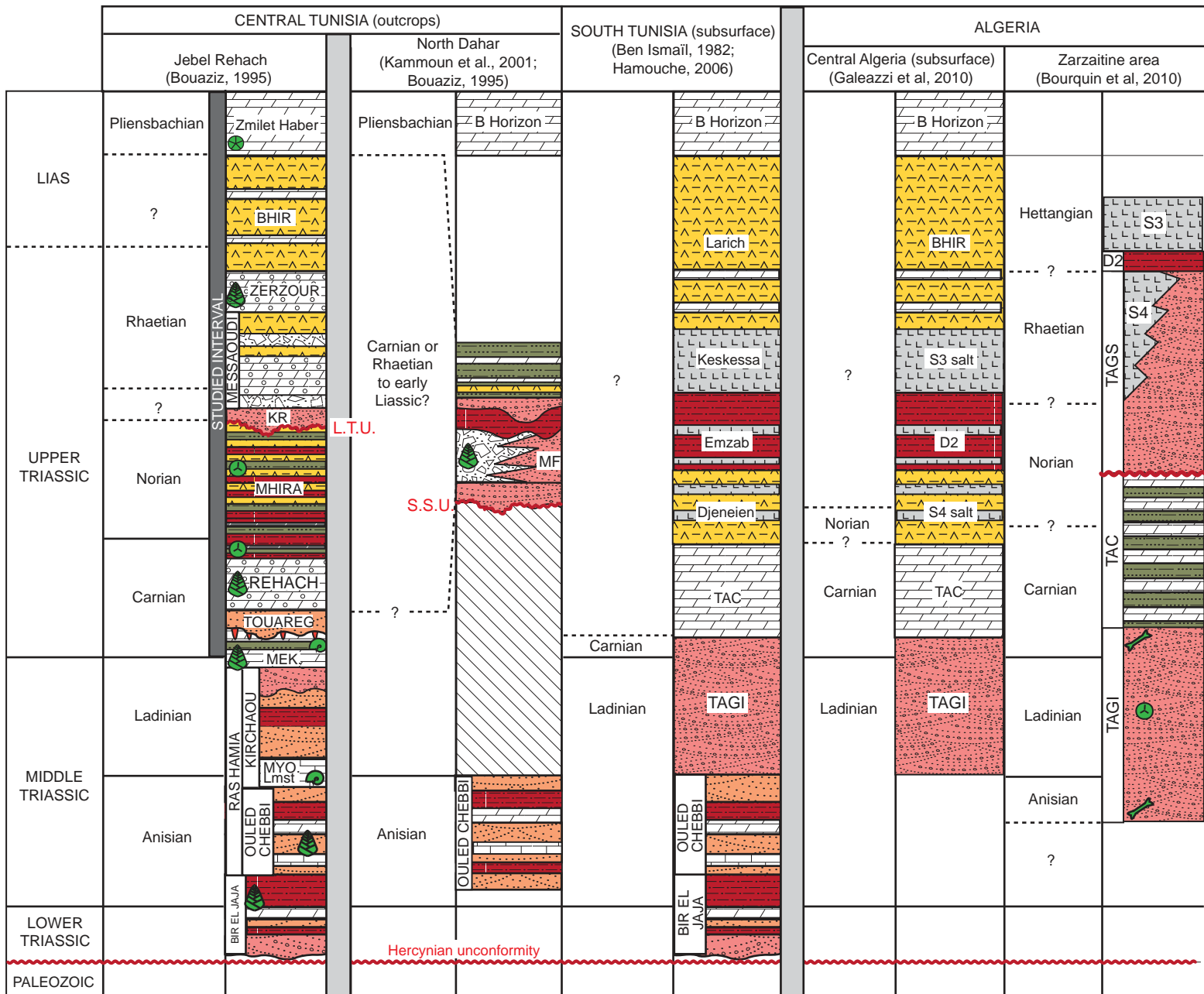
Section Name				
	Base		Top	
	Latitude	Longitude	Latitude	Longitude
Moghor	33°21'05.17"N	10°11'39.64"E	33°20'55.22"N	10°11'32.13"E
Wadi Hallouf	33°18'51.39"N	10°13'17.86"E	33°18'53.79"N	10°13'11.22"E
Sidi Stout 2	33°18'56.42"N	10°13'59.9"E	33°18'54.47"N	10°13'58.38"E
Sidi Stout 1	33°18'40.45"N	10°14'13.90"E	33°18'35.94"N	10°14'19.87"E
Kef El Anba I	33°16'22.06"N	10°18'13.3"E	33°16'20.2"N	10°18'05.5"E
Kef El Anba II	33°16'25.24"N	10°17'0.52"E	33°16'38.74"N	10°17'3.49 "E
Ouarjajin	33°14'50.9"N	10°19'39.1"E	33°14'52.2"N	10°19'33.4"E
Rijjilah I	33°0'18.04"N	10°42'59.89"E	33°0'26.63 "N	10°43'1.56"E
Rijjilah II	32°59'56.86"N	10°43'24.01"E	32°59'51.3 2"N	10°43'17.93"E
Rijjilah III	33°0'6.67"N	10°43'37.00"E	33°0'0.88 "N	10°43'36.29"E
Rijjilah IV	32°58'50.40"N	10°44'47.01"E	32°58'55.8 2"N	10°44'50.73"E
Shabat El Zitouna	32°57'9.07"N	10°46'58.89"E	32°57' 6.00"N	10°46'54.64"E
Kasbat El Drina	32°59'7.26"N	10°36'59.24"E	32°59'3. 66"N	10°36'59.45"E
Rehach quarry	32°56'55.16"N	10°50'46.64"E	32°56'35. 39"N	10°50'18.93"E
Kef El Touareg I	32°57'32.71"N	10°53'0.28"E	32°57'2 6.16"N	10°52'33.77"E
Kef El Touareg II	32°57'21.59"N	10°52'54.21"E	32°57 '14.27"N	10°52'50.55"E
Ksar Rehach	32°54'30.23"N	10°57'15.18"E	32°54'30.50 "N	10°57'9.10"E
Achaab El Messaoudi	32°56'53.05"N	10°44'49.97"E	3 2°56'42.90"N	10°44'47.89"E
Beni Ahmed I	32°55'18.22"N	10°45'22.2"E	32°55'16. 50"N	10°45'23.05"E
Beni Ahmed II	32°55'46.3"N	10°45'51.2"E	—————	—————
Ksar Mhiri	32°52'25.8"N	10°49'24.8"E	32°52'26.09" N	10°49'25.74"E
Sabkhat El Guine I	32°47'52.5"N	10°52'18.3"E	32°4 7'29.5"N	10°52'48.1"E
Sabkhat El Guine II	32°46'20.9"N	10°50'41.0"E	32° 46'18.24"N	10°50'38.30"E
Galib El Zarzour	32°54'18.5"N	10°43'43.1"E	32°54' 17.83"N	10°43'27.68"E
Galib Limesane	33°1'29.08"N	10°39'7.47"E	33°01'27. 7"N	10°39'09.6"E
Kef El Galalah	32°57'42.1"N	10°48'08.2"E	32°57'47 .5"N	10°48'27.2"E
Zmilet Haber	32°56'25.9"N	10°40'39.1"E	32°56'19.0 "N	10°40'28.9"E

Lithofacies type	Lithology, texture and diagenetic features	Sedimentary structures	Biogenic structures	Macro-paleontological content	Interpretations
<b>Carbonate facies:</b>					
(Mgr) Green Marls	Very fine and locally nodular marls	_____	Diffuse bioturbation	Bivalves, echinoids, rare ammonoids and nautiloids (Nautilus Klipsteini), nothosaurian teeth and conodonts	Lower offshore
(Dn) Nodular peloidal dolomite	Yellow to beige nodular beds of dolomitized peloidal packstone	Thin shell beds (5 cm thick) and hummocky cross stratifications	Intensive diffuse bioturbation, rare preserved <i>Thalassinoides</i> burrows	Clasts of brachiopods, oysters, sea-urchin spines and crinoids	Storm dominated upper offshore
(Dbp) Bioclastic peloidal dolomite	Grainstone to packstone	Massive beds of peloidal dolomite and wave ripples	<i>Thalassinoides</i> and <i>Rhizocorallium jenense</i> burrows	Clasts of oysters, echinoid spines, crinoid articles, and brachiopods. Crenulated coprolites	Wave dominated shoreface
(Do) Oolitic and bioclastic dolomite					
<i>Dos</i> subfacies	Dolomitized bioclastic and oolitic grainstone. Mudstone alternations	Current ripples, herring bone stratifications, horizontal and low angle stratifications, mud drapes (flaser bedding)	_____	Bivalve shells and gastropods	Tide dominated oolitic shoal
<i>Dof</i> subfacies	Oolitic packstone to grainstone. Mudstone alternations	Spring and neap tide cycles, current ripples and mud drapes (wavy and lenticular bedding)	Scarce algal mats laminations	Scarce bivalve shells	Oolitic tidal flat
(Dh) Homogeneous vuggy dolomite	Dolospar with an idiopic texture, moldic porosity and vugs of evaporite dissolution filled by dickite or microstalactitic cements	_____	_____	Dissolved bivalve shells	Subtidal hypersaline lagoon
(Ds) Stromatolitic dolomite	Dolomitized peloidal packstones, vugs of evaporite dissolution filled by dickite or micro-stalactitic cements	Fenestrae texture, desiccation cracks	Agglutinated stromatolites and <i>Gastrochaenolites</i> borings	_____	Intertidal to lower supratidal inner ramp
(Db) Dolomitic breccias	Clast supported dolomitic breccia with sandy matrix. Local intercalations of chicken wire, enterolithic and fibrous gypsum	_____	Stromatolites	_____	Collapse breccia, prolonged subaerial exposure
(Dg) Graded oolitic dolomites	Dolomitized oolitic and bioclastic grainstone to packstone intercalated in Ev facies	Sharp erosive base and vertical normal grading. Planar oblique and horizontal laminations	_____	Clasts of oysters, echinoid spines, crinoid articles	Washover deposits
<b>Evaporitic facies:</b>					
(Ev) Evaporite and stromatolite alternations					
<i>Evs</i> subfacies	Chicken wire nodules or enterolithic beds of anhydrite alternating with selenite gypsum	_____	Stromatolites	_____	Subtidal-hypersaline lagoon and sebkha
<i>Evm</i> subfacies	Yellow and green silty marls with twined gypsum layers	_____	Stromatolites	_____	Subtidal-hypersaline lagoon
(Fre) Evaporitic red shales	Red shales with beds of twined, nodular (chicken wire) or lenticular gypsum	_____	Petrified rootlets in lenticular gypsum	_____	Continental playa lake and continental sabkha
<b>Siliciclastic facies:</b>					
(Gm) Massive conglomerates	Matrix supported polygenic conglomerates. Angular to subrounded clasts of Permian reef, dolomites, sandstones and metamorphic basement rocks.	Debris flow deposits, lack of tractive current structures	_____	_____	Alluvial fan
(Fl) Red silty shales	Red to brown and locally green silty shales. Intercalations of fine grained sandstones	Type A climbing ripples in fine grained sandstones	_____	_____	Alluvial plain
(Sg) Graded sandstones	Polygenic clast support conglomerates and coarse to medium grained sandstones	Basal erosive surface overlain by graded sequences of conglomerates and sandstones with trough cross-bedding.	_____	_____	Braided channel
(Std) Cross stratified sandstones	Medium grained quartzarenite and thin silty or clay layers	Sigmoidal cross-bedding, small ripples and silt or clay drapes on the toe of cross-bedded bedforms. Few clues of palaeo-current reversals	Scarce <i>Skolithos</i> burrows	_____	Fluvial tidally influenced
(Sdm) Dolosandstone with megaplygons	Dolomitic sandstone and green shales	Tepee structures and desiccation cracks	<i>Gyrophyllites</i> burrows	_____	Supratidal to upper intertidal





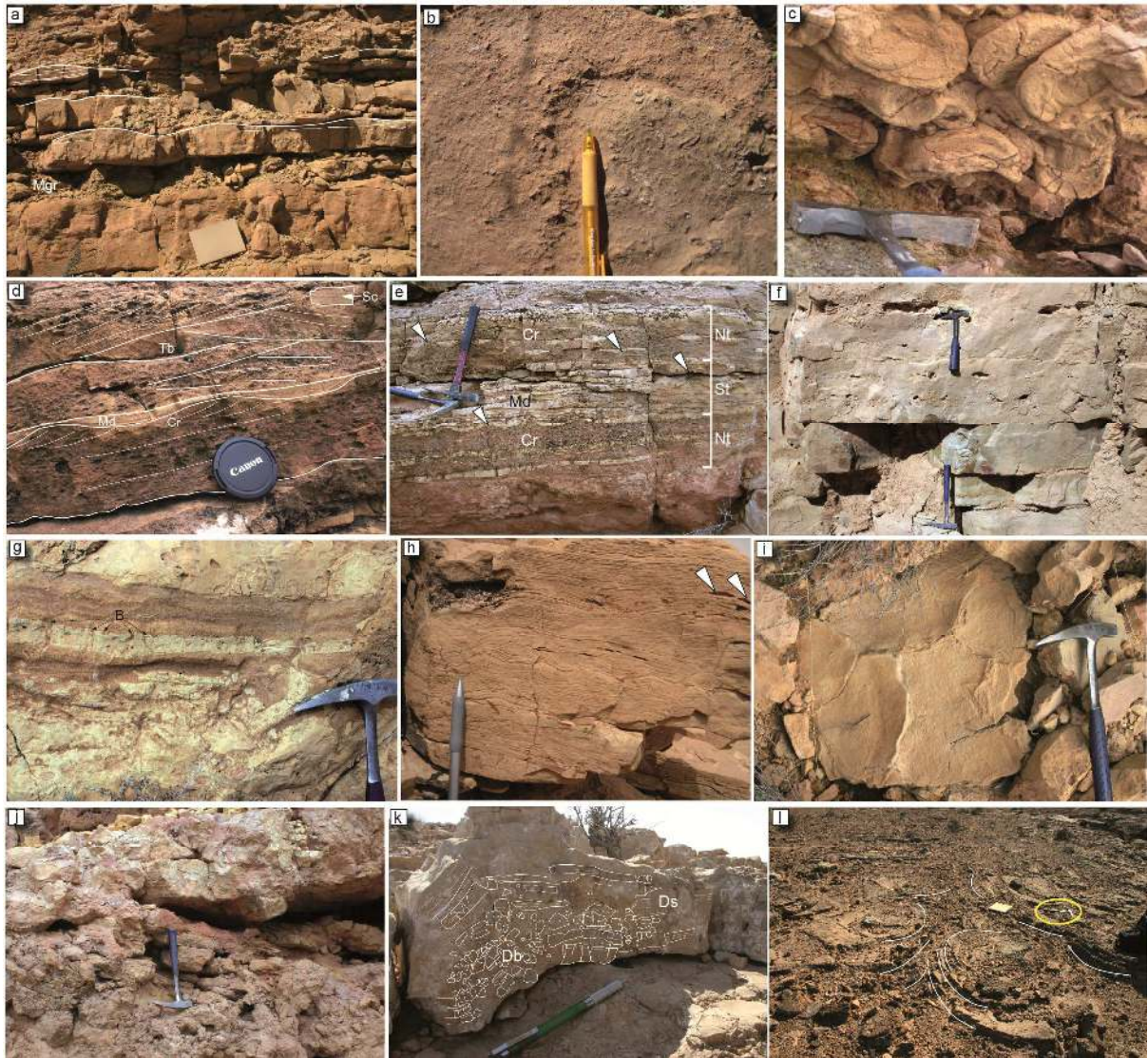
AM = Armorican Massif   CM = Central Massif   Ks = Kirsehir   PB = Paris Basin   SP = Serbo-Pelagonian terrane

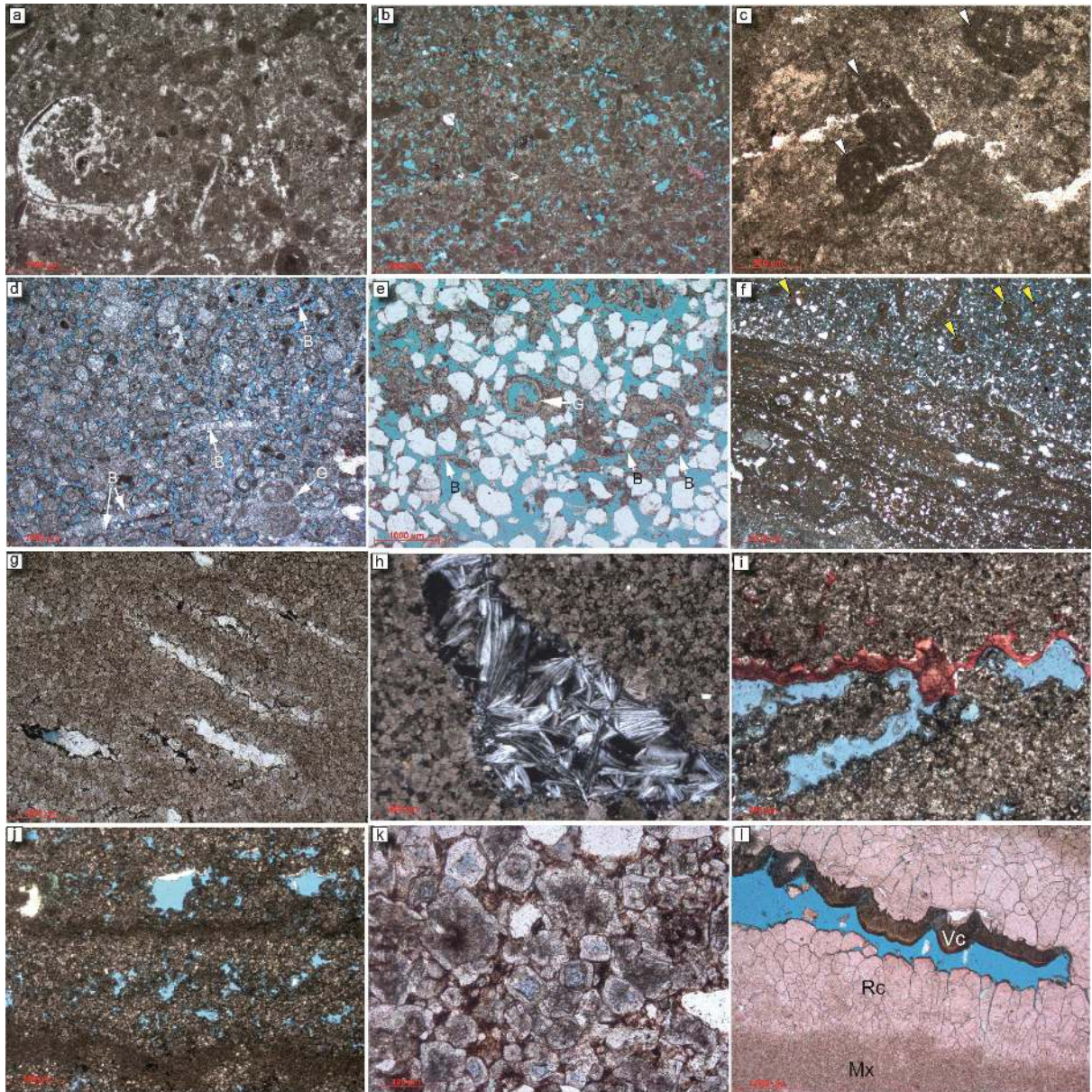


Direct dating with foraminifera    
 Direct dating with ammonites    
 Direct dating with pollens    
 Direct dating with vertebrates    
 Direct dating with echinoids

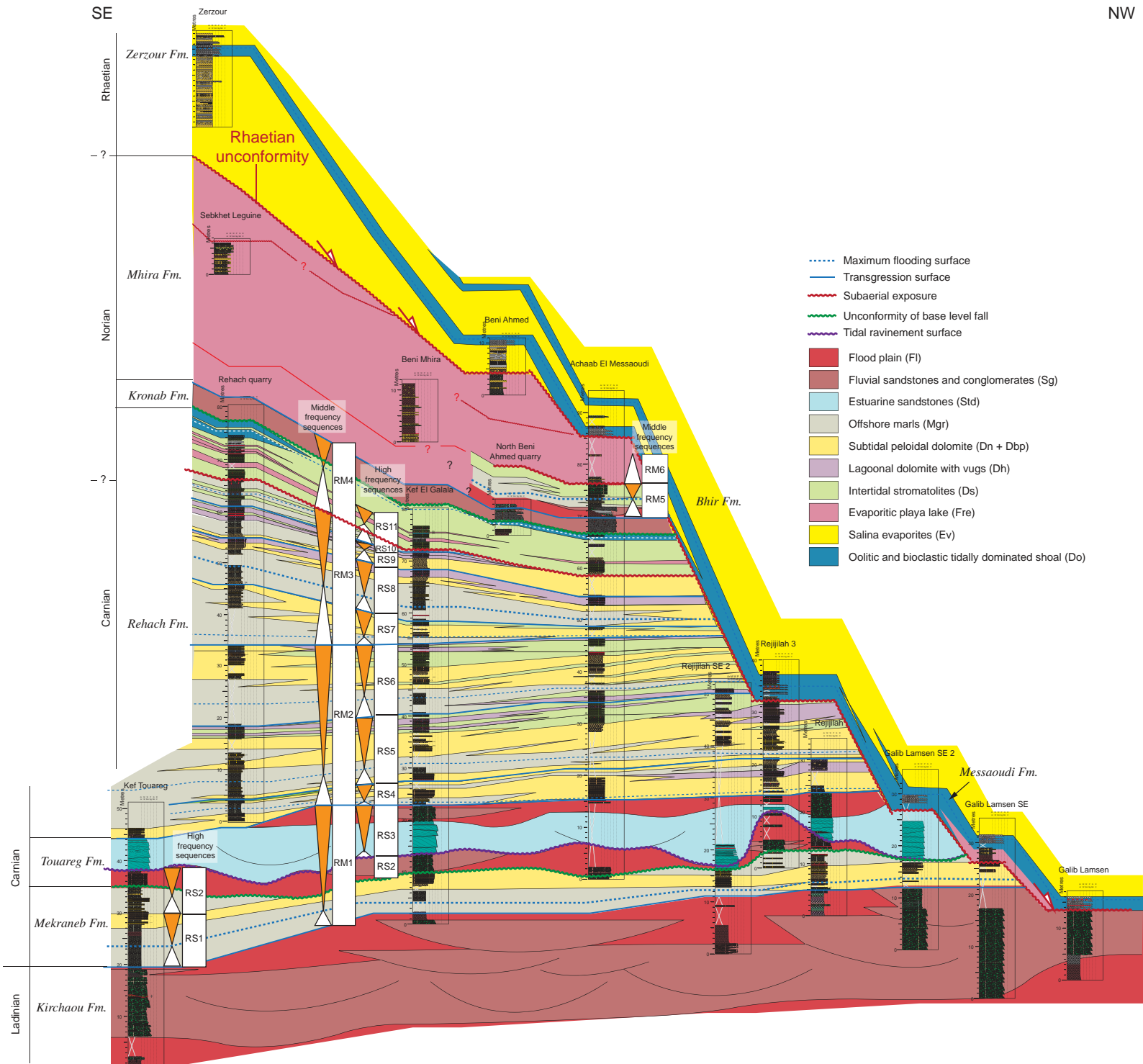
L.T.U. = Late Triassic Unconformity    
 S.S.U. = Sidi Stout Unconformity    
 MEK. = Mekraneb Fm.    
 KR = Kronab Fm.    
 MYO. Lmst = *Myophoria* limestones    
 MF = Mougou Fm.

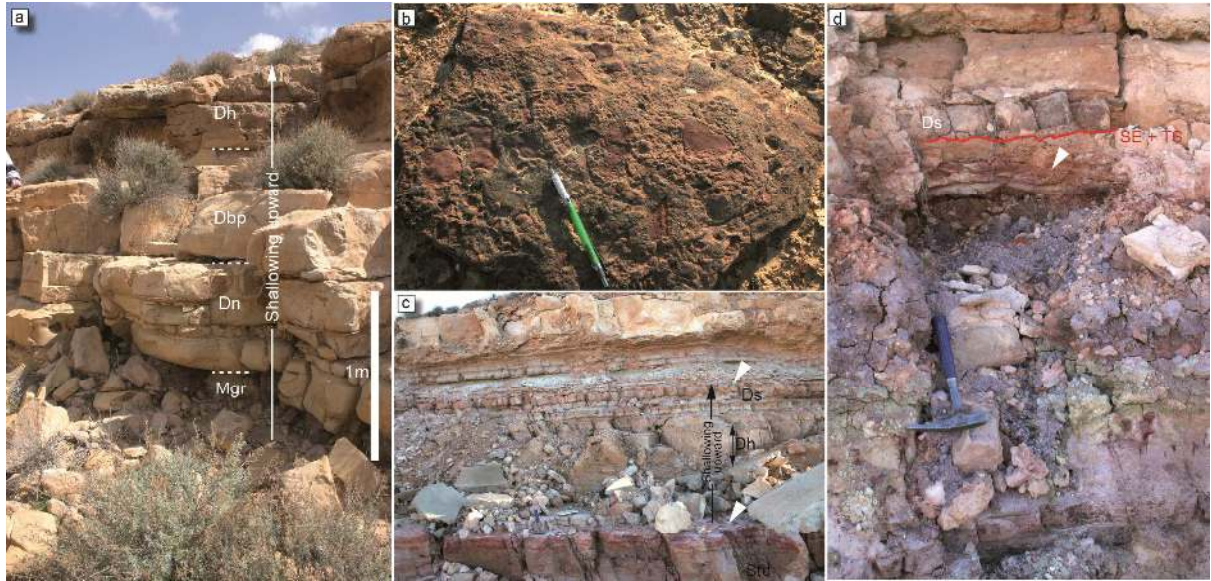
TAGI = Trias Argilo Gréseux inférieur    
 TAC = Trias Argilo carbonaté    
 TAGS = Trias Argilo Gréseux supérieur





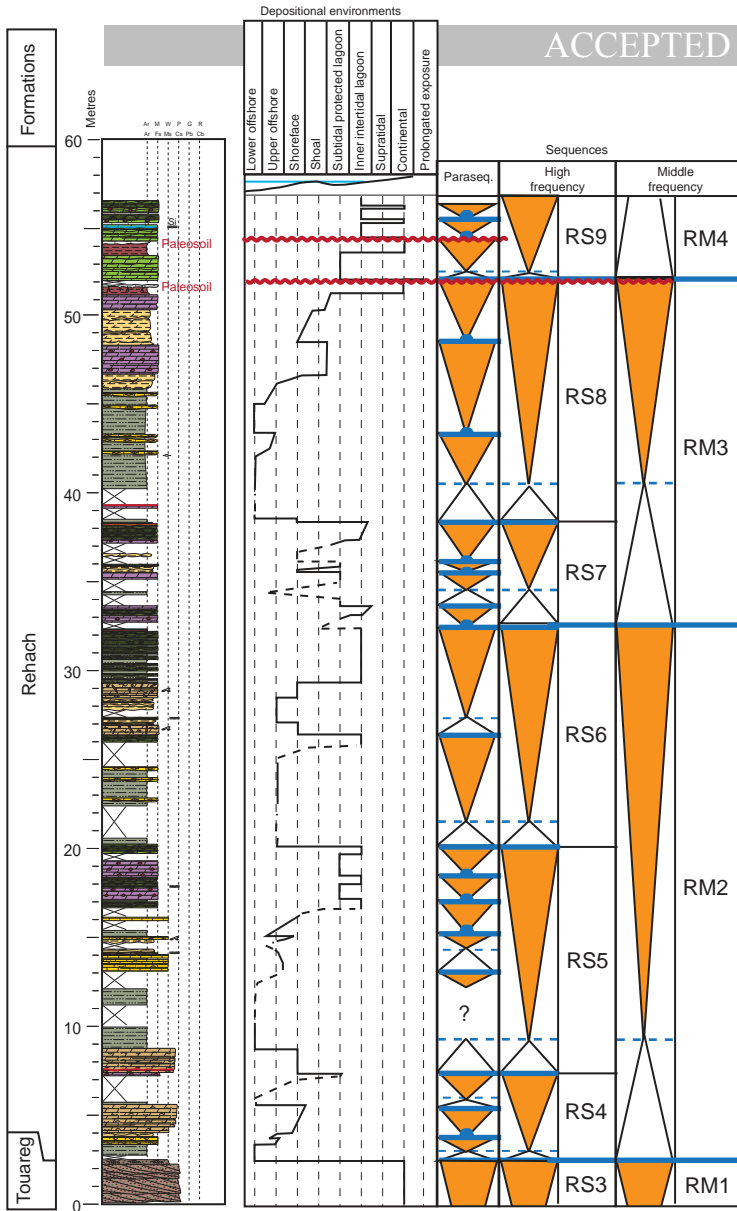




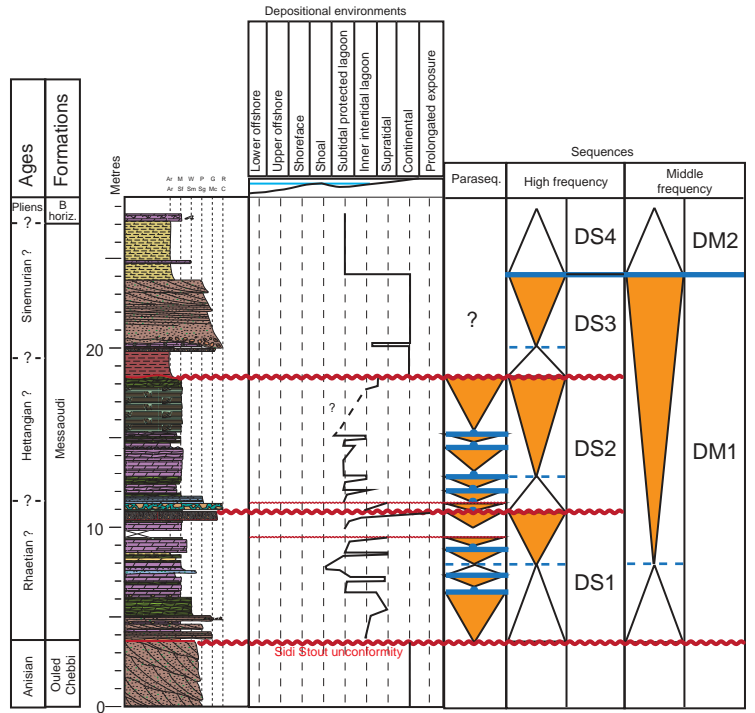


# Kef El Galala

ACCEPTED MANUSCRIPT

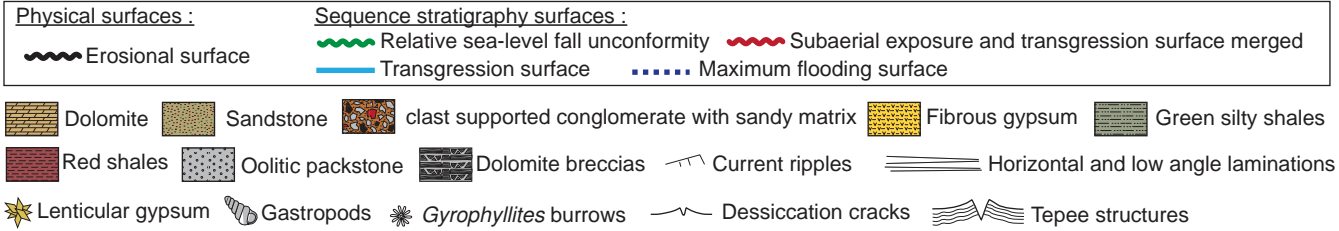
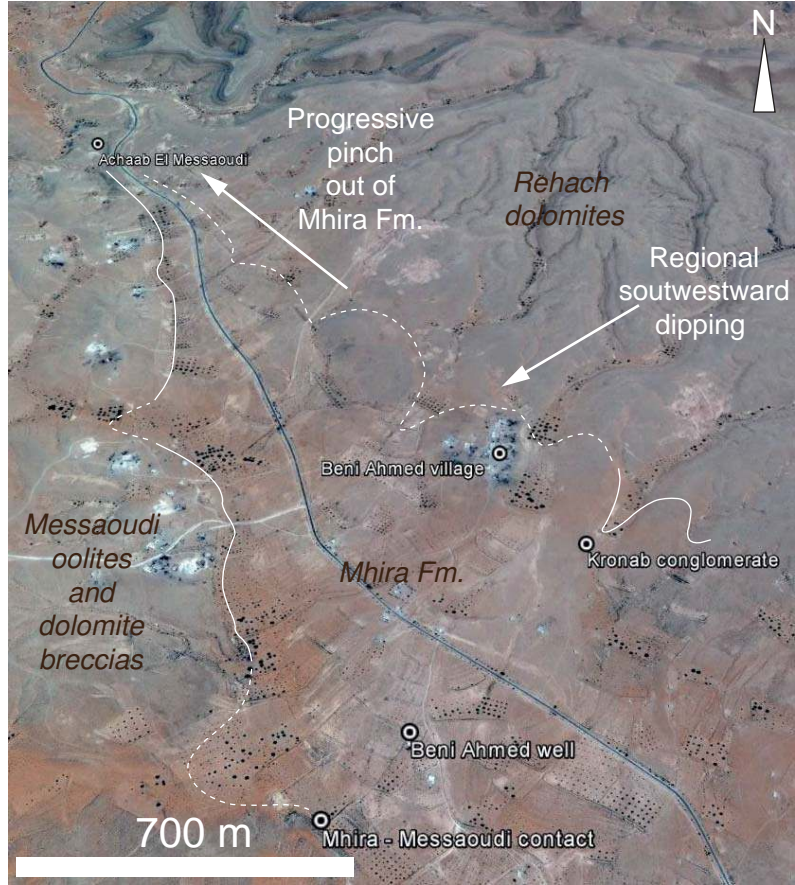
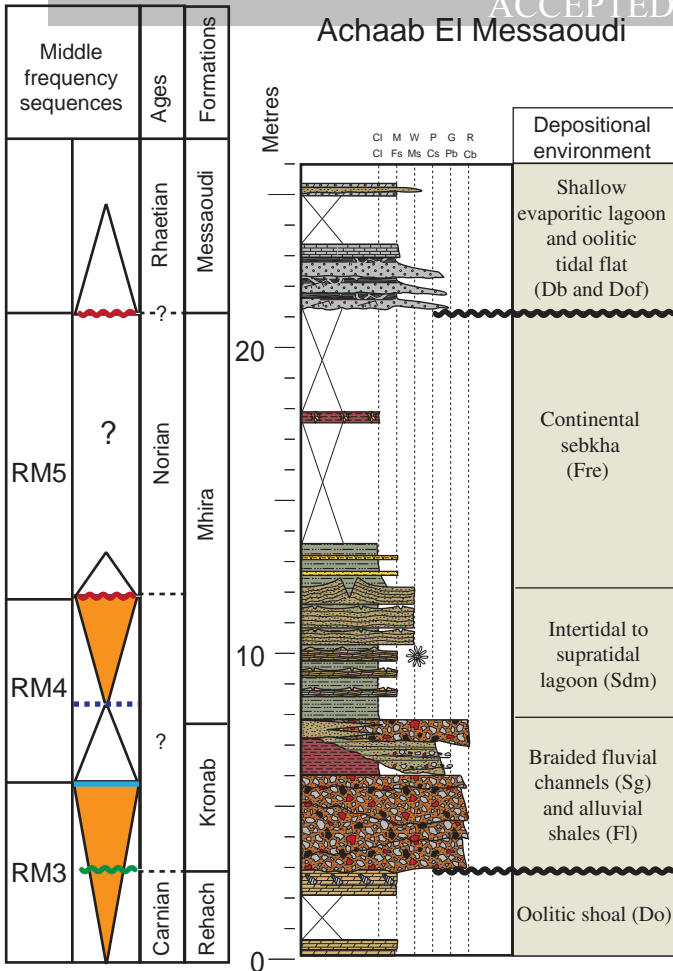


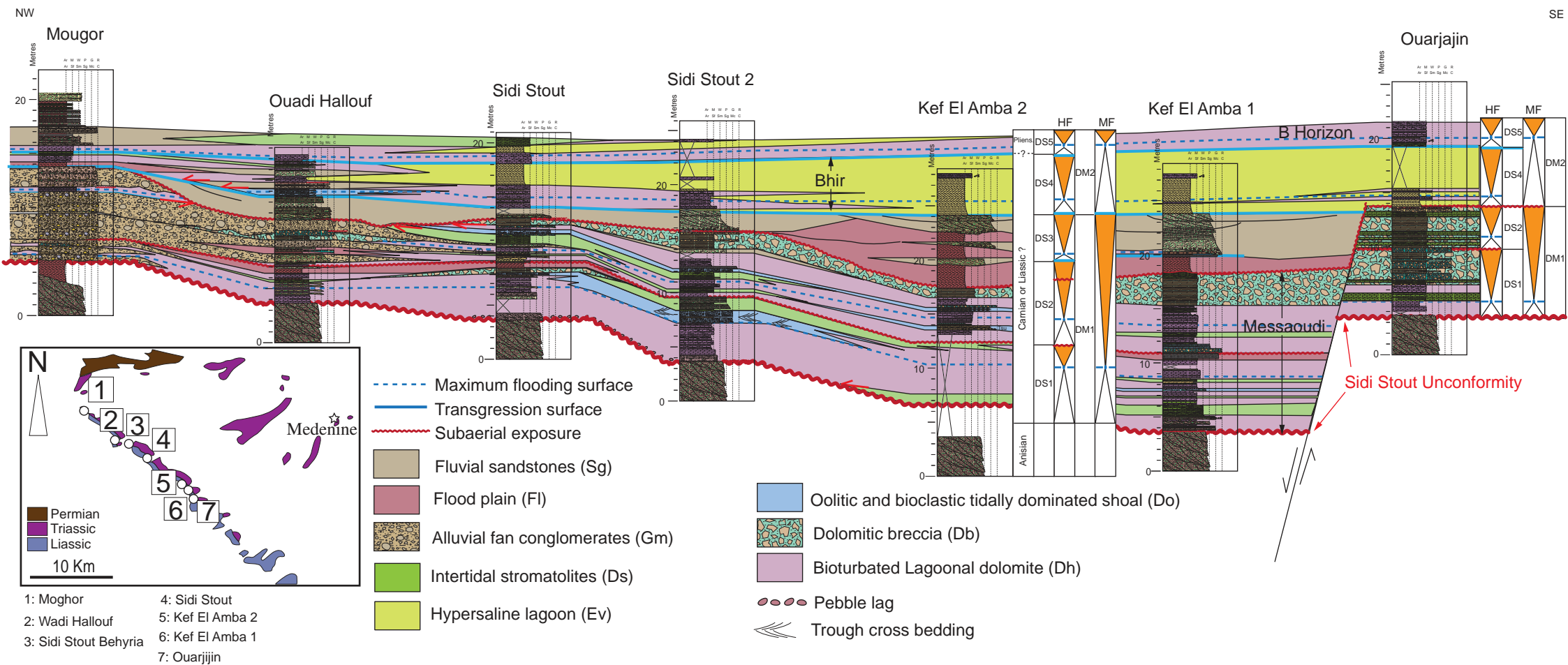
# Kef El Amba

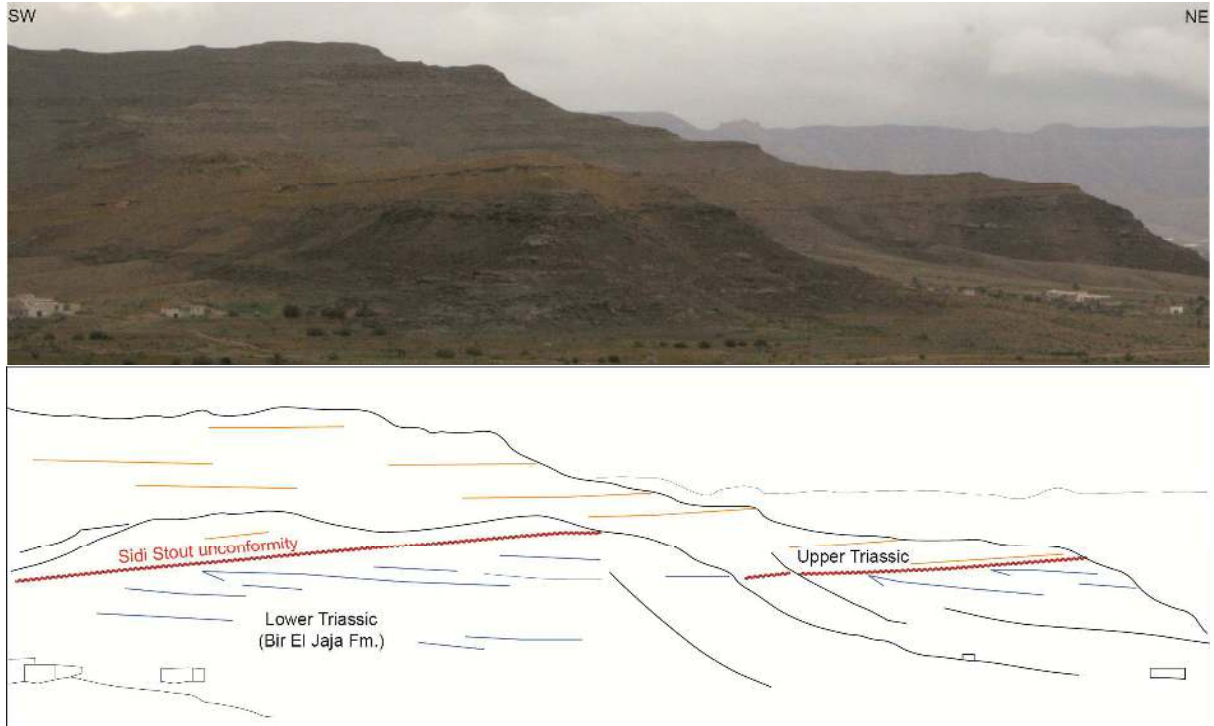


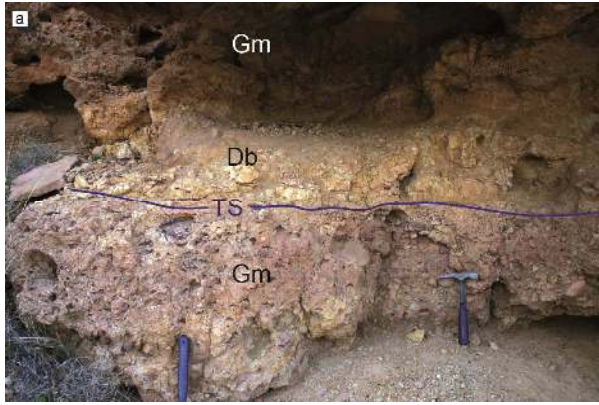
- Flood plain (Fl)
- Fluvial sandstones (Std)
- Offshore marls (Mgr)
- Lagoonal dolomite with vugs (Dh)
- Dolomite breccia (Db)
- Bioclastic peloidal dolomite (Dbp)
- Intertidal stromatolites (Ds)
- Nodular peloidal dolomite (Dn)
- Evaporitic green shales (Evm)

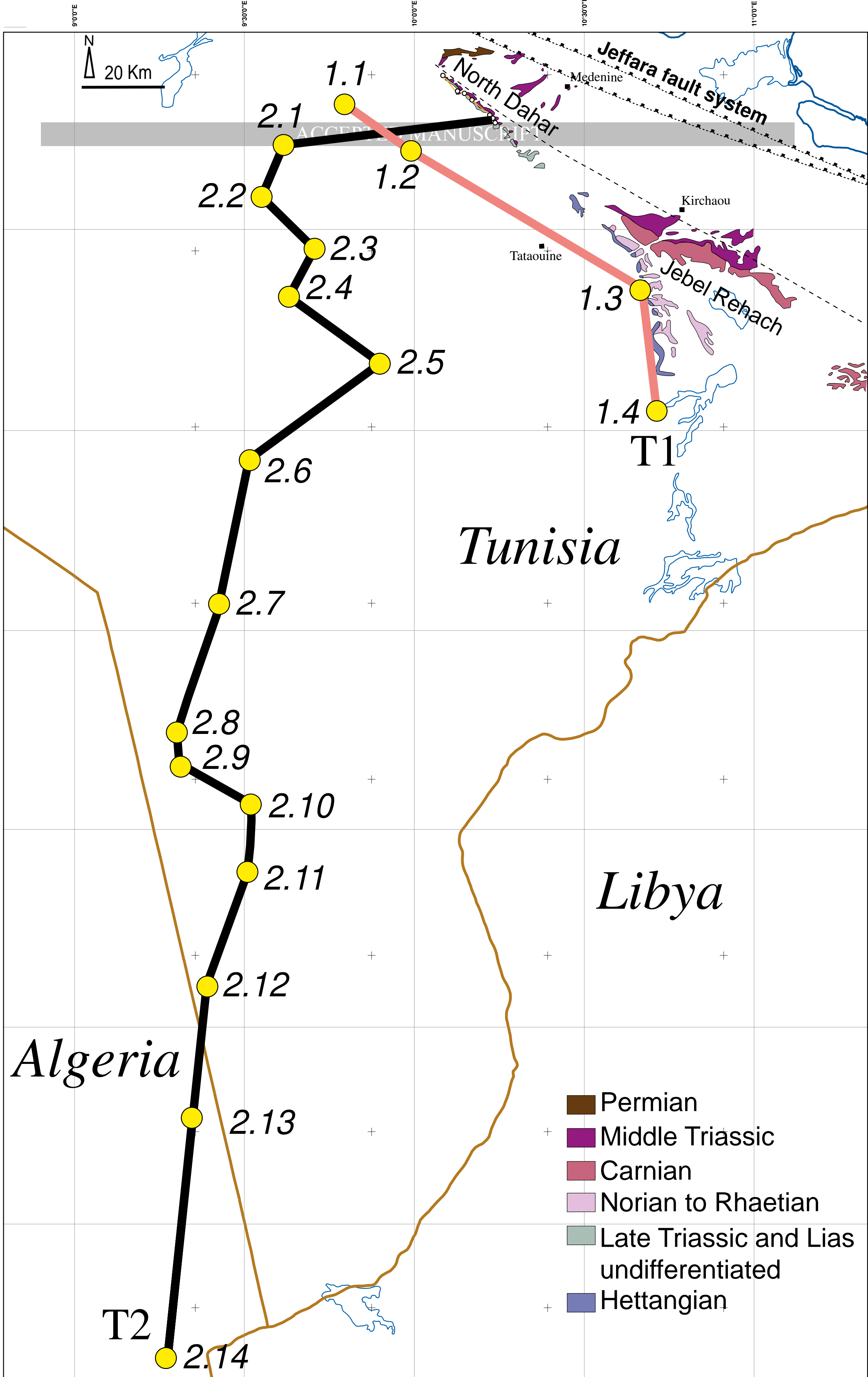
Achaab El Messaoudi

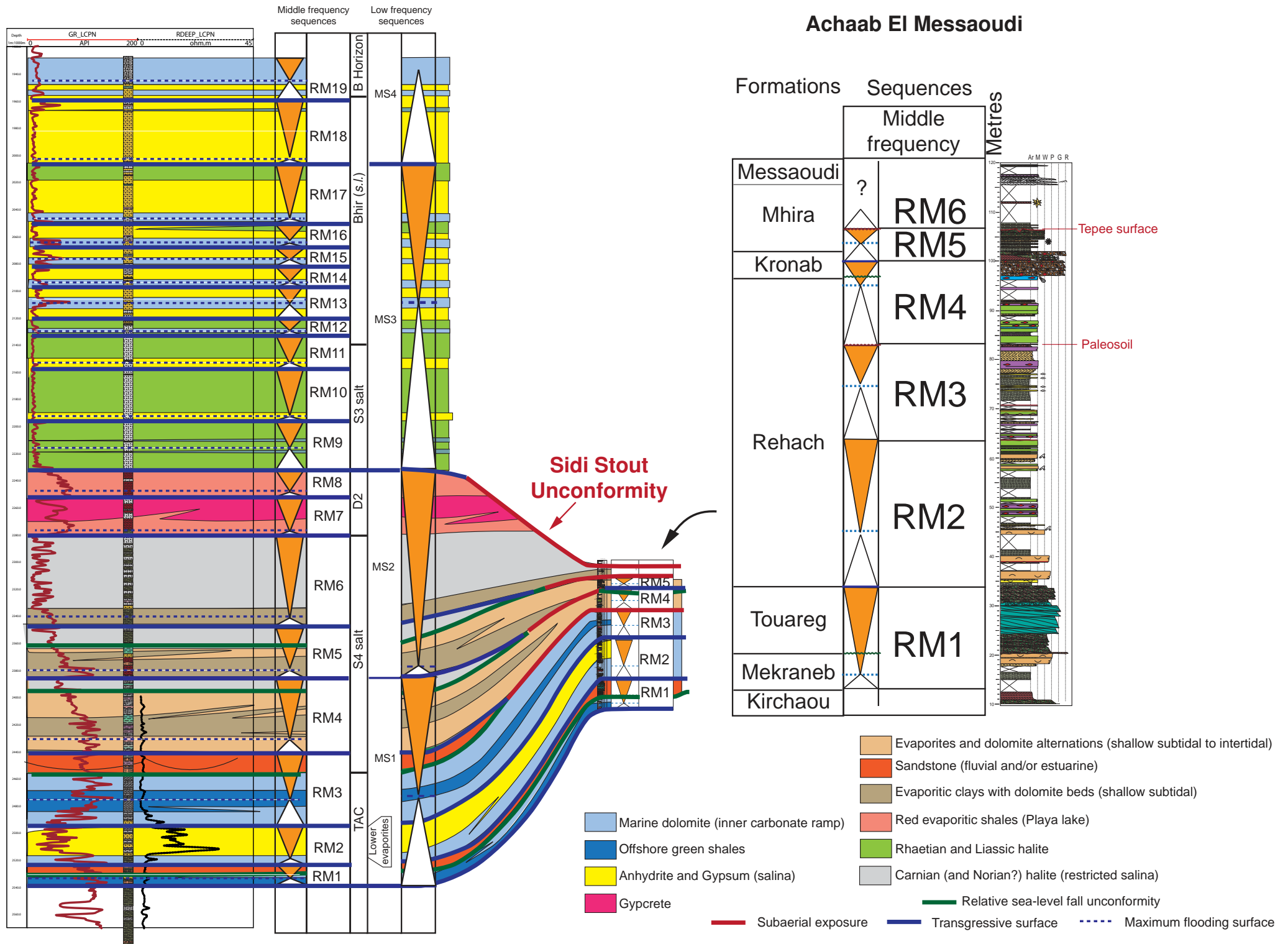






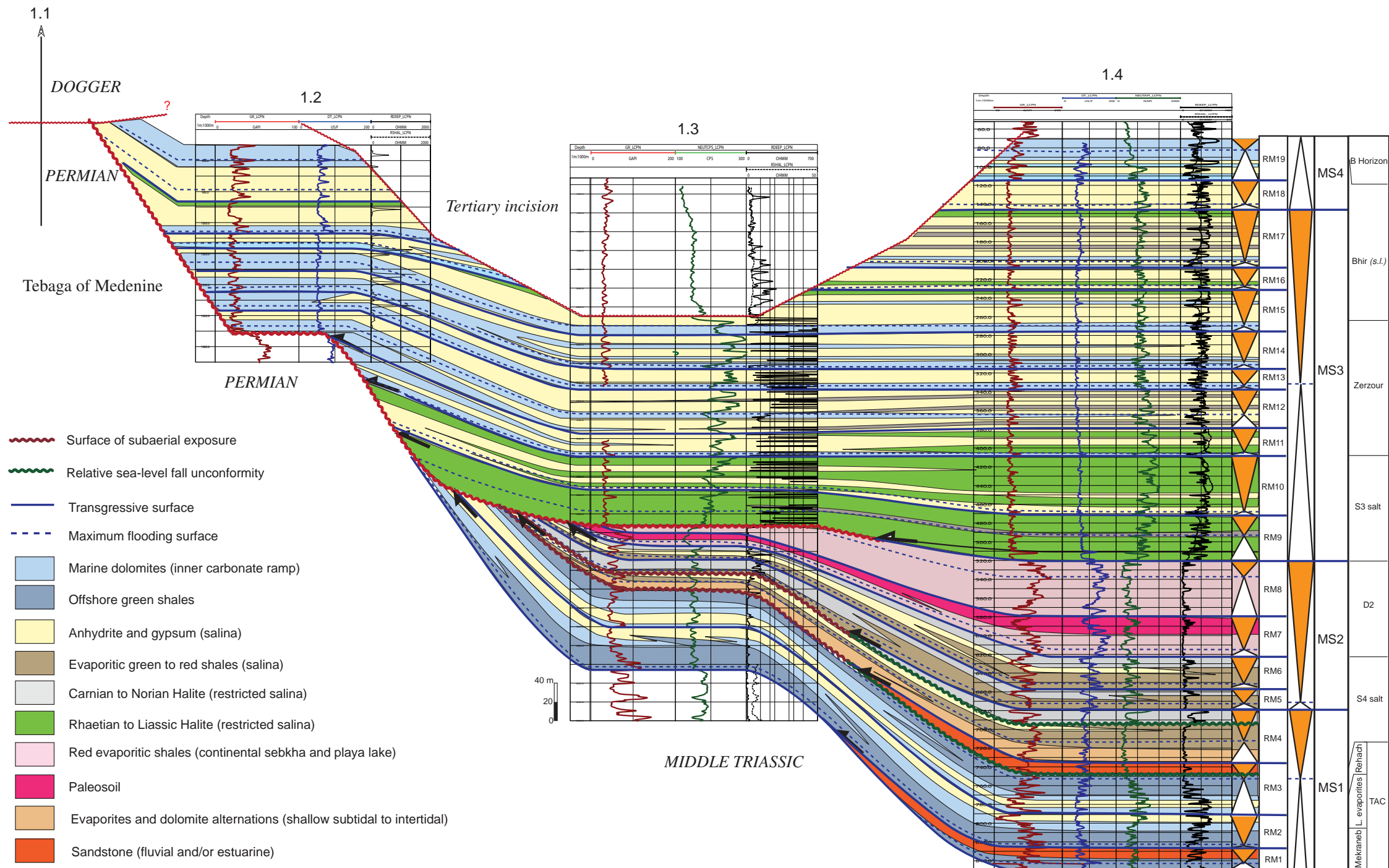


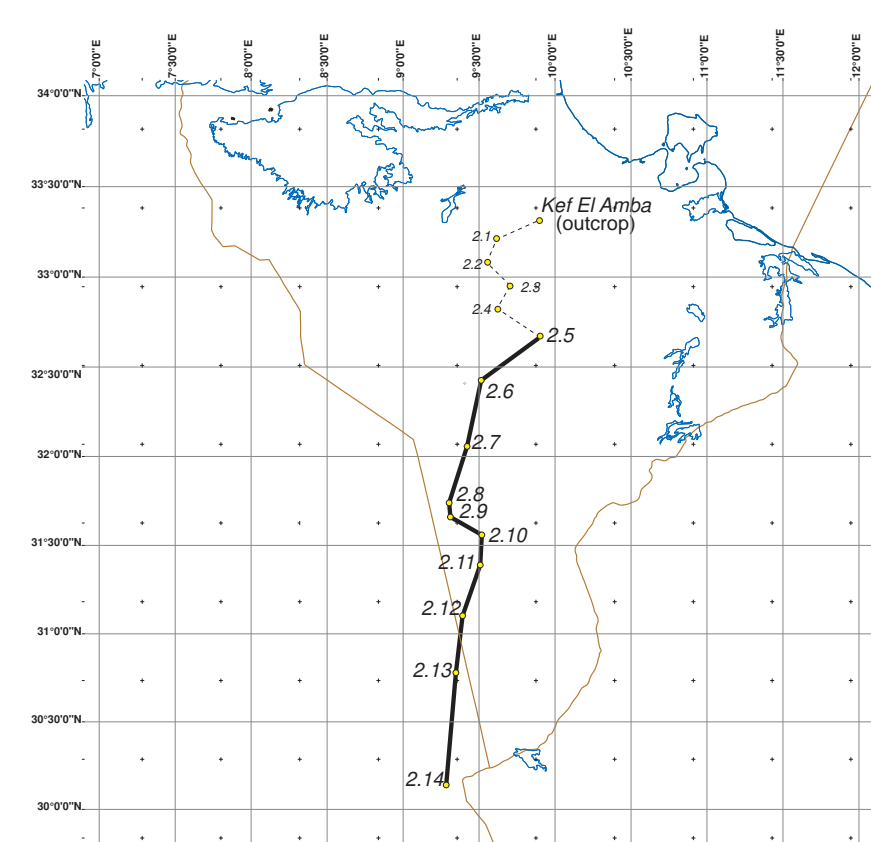
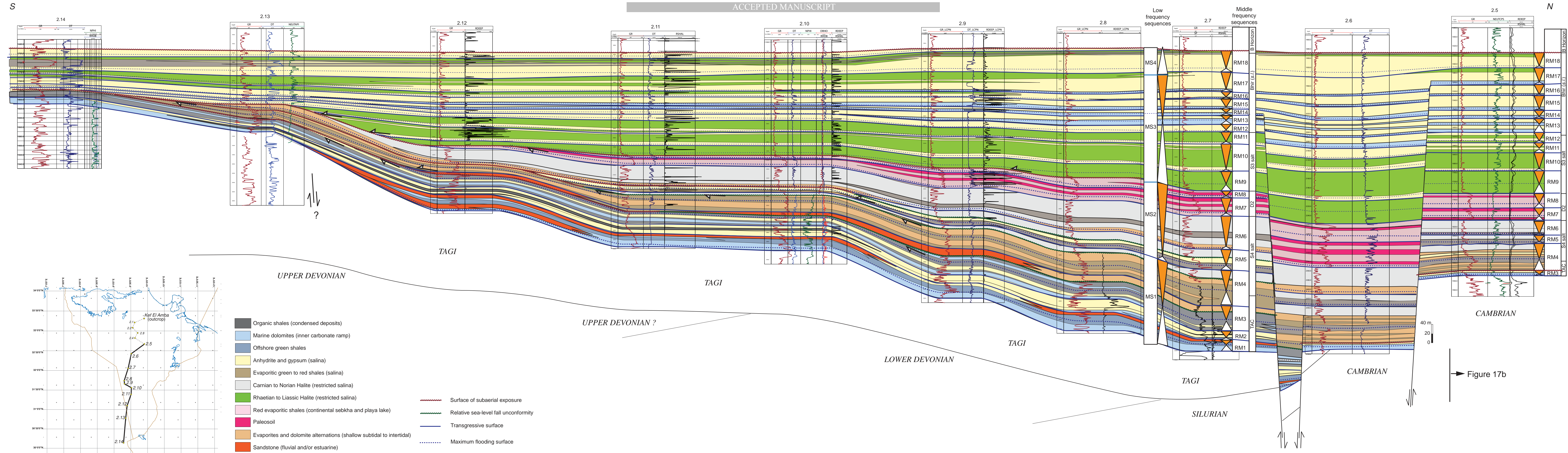


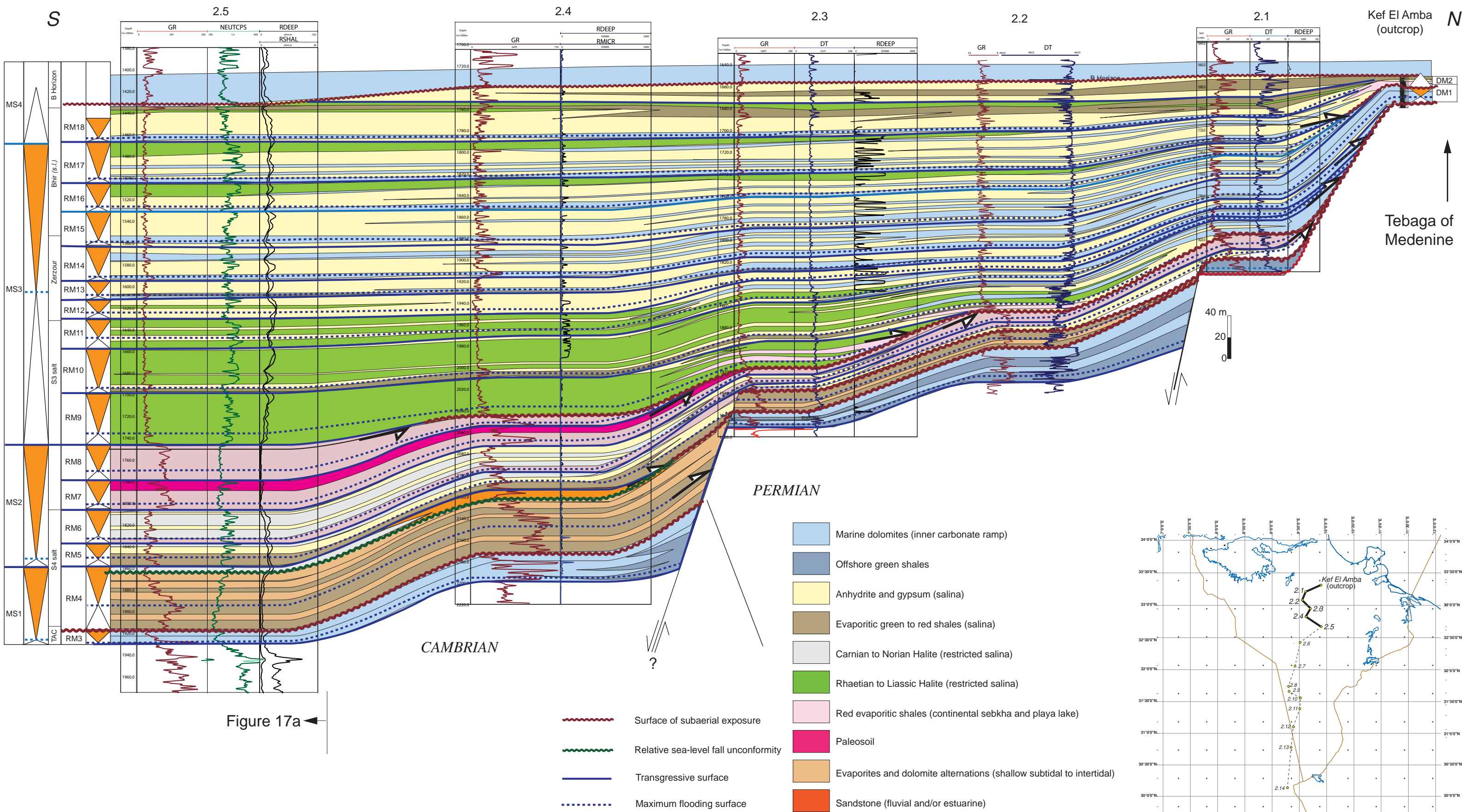


NW

SE



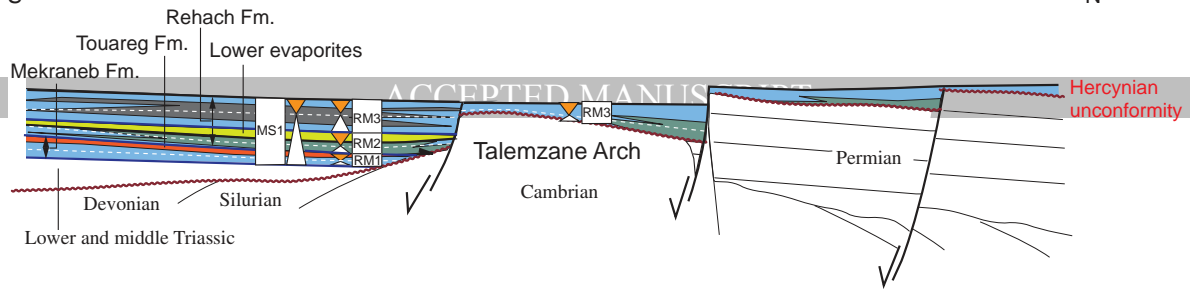




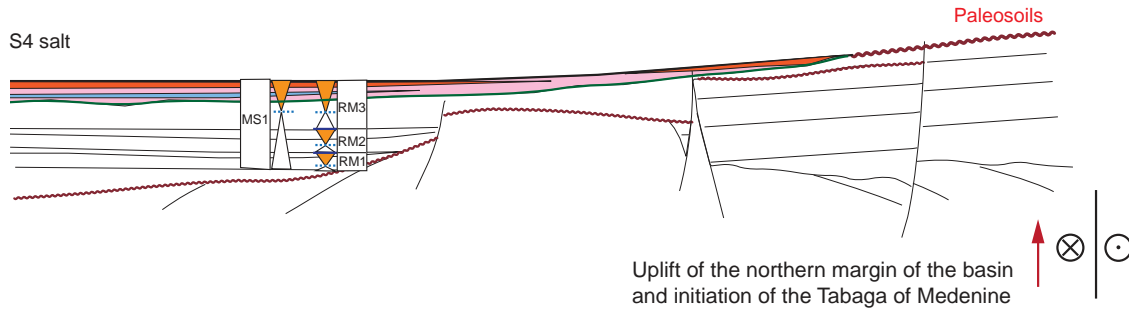
S

N

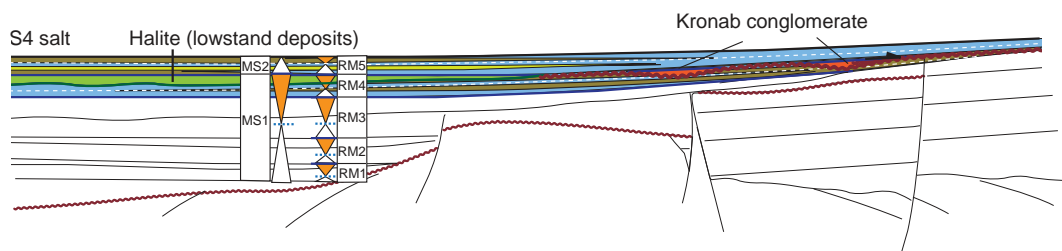
a



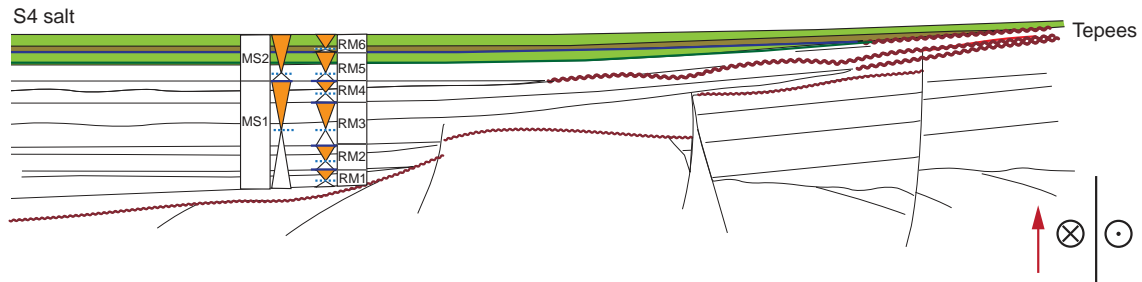
b



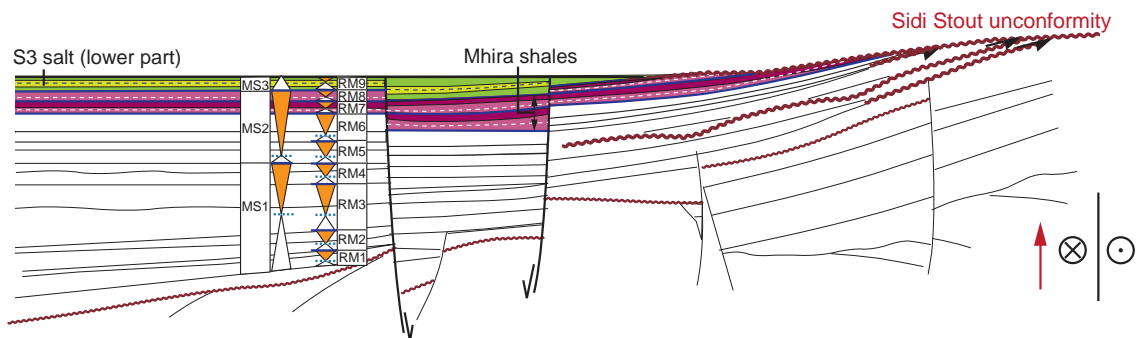
c



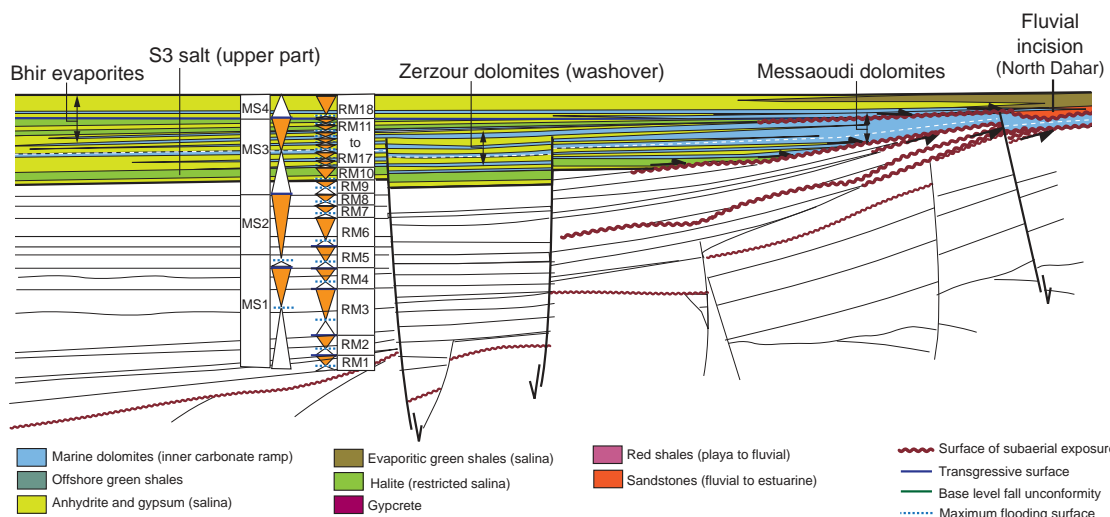
d

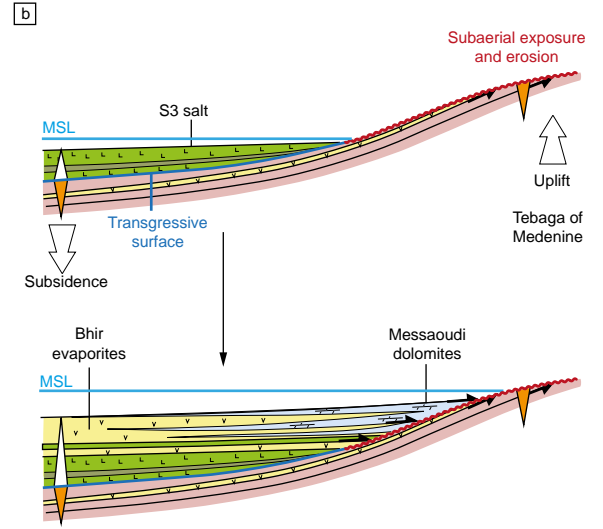
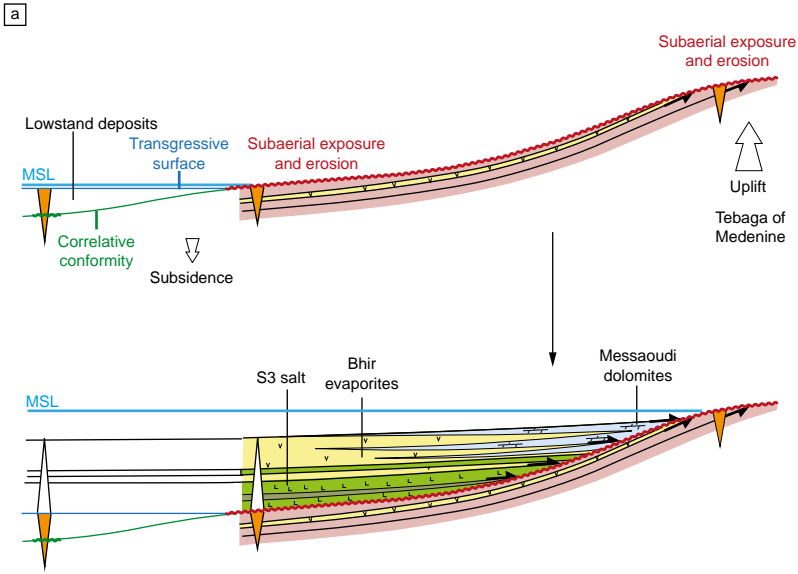


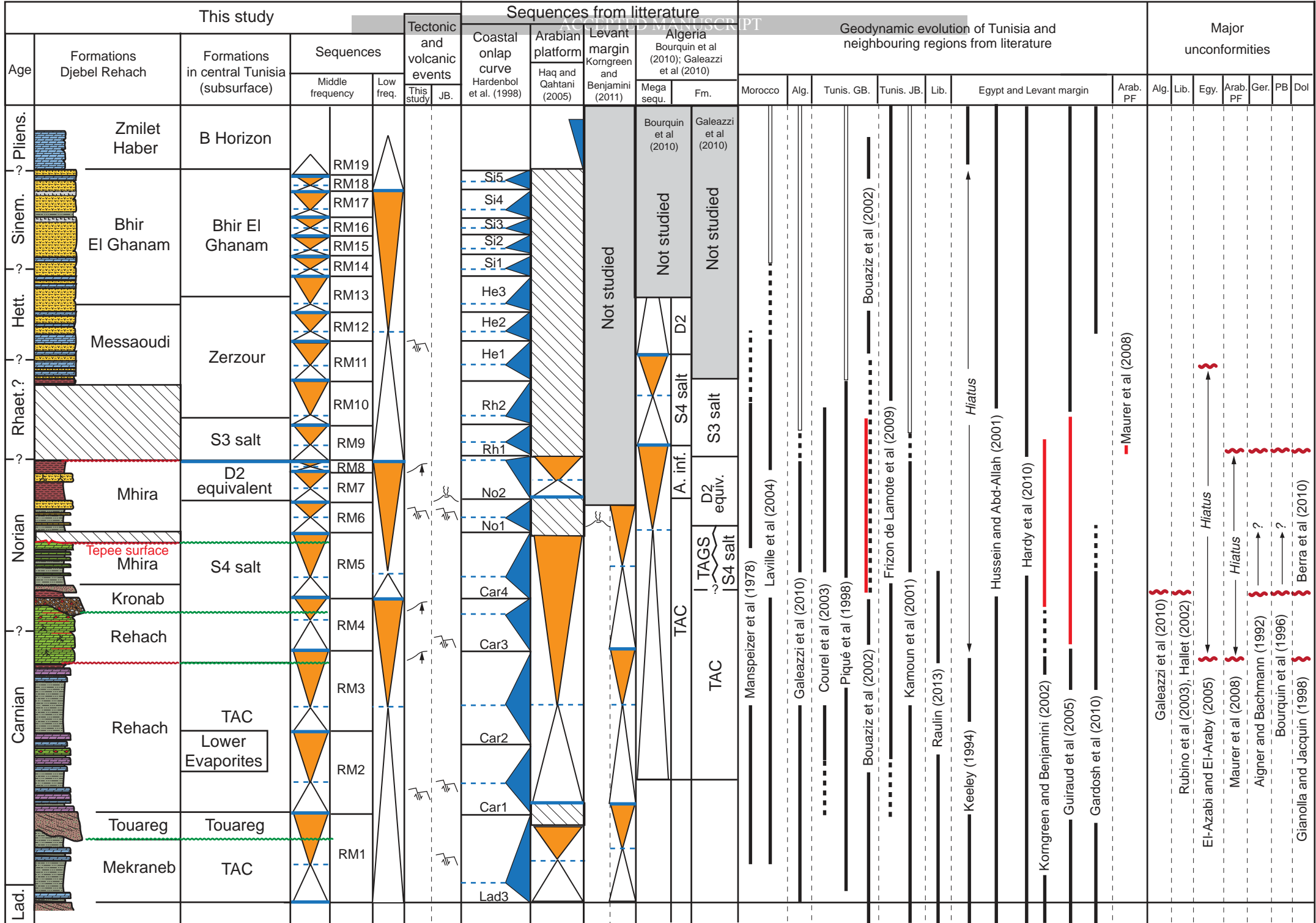
e



f







GB. = Ghadames Basin J.B. = Jeffara Basin Fm. = Formations Alg. = Algeria Lib. = Libya Mor. = Morocco Ger. = Germany PB = Paris Basin Dol = Dolomites Arab. PF = Arabian platform

A. inf. = Argiles inférieures Egy. = Egypt Normal faulting Volcanism Uplift Rifting Uplift Thermal subsidence

- First ever sequence stratigraphic framework for the Late Triassic and Early Lias of Tunisia
- Correlation and sedimentary geometries between outcrops and subsurface
- Relationships between geodynamics and sequential evolution
- Two phases of rifting separated by an uplift of the northern basin margin
- Uplift due to strike-slip movements along Hercynian faults during the Eo-Cimmerian event